University of Alberta

Finite Element Modeling of Acoustical Silencers

By:

Steven D. Bilawchuk

©

A thesis submitted to the Faculty of Graduate Studies and Research in partial fulfillment of the requirements for the degree of Master of Science.

Department of Mechanical Engineering

Edmonton, Alberta
Fall 2002

National Library of Canada
Acquisitions and Bibliographic Services
395 Wellington Street
Ottawa ON K1A 0N4
Canada

Bibliothèque nationale du Canada
Acquisitions et services bibliographiques
395, rue Wellington
Ottawa ON K1A 0N4
Canada

Your file Votre référence

Our file Notre référence

The author has granted a non-exclusive licence allowing the National Library of Canada to reproduce, loan, distribute or sell copies of this thesis in microform, paper or electronic formats.

L'auteur a accordé une licence non exclusive permettant à la Bibliothèque nationale du Canada de reproduire, prêter, distribuer ou vendre des copies de cette thèse sous la forme de microfiche/film, de reproduction sur papier ou sur format électronique.

The author retains ownership of the copyright in this thesis. Neither the thesis nor substantial extracts from it may be printed or otherwise reproduced without the author's permission.

L'auteur conserve la propriété du droit d'auteur qui protège cette thèse. Ni la thèse ni des extraits substantiels de celle-ci ne doivent être imprimés ou autrement reproduits sans son autorisation.

0-612-81364-9

Canada

University of Alberta

Library Release Form

Name of Author: Steven D. Bilawchuk

Title of Thesis: Finite Element Modeling of Acoustical Silencers

Degree: Master of Science

Year this Degree Granted: 2002

Permission is hereby granted to the University of Alberta Library to reproduce single copies of this thesis and to lend or sell such copies for private, scholarly or scientific research purposes only.

The author reserves all other publication and other rights in association with the copyright in the thesis, and except as herein before provided, neither the thesis nor any substantial portion thereof may be printed or otherwise reproduced in any material form whatever without the author's prior written permission.

2228 Brennan Court
Edmonton, Alberta, Canada
T5T 6M3

August 16 2002

University of Alberta

Faculty of Graduate Studies and Research

The undersigned certify that they have read, and recommend to the Faculty of Graduate Studies and Research for acceptance, a thesis entitled Finite Element Modeling of Acoustical Silencers submitted by Steven D. Bilawchuk in partial fulfillment of the requirements for the degree of Master of Science.

Dr. Ken R. Fyfe (Supervisor)

Dr. M. Gary Faulkner

Dr. John Beamish

13 - AUG - 2002

Abstract

Due to the increasing public awareness for noise concerns, the use of acoustical silencers is becoming more prominent. Current methods for design and prediction of performance are only reasonably accurate for specific design cases, and are unable to handle the wide variety of geometrical, environmental, and material parameters available. A numerical model, which can handle many of the various design cases and parameters, and can be implemented along with an optimization scheme is desirable.

The purpose of this thesis is to define and outline the various numerical techniques used to characterize the performance of acoustical silencers. Geometrical concerns, along with sound absorbing material, and various environmental design parameters are included and comparisons are made between the numerical and physical results obtained. Time and computational effort issues are discussed and techniques for reducing both are presented. Finally, various areas where the work can be extended in the future are mentioned.

Acknowledgements

Throughout the duration of the project, there were several key people who assisted and contributed to the work. Without the efforts and knowledge of these people the project would not have been anywhere near as successful.

First and foremost, Dr. Ken Fyfe has made life at the University much more enjoyable and enlightening. His tireless efforts to educate and inspire (along with the occasional Frisbee break) have made the last two years some of the most memorable in my life.

The members of aci Acoustical Consultants Inc. have gone out of their way to provide support and technical expertise. I have learned much from Dr. Gary Faulkner, Mr. Eugene Bolstad, and Mr. Corjan Buma.

ATCO Noise Management has also provided much in the way of support and information. They deserve credit for their continuing commitment to Engineering research in the field of acoustics.

Michelle Vigeant contributed much to the project during her summer here. Many tasks which would have taken a great deal of time were completed much faster and better due to her efforts.

Mr. Kelly Kruger and Mr. Erwin Rebke have provided much in the way of technical expertise and support, as well as equipment for testing.

The Natural Sciences and Engineering Research Council of Canada (NSERC) provided much of the funding for the work.

Last, but certainly not least, the personnel in the Mechanical Engineering machine shop have proven instrumental during the construction stage of the physical model, along with other various testing equipment.

I thank you all for your efforts. I greatly appreciate all you have done.

This Thesis is dedicated to my wife Karla who put up with me for 7 years of University, to my father who instilled in me a thirst for scientific knowledge and excitement, and to my mother who has always been there for me.

I love you all.

TABLE OF CONTENTS

1 Introduction 1
1.1 Purpose of Study 1
1.2 Importance of Work 1
1.3 Types of Silencers 1
1.4 Literature Survey 3
1.4.1 Basic Finite Element Methods 3
1.4.2 Acoustic Material Properties 4
1.4.3 Measurement Techniques and Design Criteria 6
1.4.4 Summary of Literature Review 7
1.5 Current Design Methods 7
1.6 Thesis Goals 8
1.7 Remaining Chapters 8

2 Methods for Solution 10
2.1 Introduction 10
2.2 Evaluation Criteria 10
2.2.1 Noise Reduction 10
2.2.2 Insertion Loss 11
2.2.3 Transmission Loss 12
2.3 Methods for Solution 12
2.3.1 Traditional Method 13
2.3.2 4-pole Method 14
2.3.3 3-point Method 17
2.4 Numerical Techniques 20
2.4.1 Finite Element Method 20
2.4.2 Boundary Element Method 22
2.5 Comparison of Methods for Solution 23
2.5.1 2-Dimensional Expansion Chamber 23
2.5.2 3-Dimensional Expansion Chamber 27
2.5.3 Helmholtz Resonator Example 30
2.5.4 Problems/Idiosyncrasies Encountered 31
2.6 Conclusions 34

3 Sound Absorbing Materials 36
3.1 Introduction 36
3.2 Bulk Material Properties 36
3.2.1 Flow Resistivity 37
3.2.2 Porosity 39
3.2.3 Structural Factor 41
3.2.4 Bulk Material Results 42
3.3 Sound Absorbing Materials in a Numerical Model 43

3.4 Impedance Tube Testing 43
3.4.1 Theory 43
3.4.2 Test Methods 45
3.4.3 Results 47
3.4.3.1 Flow Resistivity 49
3.4.3.2 Porosity 50
3.4.3.3 Structural Factor 51
3.4.3.4 Thickness 52
3.4.3.5 Various Materials 53
3.5 Conclusions 60

4 Data Acquisition System 61
4.1 Introduction 61
4.2 Equipment 61
4.3 Theory 65
4.4 Verification 68
4.5 Conclusions 71

5 Scale Parallel Baffle Silencer Modeling 73
5.1 Introduction 73
5.2 Scale Model 73
5.2.1 Geometry / Sections 74
5.2.2 Limitations of Scale Model 78
5.3 Measurement of Transmission Loss 80
5.3.1 Measured 3-point Method Theory 80
5.3.2 Comparison of traditional and 3-point Methods 83
5.3.3 Practical Considerations / Measurement Concerns 85
5.4 Numerical vs. Measured Scale Model Results 90
5.4.1 Sources for Discrepancies 93
5.5 Numerical vs. Empirical Scale Model Results 94
5.6 Comprehensive Parametric Study 96
5.6.1 Baffle Length 96
5.6.2 Baffle Thickness 99
5.6.3 Baffle Spacing 101
5.6.4 Percent Open Area 103
5.6.5 Staggered Baffles 103
5.6.6 Flow Resistivity Values 106
5.6.7 Porosity Values 108
5.6.8 Structural Factor Values 109
5.6.9 System Temperature 111
5.6.10 System Pressure 113
5.7 Conclusions 114

6 Design Considerations 116
6.1 Introduction 116
6.2 Computational Effort 116
6.2.1 2-Dimensional vs. 3-Dimensional 117
6.2.2 Symmetry 118
6.2.3 Multiple Models 121
6.3 Perforated Material 123
6.4 Pressure Drop 126
6.5 Conclusions 129

7 Conclusions and Future Considerations 131
7.1 Thesis Contributions 131
7.2 Future Considerations 132
7.2.1 Insertion Loss Calculation 132
7.2.2 Flow Noise 133
7.2.3 Break-Out Noise 134
7.2.4 Absorptive Materials 134
7.2.5 Low Frequency Concerns 135
7.2.6 Optimization 136
7.3 Conclusions 136

Appendix A: 2-D Acoustic FEM Derivation 137

Appendix B: 2-D Acoustic Element Derivation 140

Appendix C: Global Stiffness Matrix Assembly Example 142

Appendix D: Absorptive Material FEM Derivation 145

Appendix E: ANSYS Code for Mesh Generation 151

Appendix F: SYSNOISE Code for FEM Solution 153

References 156

LIST OF TABLES

Table 1. Bulk Acoustical Properties of Various Sound Absorbing Materials 42

Table 2. Evaluation of Frequency Accuracy of MATLAB Data Acquisition System 68

Table 3. Summary of Effects of Various Parameters on Transmission Loss 115

Table 4. Predicted Perforated Material Attenuation 126

LIST OF FIGURES

Figure 1. Various Reactive Silencers 2
Figure 2. Various Absorptive (Parallel Baffle) Silencers 3
Figure 3. *Traditional* Method for Determining Transmission Loss 14
Figure 4. 4-pole Transfer Matrix Method Measurement Points 15
Figure 5. 3-point Method Measurement Points for Transmission Loss 18
Figure 6. Finite Element Method Discretization of an Expansion Chamber Silencer 20
Figure 7. Example Boundary Element Mesh for Single Expansion Chamber 22
Figure 8. Single Expansion Chamber Dimensions 23
Figure 9a. Transmission Loss for Single Expansion Chamber with *Traditional* Method 26
Figure 9b. Transmission Loss for Single Expansion Chamber with 4-pole Method 26
Figure 9c. Transmission Loss for Single Expansion Chamber with 3-point Method 27
Figure 10. Full Three Dimensional Expansion Chamber Dimensions 28
Figure 11a. *TL* Response of 3-D Expansion Chamber 29
Figure 11b. *TL* Response of 10cm Stinger in 3-D Expansion Chamber 29
Figure 12. Three Dimensional Helmholtz Resonator 30
Figure 13. Three Dimensional Helmholtz Resonator Modeled *TL* 31
Figure 14. *TL* Response of Expansion Chamber Using Complex and Absolute Values 33
Figure 15. Numerical *TL* Response of Parallel Baffle Silencer with Complex and Absolute Values and Measured *TL* with *traditional* method 34
Figure 16. Flow Resistivity Measurement Apparatus 38
Figure 17. Porosity Measurement Apparatus 40
Figure 18. Impedance Tube Measurement Apparatus 44
Figure 19. Impedance Tube Measurement Results for ASTM Round Robin Sample 46
Figure 20. Numerical Model of Impedance Tube 46
Figure 21. Measured and modeled absorption coefficients for yellow fiberglass material 48
Figure 22. Measured and modeled absorption coefficients for ASTM round robin sample 48
Figure 23. Modeled absorption coefficient of yellow fiberglass with varying resistivity values 49
Figure 24. Modeled absorption coefficient of yellow fiberglass with varying porosity values 50
Figure 25. Modeled absorption coefficient of yellow fiberglass with varying structural factor values 51
Figure 26. Modeled absorption coefficient of yellow fiberglass with varying thickness values 52
Figure 27. Measured and Modeled absorption coefficients of Green Fiberglass, Yellow Fiberglass, and Pink Fiberglass 54
Figure 28. Measured and Modeled absorption coefficients of Permacote Grey Foam, ASTM Round Robin Sample, and Manville 814 Spin Glass 55
Figure 29. Measured and Modeled absorption coefficients of Armstrong Mineral Fiber, Kaowool 2300F Ceramic Fiber, and Kaowool 2600F Ceramic Fiber 56

List of Figures

Figure 30. Measured and Modeled absorption coefficients of 2.68, 3.0 and 4.0 pcf Whispertone Wallboard 57
Figure 31. Measured and Modeled absorption coefficients of 1, 2, and 3 layers of 6 pcf Whispertone Wallboard 58
Figure 32. Diagram of Data Acquisition Equipment Used 62
Figure 33. Data Acquisition Program with Single Channel FFT "Real Time" Data Collection 63
Figure 34. Data Acquisition Program with Dual Channel 1/3 Octave "Real Time" Data Collection 64
Figure 35. Frequency Response of Sound Card Used for Data Acquisition 69
Figure 36. Whole and 1/3 Octave Sound Pressure Level Differences Between B&K 2144 and Matlab Data Acquisition System 70
Figure 37. Dual Channel Data Acquisition with 250 Hz Signal 71
Figure 38. Scale Parallel Baffle Silencer Model 74
Figure 39. Physical Model with Test Section Door Closed 76
Figure 40. Physical Model with Test Section Door Open 77
Figure 41. Physical Model, Adjustable Baffle Detail 77
Figure 42. *TL* of Silencer Model with Full Test Section of Pink Fiberglass Insulation 79
Figure 43. Transmission Loss Comparison of *Traditional* vs. 3-point Method for Single Baffle of 100mm Thick Yellow Fiberglass Insulation 84
Figure 44. Transmission Loss Comparison of *Traditional* vs. 3-point Method for Two Baffles of 50mm Thick Green Mineral Rock Insulation 85
Figure 45. Transmission Loss with 3-point Method and Different Center-to-Center Microphone Spacing Between Points 1 & 2 for Two Baffles of 50mm Thick Green Mineral Rock Insulation 86
Figure 46. Transmission Loss with 3-point Method and Different Locations for Point 3 for Two Baffles of 50mm Thick Green Mineral Rock Insulation 87
Figure 47. Transmission Loss with 3-point Method and Different Microphone Mounting for Two Baffles of 50mm Thick Green Mineral Rock Insulation 88
Figure 48. Transmission Loss with 3-point Method and Center-Line vs. Off Center-Line Microphone Mounting for Two Baffles of 50mm Thick Green Mineral Rock Insulation 88
Figure 49. *TL* for Two 80mm Thick, 225mm Long Baffles of Pink Fiberglass Insulation 91
Figure 50. *TL* for a Single 73mm Thick, 225mm Long Baffle of Yellow Fiberglass Insulation 91
Figure 51. *TL* for Three Equally Spaced, 50mm Thick, 225mm Long Baffles of Kaowool 2600F Ceramic Fiber Insulation 92
Figure 52. *TL* Results for a Single Baffle and Two Half Baffles of Green Mineral Rock Insulation 95
Figure 53. *TL* with Varying Baffle Length (10cm – 50cm) 97
Figure 54. *TL* with Varying Baffle Length (50cm – 3.0m) 98
Figure 55. *TL* Ratio with Varying Baffle Length 98
Figure 56. *TL* Values with Varying Baffle Thickness (1cm-7cm) 100
Figure 57. *TL* Values with Varying Baffle Thickness (10cm-50cm) 100

List of Figures

Figure 58. *TL* Values with Varying Baffle Spacing (4cm-15cm) 102
Figure 59. *TL* Values with Varying Baffle Spacing (20cm-50cm) 102
Figure 60. Parallel Baffle Silencer with 2 Staggered Baffle Columns 103
Figure 61. *TL* with Equivalent Staggered and Non-Staggered Baffle Models 105
Figure 62. *TL* Values with Varying Flow Resistivity (2,000 – 20,000 mks rayls/m) 107
Figure 63. *TL* Values with Varying Flow Resistivity (20,000 – 200,000 mks rayls/m) 107
Figure 64. *TL* Values with Varying Porosity (1.0 – 0.2) 108
Figure 65. *TL* Values with Varying Structural Factor (1.0 – 5.0) 110
Figure 66. *TL* Results with Various Air Temperatures (-100°C – 150°C) 112
Figure 67. *TL* Results with Various Air Temperatures (300°C – 2,000°C) 112
Figure 68. *TL* Results with Varying Atmospheric Pressure 113
Figure 69. Planar Symmetry for Single Expansion Chamber 118
Figure 70. Axi-Symmetry for Three-Dimensional Single Expansion Chamber 118
Figure 71. Transmission Loss for Silencer with Full 3-D, Planer Symmetric, and Axi-Symmetric Numerical Models 119
Figure 72. Parallel Baffle Symmetry Example 119
Figure 73. Full Model, Half Model, and Two Half Baffle Model *TL* Results 120
Figure 74. Sound Wave Paths Through Baffles in Silencer 121
Figure 75. Fine and Coarse Mesh Sizes for Similar Geometry 122
Figure 76. Perforated Material Attenuation with Various Transparency Index Values .124
Figure 77. TL Results With and Without Perforated Metal Mesh 125
Figure 78. Entrance, Exit, and Friction Loss Factors for Various Geometries 128

1 Introduction

1.1 Purpose of Study

The purpose of this study was to investigate the various parameters involved in numerical techniques for characterization and design of acoustical silencers. More specifically, the use of the Finite Element Method (FEM) was emphasized, and factors such as accuracy, ease of use, characterization of sound absorbing materials, and computational effort were evaluated.

1.2 Importance of Work

Acoustical silencers are used on noise producing machinery to reduce the level of perceived noise. Due to the increased use of noise producing mechanical systems, and the ever-growing level of noise pollution concerns, the use of acoustical silencers is increasing rapidly. From simple, mass produced silencers (like those used on automobiles), to more complex, specific designs (such as those used on gas turbine installations), the design of effective acoustical silencers is becoming a very important facet of noise control engineering.

1.3 Types of Silencers

There are two main categories of acoustical silencers. The first category is composed of reactive silencers. These are silencers which produce sound attenuation by utilizing geometric properties to produce destructive wave interference. In a purely reactive silencer, there is no sound absorbing material used. Examples of reactive silencers include expansion chambers, side branch resonators, Helmholtz resonators, and Quincke tubes (some shown in Fig 1). These silencers can be used individually or, as is often the case, used in combination with each other to produce even more acoustical attenuation [1].

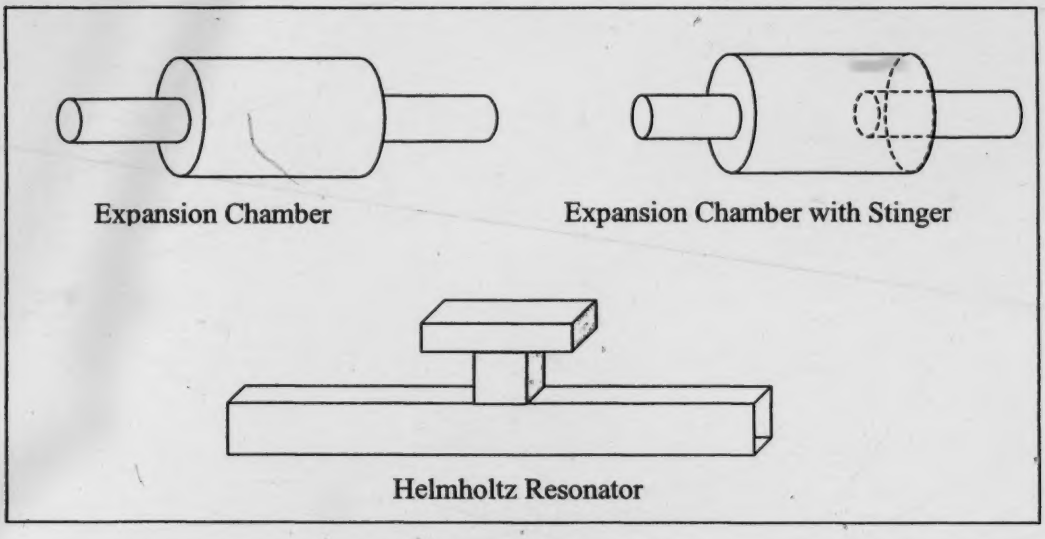

Figure 1. Various Reactive Silencers

The second category of acoustical silencers is known as absorptive. These silencers use various sound absorbing materials to produce the sound attenuation desired. For purely absorptive silencers, the geometry is typically constant throughout the silencing section, with only slight changes due to the locations of the sound absorbing material within. Examples of purely absorptive silencers include acoustically lined ducts, parallel baffle silencers (shown in Fig 2), stack insert silencers, and tubular silencers with an absorptive center "bullet". As is the case with reactive silencers, various types of absorptive silencers can be combined. Occasionally, a silencing system will consist of both reactive and absorptive silencers to provide the greatest possible sound attenuation performance over the largest possible frequency range [1].

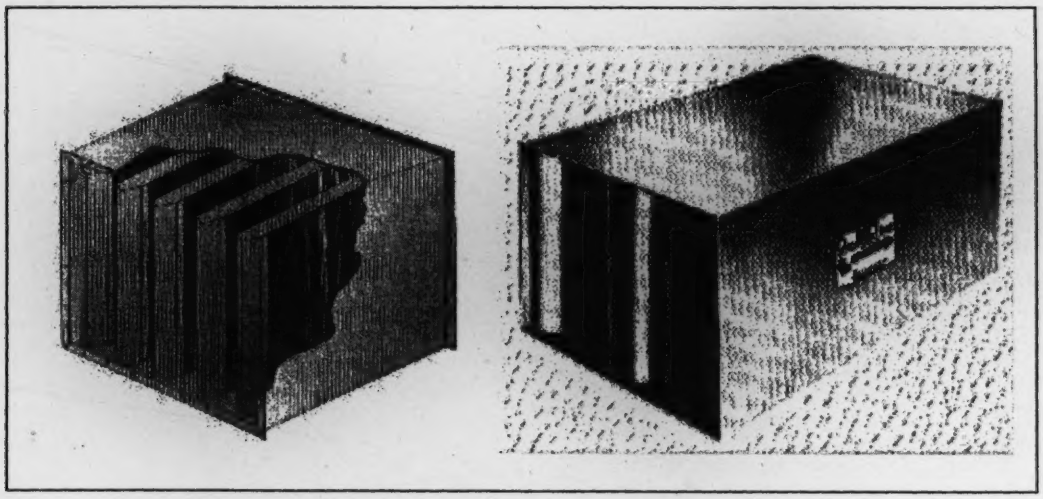

Figure 2. Various Absorptive (Parallel Baffle) Silencers
(Obtained from the Universal Silencer website, www.universalsilencer.com)

1.4 Literature Survey

There has been an abundance of work previously done regarding numerical modeling of various acoustical concerns. The literature review will be separated into three sections. The first section deals with the Finite Element Method involved in basic acoustic models. Next are the bulk acoustic material properties used and the numerical methods employed to include them in the model. Finally, the third section involves silencer measurement equipment and techniques along with investigations into design criteria other than those mentioned in more detail in the Thesis.

1.4.1 Basic Finite Element Methods

Books and papers on the subject of basic acoustic FEM methods are numerous. Some of the earliest acoustic FEM method work dates back to Gladwell [2] and Craggs [3]. Gladwell used (as a basis) the Helmholtz equation and then variational methods were used to derive the acoustic elements along with prescribed shape functions. The conditions imposed on this model were that pressure (p) and the change in pressure with distance (dp/dx) be continuous everywhere and that (dp/dx)

be zero at the ends. Craggs, using similar formulations for the FEM, investigated the use of various element types to model the modes of an acoustic cavity. Boundary conditions such as no flow (resulting in an acoustically hard surface), and pressure continuity were discussed. This was also one of the few papers to actually compare the numerical results to those obtained by measuring a physical model (the interior of a car in this case). Finally, further to the methods presented previously, Munjal [4] discussed the use of the Weighted Residual method (Galerkin) with respect to deriving an acoustic finite element.

The information obtained from these sources provided the basis for the derivations of the finite element methods, element formation, and global matrix assembly shown in the Appendices. The basic techniques were then built on and customized for the particular requirements of the Thesis.

1.4.2 Acoustic Material Properties

The characterization, measurement, and modeling of the bulk acoustic material properties are very important steps in modeling absorptive silencers. Two papers by Craggs [5, 6] were instrumental in the methods presented in the Thesis. The papers discussed the derivation of a rigid acoustical absorptive element and how this element could be coupled with the acoustical fluid (air in most cases) to model specific orientations of absorptive media. Introduction of the various bulk acoustical material properties (i.e. flow resistivity, porosity and structural factor) into the model were discussed. The methods presented were verified by comparing the numerical results obtained to those predicted using empirical methods (available at the time). The numerical models showed good agreement with the empirical models.

Buma, Craggs and Faulkner [7] presented a paper on obtaining the various bulk acoustical material properties. The paper discussed the test methods and apparati used for the measurements, along with the various mathematical equations required for the calculations. When combined with the numerical methods presented by Craggs [5, 6], the result was a full set of instructions on how to obtain the bulk acoustical material properties and include them in a numerical model.

Various ASTM measurement standards [8, 9, 10] were followed when obtaining some of the acoustical material properties. These standards covered the fundamental theories and measurement methods behind flow resistivity, random incidence sound absorption coefficients, and normal incidence sound absorption coefficients. In addition, they provided a guideline for the expected values of various materials, along with equipment limitations, and reliability and repeatability in the test methods.

Probably the most comprehensive paper on the subject is that by Attenborough [11] in which several of the various bulk material properties are derived, discussed, and evaluated. More detail is discussed for each material property than Craggs presented in his works, and many more properties which might be included into the numerical model at a future date are presented.

Testing was completed for the Thesis to compare the numerical results with physical results and it was found that the methods proposed above did not provide the most accurate numerical representation possible of the absorptive material. A further review was completed in which newer, more elaborate techniques for inclusion of the bulk material properties into the numerical model were discovered.

A paper by Peat and Rathi [12] discussed some new parameters which could be included in the model such as effective mass and the frequency dependent quantity of compressibility. Their proposed methods also account for material inhomogeneity and acoustic anisotropy. Detailed acoustic element derivations were presented along with the effects of varying the various acoustic material properties.

Kirby and Cummings [13] discussed the high and low frequency limitations of various sound absorbing material models, along with an improved method for predicting the material properties at these extreme frequency ranges.

Finally, Allard et al. [14] and Johnson et al. [15] discuss additional parameters such as permeability and tortuosity, and how they can be included into the numerical model.

1.4.3 Measurement Techniques and Design Criteria

For the methods and criteria used to quantify the performance of acoustical silencers, several papers and texts were used. Books by Bell [1] and Beranek [16] provided the necessary definitions of the various evaluation criteria. Such measurement parameters as Insertion Loss, Transmission Loss, and Noise Reduction are discussed, along with the various types of silencers and some empirical formulas for predicting their performance.

Seybert and Ross [17] discussed the use of dual microphones to measure various acoustical material properties, including the normal incidence absorption coefficient. Detailed derivations were presented for using the auto and cross power spectra to measure the relative contributions of the incident and reflected portions sound waves including the amplitude and phase information. Prasad [18] took these methods one step further and used them to measure some of the characteristics of engine exhaust mufflers such as acoustical impedance and sound source characteristics.

The final group of books and papers reviewed concerned the various additional design parameters not investigated in detail and the future direction of the work. Beranek [16] and I.D.Idel'chik [19] discussed the phenomena of pressure drop of the fluid flowing through the silencer element. Various empirical formulations for predicting the pressure drop were presented, along with the performance of various materials.

Schultz [20] presented a very comprehensive study on the effects of perforated materials used in acoustical applications. In particular, such factors as material thickness, mesh size, and mesh configuration are explored and their effects on the acoustical "transparency" of the material is quantified.

1.4.4 Summary of Literature Review

Many papers and texts have been written on the subjects presented in the Thesis. One of the main goals of the Thesis was to sort through much of the previously completed work and provide an overall summary of the methods available and to present them in such a way that they could easily by adapted.

One of the major shortcomings of essentially all of the papers reviewed is that they did not compare their results to those obtained by physical experimentation. For all of the FEM and material properties papers (including the very recent ones), the results are compared to empirically derived results. One of the major themes of the Thesis work was to compare the results obtained numerically to the results obtained physically. In order to facilitate this, physical models were constructed and then numerically modeled using their exact physical dimensions and material properties. By doing this, some of the limitations of the bulk material models presented by Craggs [5, 6] were highlighted, and newer methods were sought out to provide more accurate results.

1.5 Current Design Methods

The current methods available for silencer design consist of either simple performance calculations, or predictions based on previous empirical results [1, 4, 16, 21]. Formulas exist for the simplest of reactive silencers (single expansion chambers, Helmholtz and side branch resonators), and can be used for limited design cases. For more complicated reactive silencers or absorptive silencers however, the physical system becomes much more difficult to describe with a mathematical formula. In addition, the mathematical formulas derived for simple geometries are based on the assumption of plane wave propagation within the silencing system. Once the frequency becomes too large (wavelength becomes too small) for this assumption to be valid, the mathematical equations can no longer be used.

For results based on empirical data, the usual method is to test a variety of silencer designs and configurations, and use the gathered data to statistically predict the performance of similar designs to those tested. These methods have proven to

provide relatively accurate predictions, but are limited in that the proposed design must be of the same type which was tested to obtain the original data (a straight parallel baffle vs. a 90° elbow for example). In addition, varying operating conditions such as system temperature and pressure are difficult to include in the calculations. It is for these reasons that a numerical model is preferred to include all of the various design cases and operating conditions, as well as a larger useable frequency range.

1.6 Thesis Goals

The goals of the research were to investigate the various mathematical parameters associated with the use of computer numerical methods, namely the Finite Element Method (FEM). With a greater understanding of the use of these methods, an accurate numerical representation of a physical silencer system was the main project goal. This numerical representation was intended to have the ability to include an infinitely variable geometric configuration for the silencer systems, as well as the ability to include various sound absorbing materials and operating conditions. Finally, with all of the information gathered for proper numerical modeling, methods for solution were to be addressed to handle many of the common design cases and associated parameters. The over-riding concern with the work was to be able to compare the numerical results to those obtained by physical testing of comparable systems.

1.7 Remaining Chapters

Chapter 2 discusses the various parameters used to quantify the performance of acoustical silencers, and the methods used to obtain them. In-depth discussion and derivations of the equations used for Noise Reduction (*NR*), Transmission Loss (*TL*), and Insertion Loss (*IL*), and the methods of *traditional*, 4-pole and 3-point solutions are presented. Finally, evaluation criteria for each method is presented and a final solution technique is chosen for use in the remainder of the work.

Chapter 3 deals with the use of sound absorbing materials in acoustical silencers. The various bulk acoustical material properties are discussed, along with

methods for obtaining them, and a table of results for various materials tested in the study. The accuracy and limitations of the bulk acoustical material properties are also presented. In addition, the necessary equations required for including sound absorbing materials into the numerical model are defined, and results for normal incidence sound absorption coefficient obtained both physically and numerically are compared.

Chapter 4 covers the design and use of the digital data acquisition system for all of the acoustical measurements. The theories behind frequency dependent data acquisition are presented, along with the methods used for the research and a comparison between the custom software and commercially available data acquisition equipment.

Chapter 5 ties together the methods presented in the previous three chapters for use with a physical model of a parallel baffle silencer. The results obtained from testing of this physical model are compared to the equivalent numerical model, and sources for discrepancy are discussed. Finally, an in-depth study is presented where the various parameters associated with the numerical model are investigated to see their effects on the solution obtained. Such parameters as geometric variables with the model, operating conditions such as temperature and pressure, and sound absorbing material properties are investigated.

Chapter 6 deals with some of the various considerations for numerical design of acoustical silencers. The numerical computational effort as it relates to solution time is discussed with proposed techniques for reducing the time required. The use of perforated material in the numerical and physical models is covered, along with a discussion of evaluating the mechanical performance (pressure drop) of the silencer.

Chapter 7 concludes the contributions made by the work and outlines some of the future considerations for continued work in the area. Calculation of *IL*, along with acoustical-vibrational coupling for "break-out" noise calculations, and inclusion of fluid flow effects are discussed. Also, future work in low frequency noise control and potential optimization schemes are presented.

2 Methods for Solution

2.1 Introduction

This chapter covers the various methods and considerations for numerical solutions of acoustical silencers. Three different evaluation criteria are discussed, and one is chosen as the criteria to be used for the remainder of the work. Also, the various numerical techniques are discussed. Results are presented for simple reactive silencers for each of the numerical techniques outlines, and they are evaluated to obtain a method which is best suited for the work

2.2 Evaluation Criteria

There are several criteria used to evaluate the performance of acoustical silencers. These include Noise Reduction (*NR*), Transmission Loss (*TL*), and Insertion Loss (*IL*). Each provides frequency dependent values which describe the noise attenuation obtained by the silencer, however, each is obtained differently and has various measurement parameters which separate it from the others.

2.2.1 Noise Reduction

Noise reduction (*NR*) is defined as the sound level reduction between the inlet of the silencer and the outlet [1]. *NR* can be represented mathematically as:

$$NR = SPL_1 - SPL_2 \ , \ (dB) \tag{1}$$

where:

SPL_1 = Sound Pressure Level upstream of the silencer (dB)

SPL_2 = Sound Pressure Level downstream of the silencer (dB)

Two in-duct measurements are required, one upstream of the silencer and one downstream. The upstream measurement is obtained with the silencer in place, therefore it is subjected to both the incident sound waves propagating from the source to the silencer, and the sound waves reflecting from the silencer back towards the source. *NR* is the least used measurement criteria due to the influence of these reflected waves on the measurements.

2.2.2 Insertion Loss

IL is defined as the difference between two sound pressure levels measured at the same point in space before and after a muffler has been inserted [1]. It can be expressed mathematically as:

$$IL = SPL_{no\ silencer} - SPL_{with\ silencer}\ ,\ (dB) \tag{2}$$

where:

$SPL_{no\ silencer}$ = Sound Pressure Level measured with no silencer in place (dB)

$SPL_{with\ silencer}$ = Sound Pressure Level measured with a silencer in place (dB)

Note that $SPL_{no\ silencer}$ and $SPL_{with\ silencer}$ are to be measured outside of the silencer system at the same point in space.

IL is considered by industry to be the most desirable performance criteria due to the fact that the sound is measured outside of the silencer system and takes into account the interaction of the system with its environment. Because of this, *IL* is the criteria that most reflects how a person would perceive the performance of the silencer at some distance away from it. The difficulty with *IL* is that currently, the sound must be measured with two system configurations (i.e. with and without silencer). Also, traditional FEM cannot readily be used to calculate *IL*.

2.2.3 Transmission Loss

TL is defined as the ratio of sound intensity incident on the silencing element to the sound intensity transmitted [1]. It can be expressed mathematically as:

$$TL = SPL_i - SPL_t \ , \ (dB) \tag{3}$$

where:

SPL_i = Incident Sound Pressure Level (upstream of the silencer) (dB)

SPL_t = Transmitted Sound Pressure Level (downstream of the silencer) (dB)

TL is also a very commonly used parameter, and is easier to measure and predict than *IL*. Unlike *IL*, *TL* is measured inside the duct and, therefore, is subject to upstream noise reflection problems. Using the definition of *TL*, however, only the incident portion of the sound wave is used in the calculation. It is required, therefore, that the upstream measurement be made in such a way that the incident portion can be separated from the reflected portion. Traditionally, this was accomplished by measuring the upstream sound pressure without the silencing element in place (hence no reflected sound waves). Ultimately, *TL* was chosen because of the ease of use, and the greater ability to compare numerical results to measured values.

2.3 Methods for Solution

Each of the criteria from §2.2 can be calculated numerically, using several different techniques. The three techniques outlined in this paper are the *traditional* method, the 3-point method, and the 4-pole method. Once each method is presented, and the numerical techniques are described (§2.4), all of the methods will be compared on worked examples (§2.5).

2.3.1 Traditional Method

As mentioned previously, the definition of *TL* is the ratio of the incident intensity of sound to the transmitted intensity. Since intensity is difficult to measure, the typical method is to make use of the proportionality of intensity to the mean square pressure. As long as the inlet and outlet regions of the silencer are of the same cross section, and the properties of the fluid (density, temperature) do not significantly change, then the *TL* can be expressed as:

$$TL = 20\log_{10}\left|\frac{p_i}{p_{ref}}\ \frac{p_{ref}}{p_t}\right| = 20\log_{10}\left|\frac{p_i}{p_t}\right|,\ (dB) \tag{4}$$

where:

p_i = rms pressure of the incident wave (Pa)

p_t = rms pressure of the transmitted wave (Pa)

p_{ref} = reference rms pressure ($2\text{x}10^{-5}$ Pa)

This can be simplified to the following equation:

$$TL = SPL_i - SPL_t\ ,\ (dB) \tag{5}$$

where it is understood that SPL_i is measured without the silencer in place, and SPL_t is measured with the silencer in place, on the exhaust side of the silencer. Fig. 3 illustrates the two geometries used to measure the SPL_i and SPL_t. This method is how most standards call for the *TL* to be measured [22, 23]. The standards usually require the use of an anechoic or reverberation chamber.

For use with numerical methods, the solution requires two separate solution "runs". The first "run" would include the straight section of tube and the determination of p_i, while the second "run" would include the silencing element and p_t would be determined. This causes the solution time to essentially double. For each "run" the inlet and outlet sections need to be modeled with the characteristic impedance boundary condition applied (impedance (z) = density of fluid (ρ) x speed

of sound (c)) to mimic an anechoic source and termination. This eliminates the effects of reflected waves with in the modeled sections. In physical testing, this is accomplished by using sound absorbing material upstream and downstream of the silencer to minimize the reflected sound waves. The advantage to this numerical method is that it can be readily compared to physical measurement results on an equivalent system, however due to the increased time and effort required, it was not the preferred method.

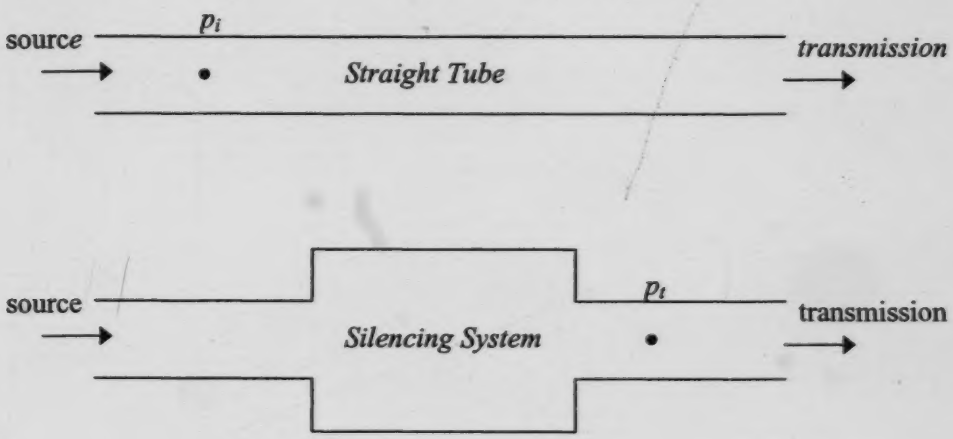

Figure 3. *Traditional* Method for Determining Transmission Loss

2.3.2 4-pole Method

The 4-pole method, as its name implies, uses 4 measurement parameters for the calculation. The derivation for the following formulas presented is well known and can be found in many papers and texts [4, 18, 24, 25], therefore a detailed derivation will not be given here. The parameters used in the formulation are the pressure and particle velocity values at the inlet and outlet of the silencer with 2 different boundary condition configurations. Figure 4 illustrates the measurement parameters for a simple expansion chamber silencer.

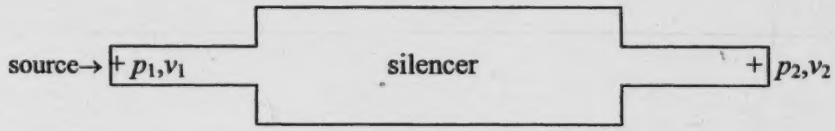

Figure 4. 4-pole Transfer Matrix Method Measurement Points

The corresponding equations (in matrix format) are:

$$\begin{bmatrix} p_1 \\ v_1 \end{bmatrix} = \begin{bmatrix} A & B \\ C & D \end{bmatrix} \begin{bmatrix} p_2 \\ v_2 \end{bmatrix} \tag{6}$$

where:

p_1 = sound pressure at the inlet (Pa)

p_2 = sound pressure at the exit (Pa)

v_1 = normal particle velocity at the inlet (m/s)

v_2 = normal particle velocity at the exit (m/s)

and

$$A = (p_1/p_2)\,|_{v_2 = 0,\, v_1 = 1}, \qquad B = (p_1/v_2)\,|_{p_2 = 0,\, v_1 = 1}, \tag{6a, b}$$

$$C = (v_1/p_2)\,|_{v_2 = 0,\, v_1 = 1}, \qquad D = (v_1/v_2)\,|_{p_2 = 0,\, v_1 = 1}. \tag{6c, d}$$

For the first configuration, the particle velocity at the inlet is set to unity (one) while the outlet is given a value of zero. Then the system is solved for pressure and particle velocity at the inlet and outlet. The second configuration keeps the particle velocity for the inlet at unity, while setting the pressure at the outlet to zero. Once again, the system is solved for the pressure and particle velocity. Once all of the values are known, the *TL* is calculated by:

$$TL = 20\log_{10}\left(\tfrac{1}{2}\left|A + \frac{B}{\rho c} + C\rho c + D\right|\right) + 10\log_{10}\frac{S_1}{S_2}\ ,\ (dB) \tag{7}$$

Again, as in the *traditional* method case, two complete runs are required for the solution. Also, the 4-pole method involves determining the particle velocity, which is a difficult quantity to measure in a physical system. Because of this, it makes the method difficult to compare to physical results. It must be noted that there is an improved formulation for the 4-pole method that is faster than the original, while still maintaining the 4-pole parameters [24]. Due to the programming options in SYSNOISE (the numerical program used in this study), however, it was not possible to evaluate the improved 4-pole method and compare it to the other methods.

The greatest advantage to the 4-pole method is that the values of the 4-pole parameters can be used for adjoining sections of acoustical elements (i.e. additional silencers or ducts, etc...) This is advantageous when the silencer is to be modeled as part of a much larger system. The other sections can be modeled separately, and then the silencer can be added in and the overall performance can be calculated. This is opposed to the *traditional* and 3-point methods where the entire system must be modeled as one complete geometry. Therefore, for individual system component design, the 4-pole method is better, and for whole system design, the 3-point method is better (as will be shown in §2.3.3). It is at this stage in the design, where the method used would be chosen.

One important note relates to the use of complex numbers. The pressures calculated during the numerical solution with the 4-pole method will all be complex. These numbers MUST be kept complex for use in the equations, and only converted to absolute values at the final *TL* calculation step. Keeping the numbers complex will prevent loss of phase information. If the pressures are converted to absolute values early in the calculation stage, the final results will be skewed from the actual values.

Ultimately, due to the increased computational time required and the difficulty to compare to physical results, the 4-pole method was not chosen for the remainder of the work.

2.3.3 3-point Method

The final method for calculating *TL* is known as the 3-point method. As its name implies, three locations are used to determine the pressure. The derivation of the 3-point method equation begins with the one-dimensional wave equation [26].

$$c^2 \frac{\partial^2 p}{\partial x^2} - \frac{\partial^2 p}{\partial t^2} = 0 \tag{8}$$

Eq. (8) is the pressure wave equation for planar propagation where c represents the speed of sound of the medium. Using separation of variables leads to a solution of the form:

$$p(x,t) = p(x)e^{i\omega t} \tag{9}$$

Eq. (9) can now be substituted into Eq. (8) to produce the following ordinary differential equation and corresponding assumed solution:

$$\frac{d^2 p(x)}{dx^2} + k^2 p(x) = 0 \tag{10}$$

$$p(x) = Ae^{sx} \tag{11}$$

where $k = \omega/c = 2\pi f/c$ which is known as the wave number. Substituting the assumed solution, Eq. (11), into Eq. (10) yields the final solution for pressure as a function of distance, x.

$$p(x) = A_1 e^{ikx} + A_2 e^{-ikx} \tag{12}$$

Where A_1 and A_2 are found from the boundary conditions of the problem. The two terms of Eq. (12) represent the waves traveling in the positive and negative directions. Note that Eq. (12) is independent of time. This can be explained in two ways. First,

Eq. (12) is solving for pressure under the assumption that the system is already in a "steady" state of harmonic oscillations. Therefore the time dependence terms can be ignored. The second reason is that if the time dependent terms are carried through with the further derivations, they eventually cancel out anyway and so they were dropped early to avoid confusion and clutter. At this point, the pressure value, $p(x)$, could be substituted into Eq. (9) to get the full solution of the original wave equation but this is not necessary due to the time independent calculations used.

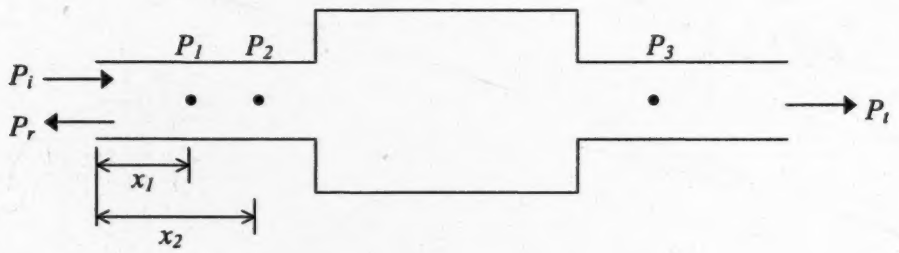

Figure 5. 3-point Method Measurement Points for Transmission Loss

Figure 5 illustrates the three measurement positions, required for the 3-point method, in a single expansion chamber silencer. Applying the first two measurement points to Eq. (12) results in the following two equations:

$$p_1 = p_i e^{-ikx_1} + p_r e^{+ikx_1} \tag{13}$$

$$p_2 = p_i e^{-ikx_2} + p_r e^{+ikx_2} \tag{14}$$

where:

p_1 = rms pressure at point 1 (Pa)
p_2 = rms pressure at point 2 (Pa)
p_i = rms pressure of incoming wave (Pa)
p_r = rms pressure of reflected wave (Pa)
x_1 = distance from silencer inlet to point 1 (m)
x_2 = distance from silencer inlet to point 2 (m)

The reason that two points are required at the inlet section is because there exists an incoming wave (from the source) and a reflected wave. This reflected wave results from the geometry of the silencing element, (expansion in this case). For the *TL* calculation, we are only interested in the incoming waves. More specifically, the *TL* calculation compares the incoming sound pressure at the inlet section of the silencer to the transmitted sound pressure at the exit section. By solving the system of Eqs. (13) and (14), we can isolate this incoming pressure value and discard the reflected pressure value. After some manipulation, p_i is given by:

$$p_i = \frac{p_1 e^{-ikx_1} - p_2 e^{-ikx_2}}{e^{-i2kx_1} - e^{-i2kx_2}} \tag{15}$$

Note that the distances x_1 and x_2 are not critical (as discussed in §2.5.4), and that the equation can also be re-arranged so that only the measurement point spacing, x_{12} (i.e. $x_2 - x_1$) is required.

$$p_i = \frac{p_1 - p_2 e^{-ikx_{12}}}{1 - e^{-i2kx_{12}}} \tag{16}$$

Now that the incoming and exiting pressure values are known, the *TL* can be calculated simply as follows:

$$TL = 20 \log_{10} \left| \frac{p_i}{p_3} \right| \tag{17}$$

where:

p_3 = rms pressure at point 3.

The pressure at point 3 can be read directly since the termination at the exit is given the characteristic impedance ($z = \rho c$). This means that there are no reflected waves and thus the pressure at point 3 consists only of the transmitted waves.

As noted in the 4-pole method section, the calculated pressures will be complex. For the most accurate results, these numbers MUST be kept complex until

the final *TL* calculation. This will ensure that phase information is not lost, as would be the case if the complex values were converted to absolute values.

Essentially the 3-point method is just as accurate as the *traditional* and 4-pole methods, and can be implemented in a numerical scheme faster and easier. After much testing and comparing, the 3-point method was finally chosen as the method for use with the rest of the research work.

2.4 Numerical Techniques

Each of the various calculation methods can be implemented with one of two fundamental numerical techniques. The Finite Element Method (FEM) and Boundary Element Method (BEM) are widely used for various engineering problems, and can each be applied to acoustical concerns.

2.4.1 Finite Element Method

As its name implies, the FEM divides the modeled region into many discrete finite elements. This means that, for 2-dimensional systems, the entire area is considered and for 3-dimensional systems, the entire volume is considered. Fig. 6 contains an example of an expansion chamber silencer which has been discretized in a FEM mesh.

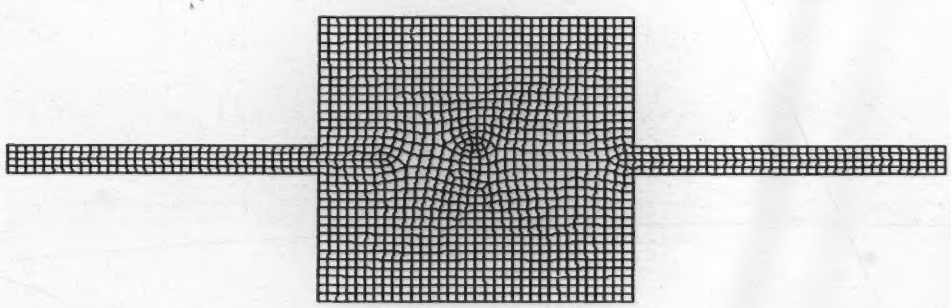

Figure 6. Finite Element Method Discretization of an Expansion Chamber Silencer

The acoustic wave equation is then solved in each of these smaller regions based on information from the neighboring regions. The FEM is primarily used when only the interior acoustic field of the silencer is to be computed. Solving purely exterior problems, or coupled interior-exterior problems with the FEM, requires large domains to be modeled with approximate terminating boundary conditions. Alternatively, infinite elements, like the wave envelope method proposed by Fyfe and Cremers [27] can be used in these situations. Both strategies require extensive convergence testing to be trusted. In other words, to implement this method, the outside regions of the silencer must be modeled, which is quite difficult to do with the FEM. For these reasons, the current FEM is not well suited for Insertion Loss calculations and should be restricted to Transmission Loss calculations.

In order to perform the Transmission Loss calculations, the desired region is divided up into a grid of nodes and elements. The fundamental theory behind FEM shows that each element interacts only with the elements directly adjacent to it. With wise node numbering, the result is a banded coefficient matrix for the resulting system of equations, which can be solved faster than a full coefficient matrix. The biggest advantage associated with the FEM is that, since the entire area is considered for calculation, there also exists the ability to assign different element types, and material properties (such as flow resistivity, porosity, density, and speed of sound) to different sections of the mesh (refer to Chapter 3). This is useful when trying to properly model absorptive materials because different sections of the mesh can be given different properties while still connected ("talking") to each other.

Refer to Appendix A for a 2-D acoustic FEM derivation, Appendix B for a 2-D acoustic element derivation, and Appendix C for a global stiffness matrix assembly example.

2.4.2 Boundary Element Method

Unlike the FEM, the BEM (based on Green's theorem) is only concerned with the boundary of the geometry in question. This means that only the perimeter of the area in 2-dimensions or the surface area of the volume in 3-dimensions is required. Fig. 7 illustrates a simple BEM model of an expansion chamber silencer. Each of the dots represents an element node, and the lines interconnecting the dots represent the elements themselves.

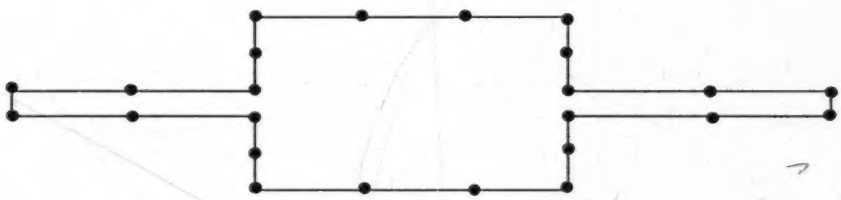

Figure 7. Example Boundary Element Mesh for Single Expansion Chamber

The biggest advantage of the BEM is that it can be used to compute the interior, exterior, or both fields simultaneously. It is for this reason that the BEM is best suited for *IL* calculations. The BEM only requires the perimeter of the silencer to be divided into nodes and elements and then solved. Also unlike the FEM, each node in the BEM mesh is inter-linked with every other node, which forms a full coefficient matrix. The system of equations is essentially the same as the FEM (i.e. Eq. 50 in Appendix A) but there are no zeros in the coefficient matrix. This greatly increases the computational time as the number of nodes increases. Finally, with regard to absorption, since elements exist as lines (or areas in the 3-dimensional models) only acoustical impedance values can be assigned to them. Bulk properties such as porosity and density cannot be applied in the BEM. It is for these reasons that the FEM is more appropriate for performing *TL* calculations, and was chosen for this work.

2.5 Comparison of Methods for Solution

Now that each of the different methods for solution have been defined, an in-depth comparison is required to support the decision to use the 3-point FEM as the method used for the remainder of the work.

2.5.1 2-Dimensional Expansion Chamber

In order to compare the virtues of the *traditional*, 4-pole and 3-point methods, with both the FEM and BEM, a single expansion chamber silencer was chosen. This particular system was chosen because the plane wave theoretical values for *TL* are well established and the geometry is relatively simple [1]. Fig. 8 shows the geometry of the modeled silencer (length of 1.2m and an expansion ratio of 5).

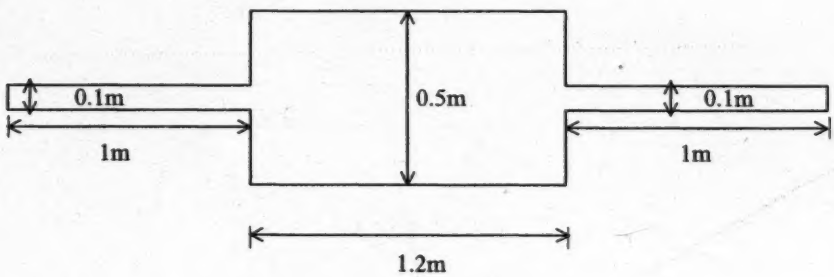

Figure 8. Single Expansion Chamber Dimensions

The theoretical *TL* curve can be calculated by [1]:

$$TL = 10\log_{10}\left[1+\frac{1}{4}\left(m-\frac{1}{m}\right)^2 \sin^2 kL\right], \ (dB) \tag{18}$$

where:

m = area ratio of inlet/outlet section to expansion chamber section

k = wave number (1/m)

L = expansion chamber length (m)

The FEM and BEM meshed models are similar to those represented in Figs. 6 and 7 respectively. Figs. 9a, 9b, and 9c illustrate the results obtained with the *traditional*, 4-pole and 3-point methods respectively for both FEM and BEM. It can be seen that the results for both the *traditional* and 3-point methods overlay each other exactly. The 4-pole FEM results match those of the other methods, and the 4-pole BEM results are also very close to the other BEM results. Note that all three methods follow the theoretical curve up until approximately 550 Hz. The reason the results start to diverge from theory at this point is a result of the assumptions used to derive Eq. (18). The derivation assumes that the sound waves are propagating in a planar fashion throughout the frequency range. This assumption becomes invalid at approximately the point when the sound wavelengths become smaller than the expansion chamber diameter. Once the wavelengths become too small (frequency becomes too large), the theoretical equation is no longer able to properly predict the performance of the system. Even though the theoretical curve is no longer valid after 550 Hz, it is still shown in each figure to illustrate how the numerical results are different from the theoretical beyond this point.

In terms of computational time required for solution, the 3-point method was noted to be generally faster than both the *traditional* and 4-pole methods. Again, this was mainly due to the fact that the 3-point method only required one computational "run" while the other two methods required two separate "runs". Also, the FEM was much faster than the BEM due to the fact that the BEM utilizes a full coefficient matrix when solving, while the FEM coefficient matrix is only partially populated. It should be noted that a comprehensive study regarding the time parameters was not completed for the paper and, as such, no specific time differences will be reported.

In terms of ease of use and adaptability, the differences between the 3-point method and 4-pole method were minor. The 3-point method was a little bit faster to modify and restart than the 4-pole method, however, compared to the overall computational times required, this difference was not an issue. It would be easy to automate the system to make a change, perform the run, record the results, and then start over again. The *traditional* method, however, was much more cumbersome to use due to the fact that two separate geometries were required (one for the straight

tube and one for the silenced section) and two separate FEM/BEM runs were required. An important note to make regarding the traditional method is with regards to the un-silenced geometry. This geometry is essentially a long, straight, unlined tube which has an induced particle velocity at one end and anechoic terminations at both ends. The acoustic response of this geometry is easy to solve using analytical methods, and therefore, the un-silenced FEM/BEM "runs" are not necessarily required. However, this only applies to simple geometric cases, and other more complicated geometries and operating conditions, may make an analytical solution more difficult than a numerical one. Therefore, the use of a numerical solution was employed throughout to handle all design cases.

Overall, the 3-point method was faster and somewhat easier to work with, from a programming standpoint, than the other two methods used. Also, the 3-point method can be implemented in a physical testing scheme much better than the 4-pole method (as seen in §5.3.1). The particle velocities required for the 4-pole method are difficult to measure, compared to the rms pressures required for the 3-point method.

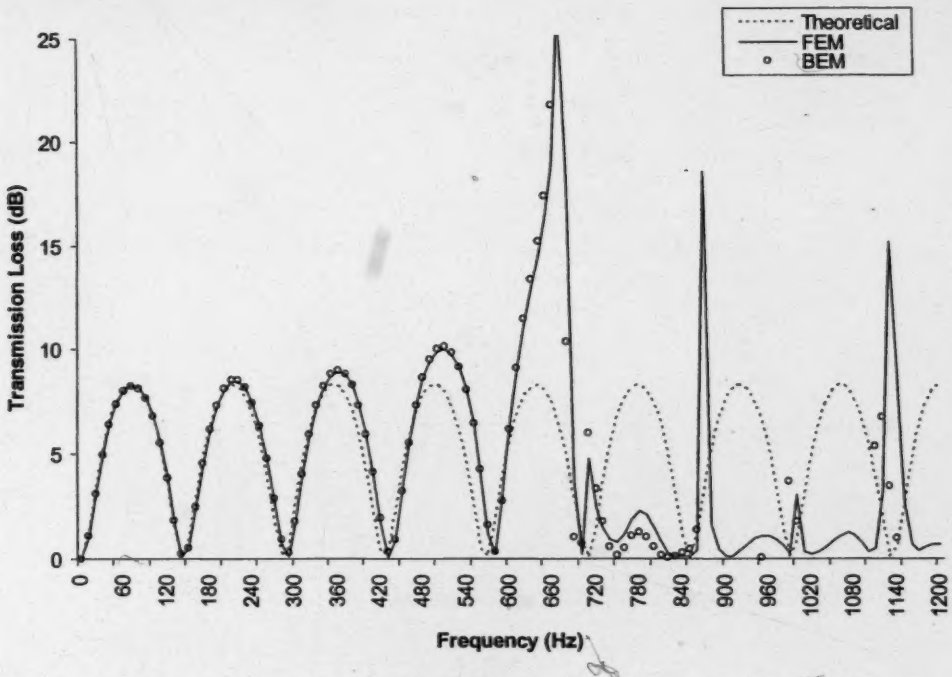

Figure 9a. Transmission Loss for Single Expansion Chamber with *Traditional* Method

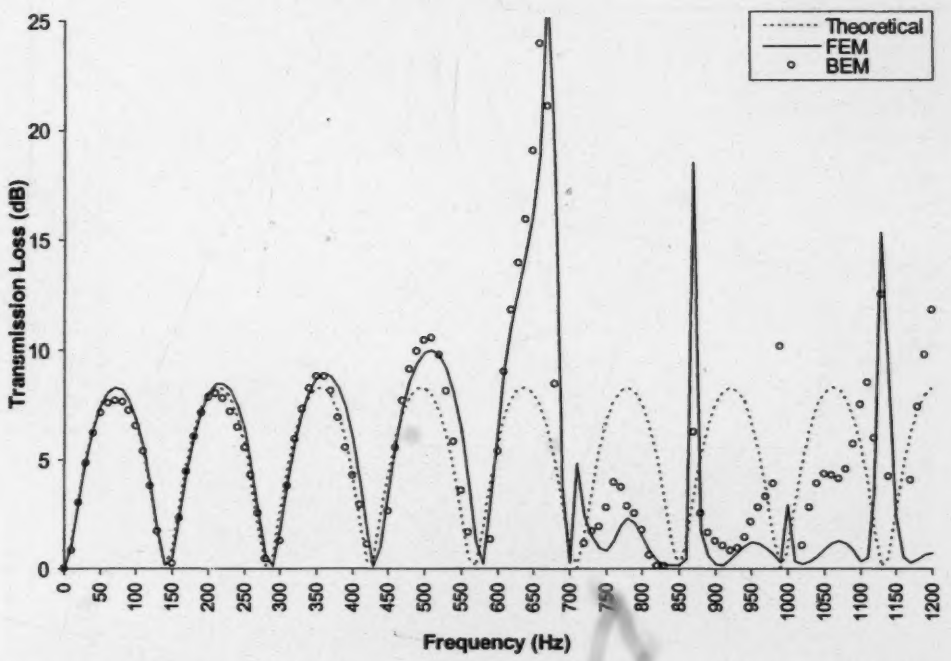

Figure 9b. Transmission Loss for Single Expansion Chamber with 4-pole Method

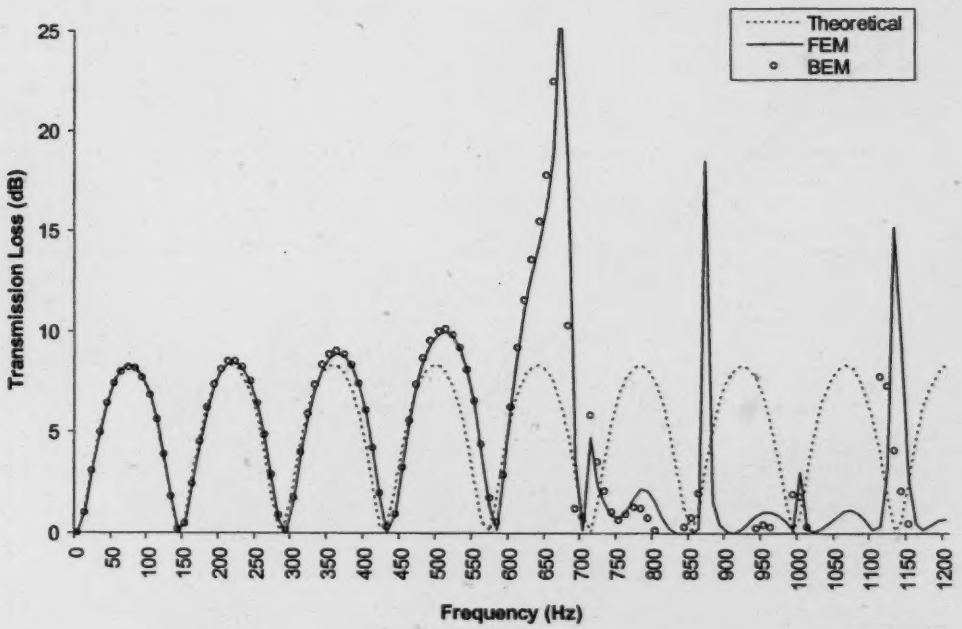

Figure 9c. Transmission Loss for Single Expansion Chamber with 3-point Method

2.5.2 3-Dimensional Expansion Chamber

To further verify the accuracy and viability of the 3-point method, a comparison was performed with actual measured data from a three-dimensional, round, single expansion chamber silencer as shown in Fig. 10. The *TL* results were measured and modeled for the case of just the expansion chamber and for the case of the expansion chamber with a 10cm stinger (quarter wave tube resonator) inserted into the exit side. The results are shown in Figs. 11a and 11b for the cases of without and with the stinger respectively. Note that for Fig 11b, the *TL* results for the expansion chamber alone were subtracted from the *TL* results for the chamber and stinger, resulting in the *TL* effect of the stinger alone. It can be seen that the results matched very well in both cases.

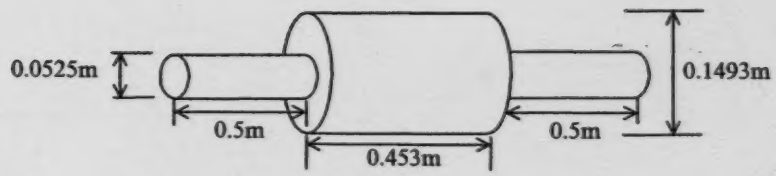

Figure 10. Full Three Dimensional Expansion Chamber Dimensions

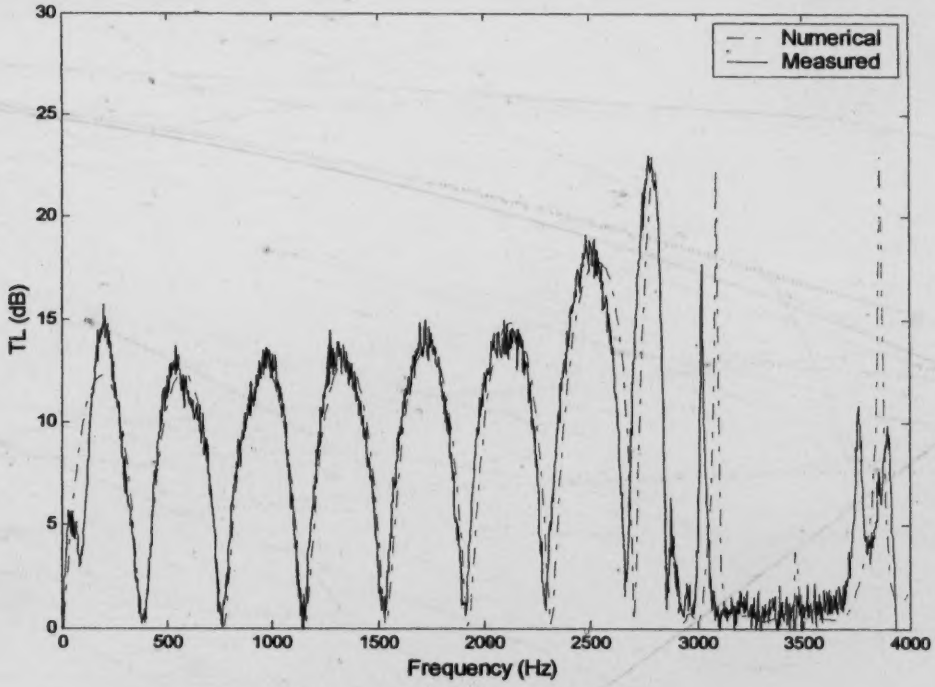

Figure 11a. *TL* Response of 3-D Expansion Chamber

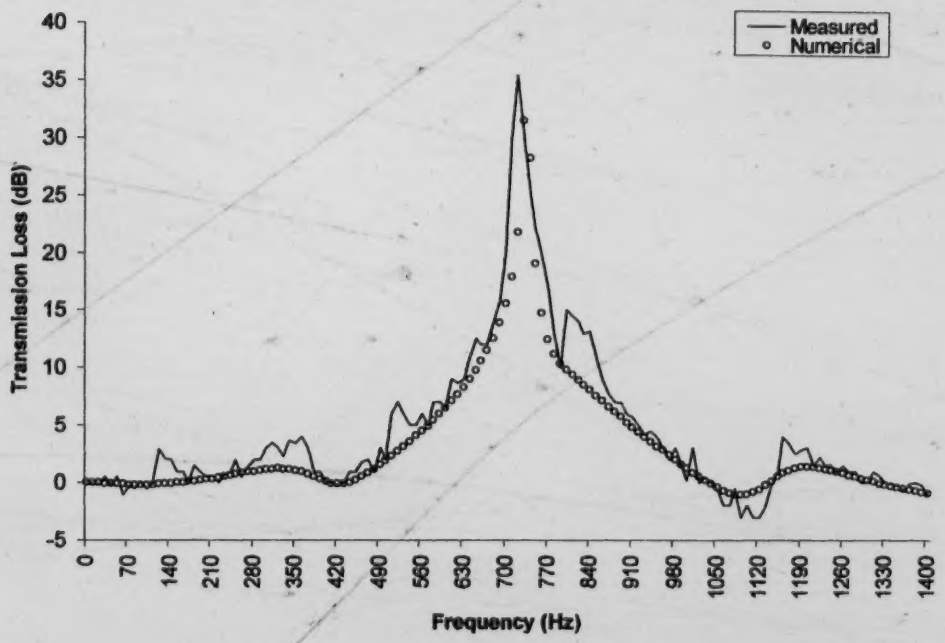

Figure 11b. *TL* Response of 10cm Stinger in 3-D Expansion Chamber

2.5.3 Helmholtz Resonator Example

One final design that was modeled was that of a simple Helmholtz resonator. Again, the theory behind the response of such geometry is well established [1] and, therefore, lends itself quite well to comparison. The resonant frequency (frequency of greatest attenuation) for a simple Helmholtz resonator is given by:

$$f_r = \frac{c}{2\pi}\sqrt{\frac{A}{LV}} \tag{19}$$

where:

c = speed of sound of the medium (m/s)
A = cross sectional area of the *neck* of the side branch (m^2)
L = effective length of the *neck* = Length + $0.8\sqrt{A}$ (m)
V = volume of the cavity (m^3)

Equation (19) shows that the TL of a single Helmholtz resonator should peak at one specific frequency and then decrease sharply on either side back down to zero. In the case of the geometry shown in Fig. 12, the theoretical frequency of maximum TL should occur at 201.7 Hz.

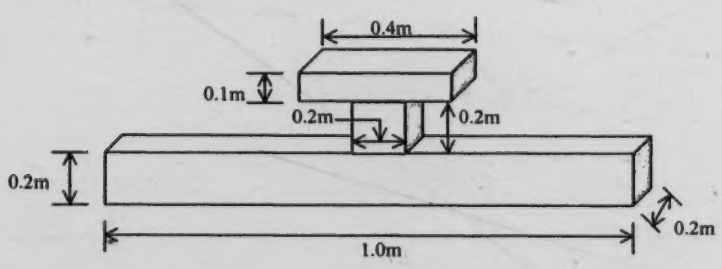

Figure 12. Three Dimensional Helmholtz Resonator

Fig. 13 shows the response of the two-dimensional model. Again, it is apparent that the 3-point method modeled the system very well compared to the theoretical values. Both two-dimensional and three-dimensional models were evaluated and found to match each other within numerical and experimental accuracies.

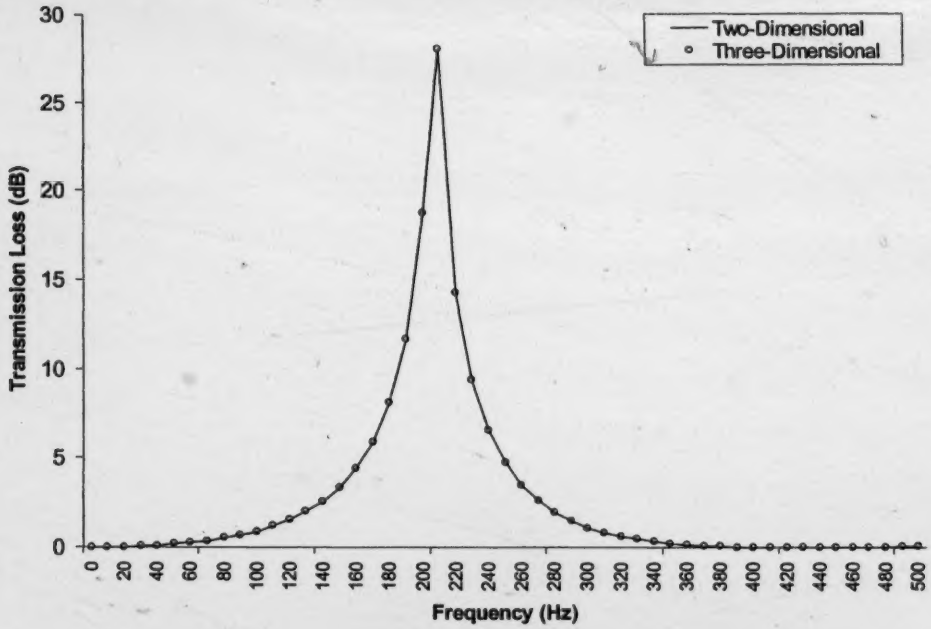

Figure 13. Three Dimensional Helmholtz Resonator Modeled *TL*

2.5.4 Problems/Idiosyncrasies Encountered

For all three methods there were a few interesting idiosyncrasies associated that are worth mentioning. For example, for each method, varying the length of the inlet and outlet sections of the silencer (varying inlet/outlet lengths from 10% of silencer length to 200% of silencer length) had a very little effect on the calculated *TL*. Only at a few frequencies were any differences realized, and the largest of these differences was never more than 0.5dB. In terms of time, shorter inlet and outlet sections required fewer elements for the mesh. Therefore, it would be advantageous to make the inlet and outlet sections shorter if for no other reason than to save computational effort and time. Through much testing, an inlet/outlet length of 10% of the silencer length was found to be an acceptable minimum length.

The derivations for all three methods evaluated assume plane wave behavior at the inlet and exhaust sections. This is only valid for frequencies up to the point where higher order modes begin to propagate. Beyond this range, the numerical

results become increasingly dependent on the choice of measurement location. This was noticed in numerical models as well as in physical system testing. Numerical and physical testing indicates that differences arising from this phenomenon are small compared to the TL values obtained. A more detailed analysis of these differences is presented in §5.3.3.

With the *traditional* method, the main concern was with reflections from the source side of the geometry. Some of the sound was reflected from the expansion chamber, back to the source, and then reflected from the source back to the expansion chamber. This set up a standing wave that was not realized when the straight tube (with the characteristic impedance at the outlet) was used. When the post silencer measurement, p_t, was taken, this standing wave was present. This resulted in a very large effect on the overall *TL* results (to the point where they were completely different from theoretical). As mentioned before, the way to eliminate this was to simply model the inlet face with a unit amplitude of vibration and to give it the characteristic impedance so that all of the waves reflecting towards it were absorbed and a standing wave was not formed. In actual tests, the way to prevent the formation of standing waves was to install light sound absorbing fibrous material in between the source and the first measurement point, as well as in between the last measurement point and the termination, so that the effects of reflected waves could be greatly reduced.

With regard to the 3-point method, the most important area for concern was the use of complex numbers in the calculation (as mentioned previously). When the pressures were converted into absolute values (or measured as absolute values with a real time analyzer or single channel FFT analyzer) there were differences with the *TL* values calculated. With a purely reactive silencer, these differences were small, however with absorption included in the model, the differences were larger. Figs. 14 and 15 show the *TL* results using complex and absolute values in the calculation for a modeled reactive silencer and absorptive silencer respectively. Fig. 14 shows a modeled simple expansion chamber, while Fig. 15 shows the results with a measured parallel baffle silencer with the *TL* calculated from absolute values of the 3-point method compared to the *TL* calculated using the *traditional* method (taken as the

correct values). Note that the differences between the complex and absolute pressure values are small, however, the more accurate results were obtained with the complex values.

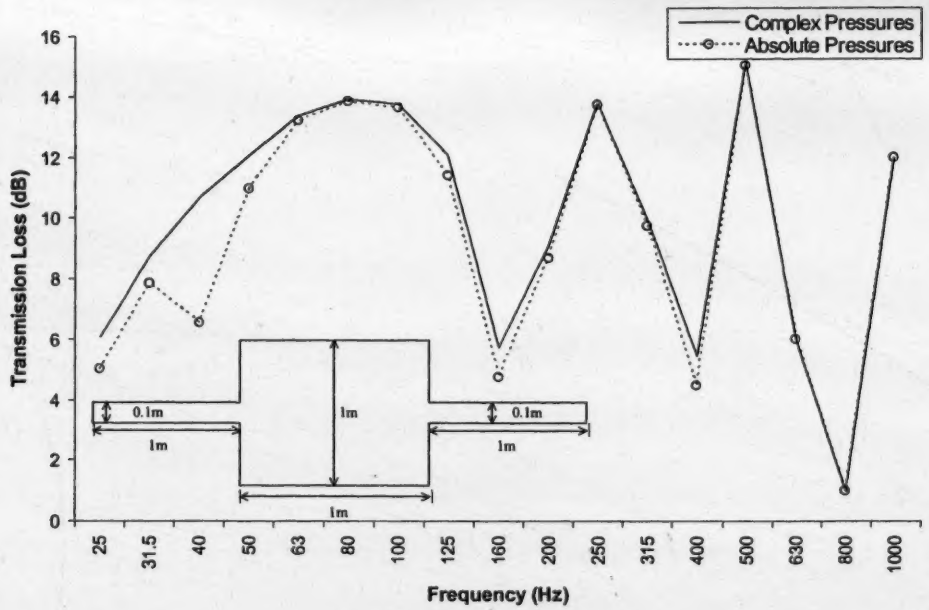

Figure 14. *TL* Response of Expansion Chamber Using Complex and Absolute Values

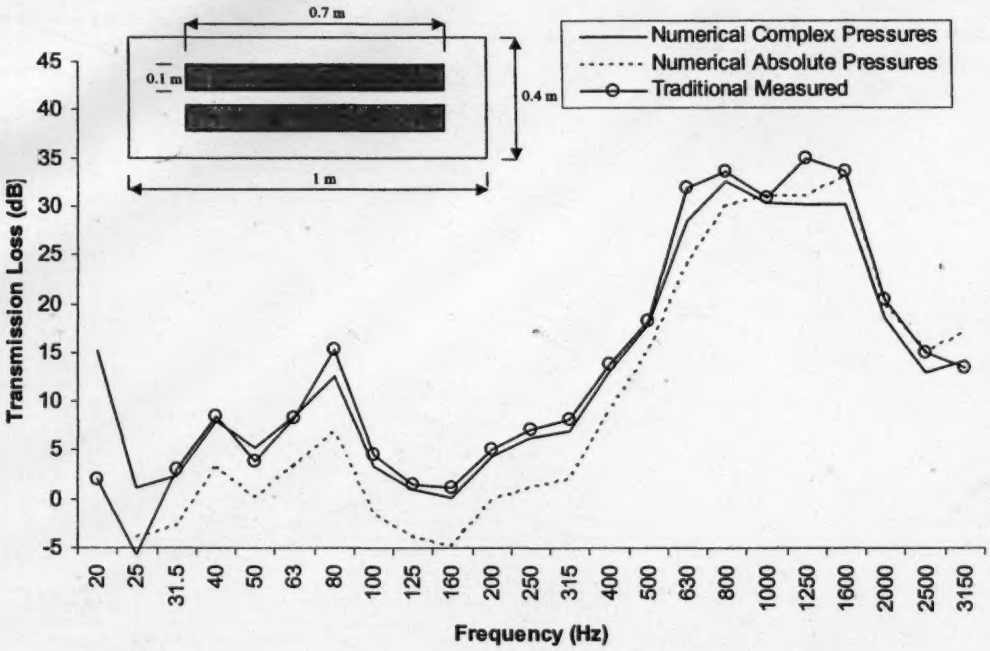

Figure 15. Numerical *TL* Response of Parallel Baffle Silencer with Complex and Absolute Values and Measured *TL* with *traditional* method

2.6 Conclusions

There are several evaluation criteria and solution methods to predict the performance of acoustical silencers. Due to the reflection influences measured by Noise Reduction, and the difficulty associated with obtaining Insertion Loss, Transmission Loss was chosen as the criteria which would be used for the measurements and numerical predictions. After much testing and comparison, the FEM was chosen as the numerical scheme. The FEM is faster than the BEM, and has the ability to incorporate bulk sound absorbing materials. Finally, the 3-point method was chosen over the *traditional* and 4-pole methods because it was easier to use and faster to implement. Also, the numerical results obtained by the 3-point method can be directly compared to those measured from a physical model, as opposed to the 4-pole results which are much more difficult to obtain from a physical model. The 3-point method was used to model several different types of reactive silencers with

varying geometries. Simple expansion chambers, stingers, and Helmholtz resonators were modeled and found to match very well with theoretical and measured results.

Based on the results obtained in this chapter, the 3-point FEM will be the method used to calculate the *TL* for the remainder of the Thesis.

3 Sound Absorbing Materials

3.1 Introduction

In addition to the noise reduction realized by simple reactive silencers, various sound absorptive materials can be used to gain further attenuation. In many situations, where the mechanical effects of the silencer on the system are critical (refer to §6.4), sound absorbing materials are used instead of reactive elements because of the reduced pressure drop.

This chapter discusses some of the various bulk material properties associated with sound absorbing materials, and how they are obtained. Numerical and physical results obtained in an acoustical impedance tube are compared, and an extensive list of results obtained for various sound absorbing materials is presented.

3.2 Bulk Material Properties

Materials absorb sound by two primary phenomena. At high frequencies, absorption involves an adiabatic (high frequencies) and isothermal (low frequencies) heat transfer in the interstices of the material due to the gaseous expansions and rarefactions along the pore edges and in the voids themselves [16]. The second method for absorption occurs at low frequencies in which the vibration of the fibers causes fiber bending and fiber-to-fiber rubbing. Both of the above operations essentially change the acoustical wave energy into heat. It is in this transfer where the sound wave loses energy and becomes "attenuated".

Most sound absorbing materials are composed of some sort of foam or fiber material. Typical materials are fiberglass insulation (both soft and rigid), cotton and woolen materials (such as fabrics, carpets, upholstery, and curtains), and steel wool and ceramic meshes (used in high temperature exhaust silencers). All of these materials can be characterized by their bulk acoustic material properties. These include flow resistivity (R), porosity (Ω), and structural factor (K_s).

3.2.1 Flow Resistivity

The flow resistivity, R, is defined as the specific flow resistance per unit thickness [16]. As its name implies, it is essentially the measure of the resistance of the material to having a fluid flowing through it. Mathematically it is defined as:

$$R = -\frac{t S \Delta p}{V \Delta x} \qquad \text{(mks rayls/m)} \qquad (20)$$

where:

t = time period for test (s)

S = face area for specimen (m^2)

V = volume of air passing through specimen (m^3)

Δx = thickness of specimen (m)

Δp = static pressure difference across specimen (Pa)

The ASTM C 522-87 standard illustrates one way to measure the flow resistivity [8]. The test involves placing a specimen of known thickness in a tube, shown in Fig. 16, which is connected to a supply air source. The air is turned on and the volume flow rate and pressure difference (across the material) are measured. Using Eq. (20), the specific flow resistivity can then be calculated.

The accuracy of the flow resistivity measurement apparatus was verified by using an ASTM round robin test sample [28]. The round robin results for the test sample averaged approximately 44,000 mks rayls/m, while the value obtained in the measurement apparatus was 44,829 mks rayls/m with a standard deviation of only 3048 mks rayls/m. In addition, results obtained from various materials matched what would intuitively be expected based on density and thickness. These results indicated that the measurement apparatus was quite accurate and repeatable (based on the standard deviations obtained) as long as it was used within the flow parameters outlined in the ASTM standard. These parameters state a normal flow velocity of 0.5 to 50 mm/s, a pressure drop across the specimen of 0.1 to 250 Pa, and a flow resistivity ranging from 100 to 10,000 mks rayls (note the units are mks rayls, not mks rayls/m as commonly used).

Flow resistivity values for most sound absorbing materials range between 5,000-60,000 mks rayls/m, although some materials, such as acoustical ceiling tiles, can have much higher values. Typically, higher flow resistivity values result in greater sound absorption. This starts to work in a negative way when the material becomes so dense, that it becomes a reflector rather than an absorber (the range for this is also dependent on the porosity and structural factor).

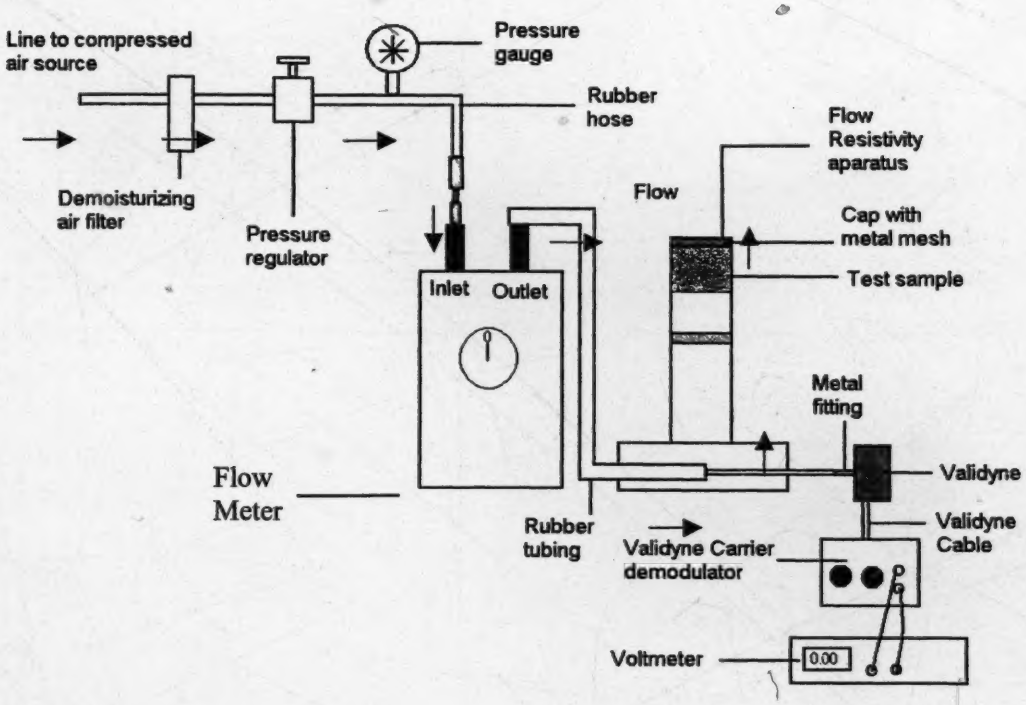

Figure 16. Flow Resistivity Measurement Apparatus

3.2.2 Porosity

The porosity of the material, Ω, is defined as the ratio of the volume of the pores or voids, V_v, on the material to the total volume, V_t [16].

$$\Omega = \frac{V_v}{V_t} = 1 - \frac{\rho_a}{\rho_f} \tag{21}$$

where:

ρ_a = average bulk density of the porous material (kg/m^3)

ρ_f = density of the fibers (kg/m^3)

The porosity is, therefore, a positive number smaller than or equal to 1, with 1 being for open air and 0 being for a completely solid material.

One method to determine the porosity of a material involves using a water column apparatus and an equation derived from Boyle's law [7]. Fig. 17 shows the apparatus used. By changing the height of the left capillary tube, the values of h_1 and h_2 can be determined. The volume of voids in the specimen, V_v, can be calculated by [7]:

$$V_v = \left\{\left(1 + \frac{P_1}{h_2 - h_1}\right) \times (A_t h_1) - (A_t l_a + V_{cn})\right\} \tag{22}$$

where:

P_1 = atmospheric pressure (mm H_2O)

h_1 = difference in water height, on specimen side, from rest position to new position after left capillary tube has been raised (mm)

h_2 = difference in water height, on capillary tube side, from rest position to new position after left capillary tube has been raised (mm)

A_t = cross sectional area of inside of tube (mm^2)

l_a = length of excess air in tube between water and specimen (mm)

V_{cn} = corrected volume is the amount of air above specimen including air trapped in valve (mm^3)

V_v can then be used in Eq. (21) to calculate the porosity.

The porosity measurement apparatus was calibrated by placing a solid metal piece of known volume inside the test section. The porosity of this solid piece and open volume was measured and compared to the porosity calculated from the two known volumes. Based on the volume of the solid block, and the total volume of the test chamber, the porosity was calculated to be 0.832. The value obtained using the apparatus was 0.827 with a standard deviation of 0.025. In addition, similar to the flow resistivity apparatus, the results obtained from various materials matched the intuitively expected values, and the measurements were very repeatable (based on the small standard deviations obtained).

Note: The left capillary tube is shown raised

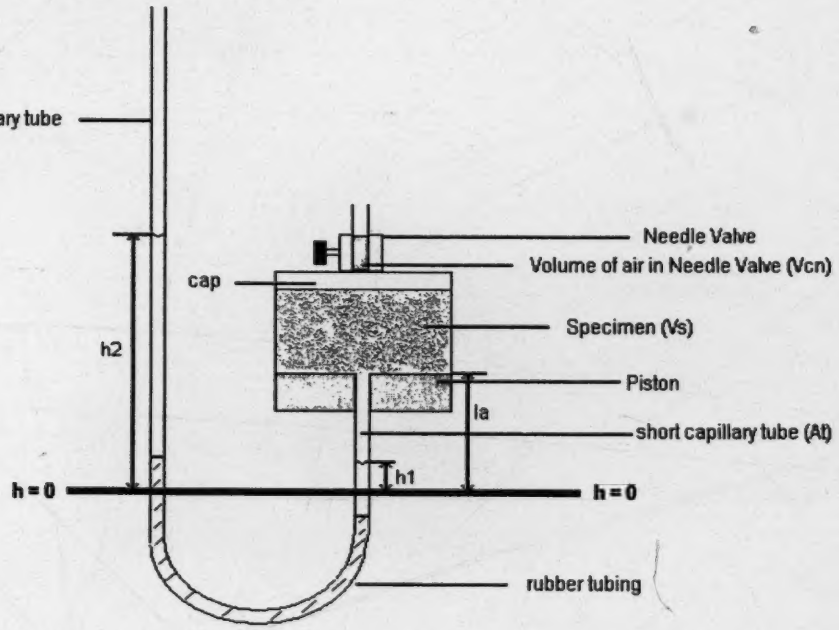

Figure 17. Porosity Measurement Apparatus

3.2.3 Structural Factor

The structural factor, K_s, is a value that takes into consideration the pores and cavities that are perpendicular to the propagation direction of the traveling wave and their effect on the acoustical behavior of the material [16]. Typically the values range between 1 and 1.3, with 1 having no effect on the calculations. According to Beranek, the structural factor could be basically thought of as an empirical multiplication factor to take into account those parameters that the other material properties do not. It can be calculated by the following formula:

$$K_s = \Omega^2 \,\mathrm{Re}\left\{\left(\frac{Z_a}{Z_o}\right)^2\right\} \quad (\textit{unitless}) \tag{23}$$

where:

Ω = Porosity

Z_a = The complex characteristic impedance of the material ($kg/m^2 \cdot s$)

Z_o = The characteristic impedance of the gas in the voids between fibers ($kg/m^2 \cdot s$)

It was found, however, that the value for structural factor was better determined through a systematic approach of convergence testing (refer to §3.4.2). By this, the structural factor did indeed act as a correction factor to bring the numerical results even closer to the measured results. This is also advantageous if one does not have the means to acquire the complex impedance of the material.

3.2.4 Bulk Material Results

Various materials were tested and values for flow resistivity, porosity, and structural factor were obtained for each. Table 1 displays the results obtained for the different materials. It can be seen that, in general, as the flow resistivity increases, the porosity decreases and vice versa. This is intuitively expected since a decrease in porosity means that the material's density is increasing, which would make it more difficult for fluid to flow through it.

Table 1. Bulk Acoustical Properties of Various Sound Absorbing Materials

Material	Thickness (mm)	Resistivity (mks rayls/m)	Porosity	Structural Factor
Green Fiberglass (mineral rock)	49	70137	0.807	2.0
Yellow Fiberglass (Fiberglass Canada Inc.)	73	14371	0.827	1.2
Pink Fiberglass R-12 (Owens Corning)	80	7484	0.846	1.1
Permacote Linacoustic Grey Foam	25	13159	0.627	1.6
ASTM E 1050-98 Round Robin Sample	25	44829	0.694	2.5
MANVILLE 814 Spin-glass, plain	34	21939	0.794	1.4
ARMSTRONG mineral fibre SA 1589 9-81 J	18	387417	0.809	4.0
Kaowool Ceramic Fiber (2300F)	50	64787	0.786	2.0
Kaowool Ceramic Fiber (2600F)	50	105614	0.799	2.0
2.68 PCF Whispertone Wallboard (Schuller)	36	19378	0.858	1.3
3.0 PCF Whispertone Wallboard (Schuller)	25	20058	0.824	1.6
4.0 PCF Whispertone Wallboard (Schuller)	25	24992	0.808	1.8
1 layer 6 PCF Whispertone Wallboard (Schuller)	25	65381	0.829	2.0
2 layers 6 PCF Whispertone Wallboard (Schuller)	49	60105	0.829	2.0
3 layers 6 PCF Whispertone Wallboard (Schuller)	73	59964	0.829	2.5

3.3 Sound Absorbing Materials in a Numerical Model

Once the various bulk material parameters are known, they can be included in the numerical model. Refer to Appendix D for a full derivation of how the material properties can be included, along with the assumptions involved.

3.4 Impedance Tube Testing

In order to verify the ability of the numerical formulations to incorporate sound absorbing materials, an experiment was devised where results were obtained and compared for a physical model and an equivalent numerical model.

3.4.1 Theory

One way to characterize a sound absorbing material is by its absorption coefficient. The absorption coefficient (α) is defined as a ratio of the sound energy absorbed to the sound energy incident on the material [16]. For the purposes of this work, only the normal incidence absorption coefficient was explored. Further work could compare the numerical calculations of the random incidence absorption coefficient similar to that measured using ASTM C 423-00 [9].

One method for calculating the absorption coefficient is using an impedance tube and two microphones [10, 17, 29]. The apparatus, shown in Fig. 18, consists of a long tube with a sound source at one end, and the specimen at the other (backed by a hard reflective surface).

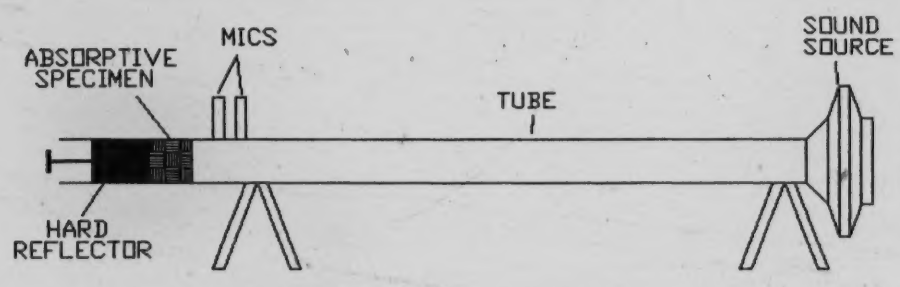

Figure 18. Impedance Tube Measurement Apparatus

The two microphones are placed in close proximity to each other and to the specimen at the outer edge of the tube. Using a dual channel simultaneous data acquisition system with FFT capabilities (such as an FFT analyzer), the cross power spectra, G_{12}, and the auto power spectra, G_{11}, can be measured, and the transfer function, H, can be calculated using:

$$H = \frac{G_{12}}{G_{11}} \tag{24}$$

Note that G_{11} and G_{12} are averaged quantities. Using H, the complex reflection coefficient can be calculated with [29]:

$$R = \left(\frac{H - e^{-jks}}{e^{jks} - H} \right) e^{j2k(l+s)} \tag{25}$$

where:

R = complex reflection coefficient

H = transfer function

k = wave number, $2\pi f/c$ (m^{-1})

s = center-to-center spacing of microphones (m)

l = distance from the test sample to the nearest microphone (m)

Once R is known, the absorption coefficient is calculated simply from:

$$\alpha = 1 - |R|^2 \tag{26}$$

It should be noted that once R is known, many other parameters (such as the normal specific acoustic impedance ratio) can be calculated. For the purposes of this Thesis, however, the calculations were limited to the absorption coefficient. Also note from Eqs. (25) and (26) that the absorption coefficient is frequency dependent, thus it is not just one specific value, rather a series of values over a wide frequency range.

3.4.2 Test Methods

The absorption coefficients were measured following the ASTM E 1050-98 standard [10]. The accuracy of the device was verified by checking the results of a closed cell foam material to the results of an ASTM round robin test for that exact material. The results of this test are shown in Fig. 19, with the accepted and measured curves shown. Each material was then measured several times to obtain an average value. Similar to the flow resistivity and porosity data, the absorption coefficients measured had a very low standard deviation associated with them.

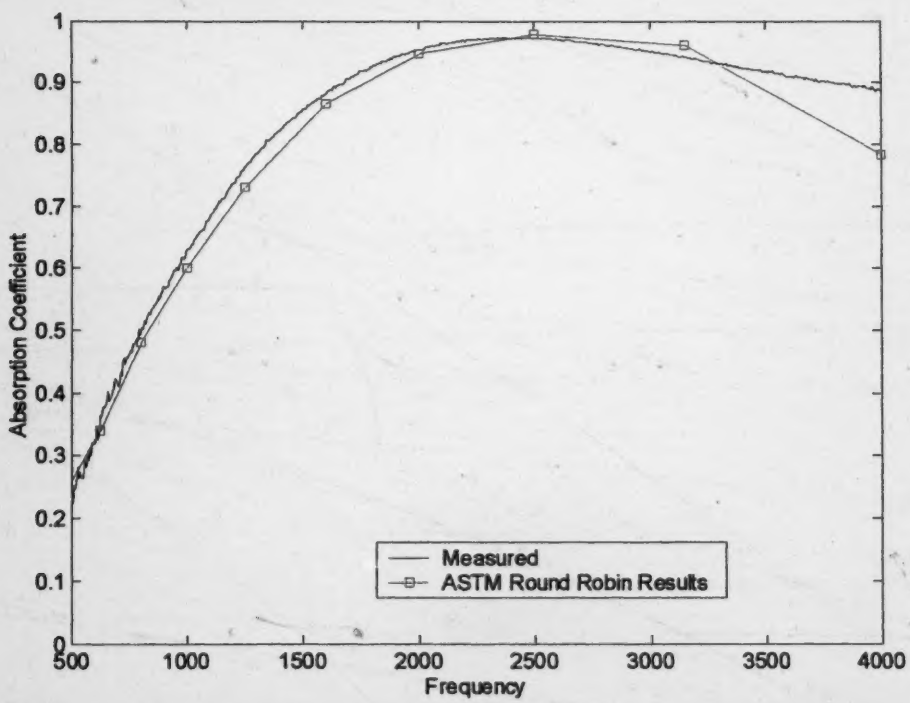

Figure 19. Impedance Tube Measurement Results for ASTM Round Robin Sample

All FEM calculations were performed using SYSNOISE [30]. To begin with, the geometry of the impedance tube was created using ANSYS [31] (to define the nodal coordinates and element connectivity). The geometry was then exported from ANSYS, and imported into SYSNOISE. Fig. 20 shows the meshed impedance tube geometry.

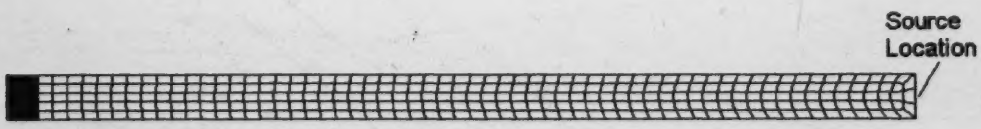

Figure 20. Numerical Model of Impedance Tube
(shaded region represents absorptive material)

Note that the geometry shown is equal to that of the physical model, but the length of the numerical model is not required to be equal to the length of the physical model. This is because only the normal impedance is modeled and the waves are assumed planar, therefore the distance between the vibration source and the absorptive material can be made much shorter in the numerical model (only a few elements in length) without affecting the results. This will save on solution time, however, the model was quite small to begin with so the time saved was not great. Next, the boundary conditions and material properties were assigned. The source section was given a uniform unit vibration velocity (to mimic a sound source), and all other surfaces were made acoustically "hard". Then elements in the test section (for the acoustic material to be tested) were given the flow resistivity and porosity values that were previously determined. Finally a structural factor of 1 was chosen as a start, and the value was slightly modified to obtain the closest possible match between the measured and numerical absorption coefficient curves.

3.4.3 Results

Once the model was solved and the absorption coefficients were calculated, at all of the frequencies of interest the results were compared to those obtained in the physical impedance tube. Based on the results, the structural factor was modified until the numerical curve came as close as possible to the measured curve. Fig. 21 and Fig. 22 show the final results obtained for a sample of the yellow fiberglass insulation and the ASTM round robin sample foam respectively. Note that the numerical curves follow the measured curves quite well and are within error over most of the useful range.

In order to obtain the errors associated with the numerical model, a sensitivity analysis was performed on the various parameters defining the absorptive material. Each parameter was looked at independently to see the effects of a large range of values.

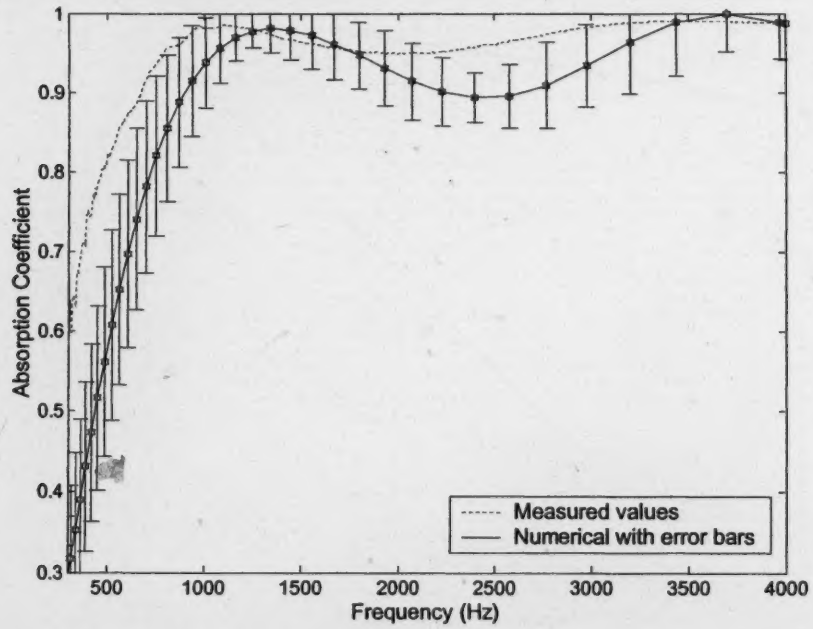

Figure 21. Measured and modeled absorption coefficients for yellow fiberglass material

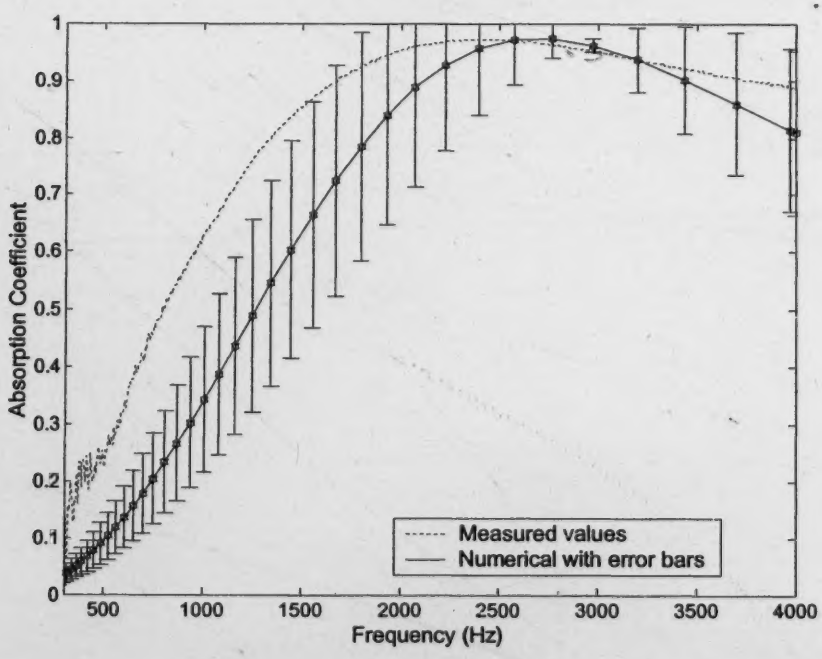

Figure 22. Measured and modeled absorption coefficients for ASTM round robin sample

3.4.3.1 Flow Resistivity

It was noticed that as the flow resistivity was increased, the absorption coefficient increased up to a certain point where the material became too dense and started acting as a reflector more than an absorber. The range where this phenomenon takes place is dependent on the other parameters. Also, as the flow resistivity increased, the differences in absorption coefficient values decreased, therefore the dependence on flow resistivity decreases as the values increase. Figure 23 shows the effects of varying the flow resistivity between ± one measured standard deviation for the yellow fiberglass specimen. It can be seen that the differences were small, mainly due to the small standard deviations associated with obtaining the flow resistivity values.

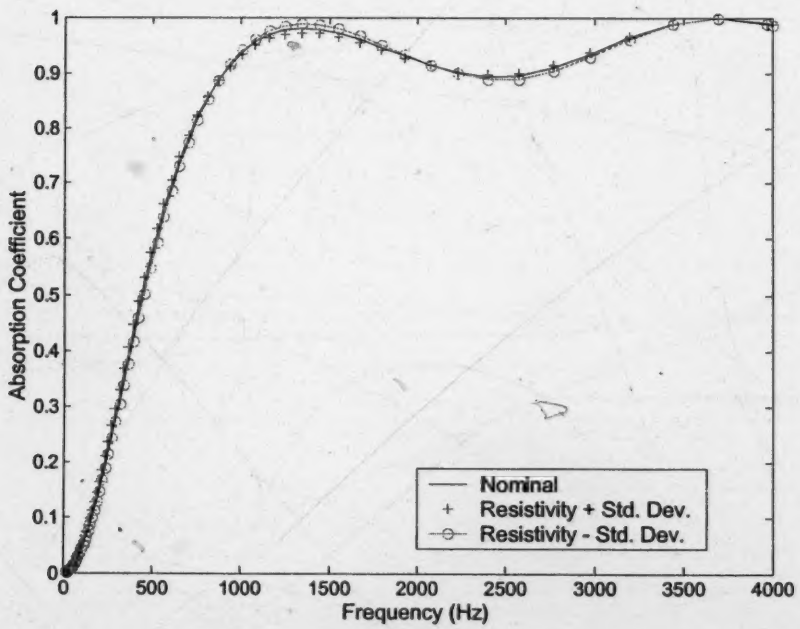

Figure 23. Modeled absorption coefficient of yellow fiberglass with varying resistivity values

3.4.3.2 Porosity

It was noticed that as the porosity decreased, the absorption coefficients decreased. This is due to the increased density of the material which resulted in the pores becoming more closed. Figure 24 shows the effects of varying the porosity values between ± one measured standard deviation for the yellow fiberglass specimen. It can be seen that the differences were small, mainly due to the small standard deviations associated with obtaining the porosity values.

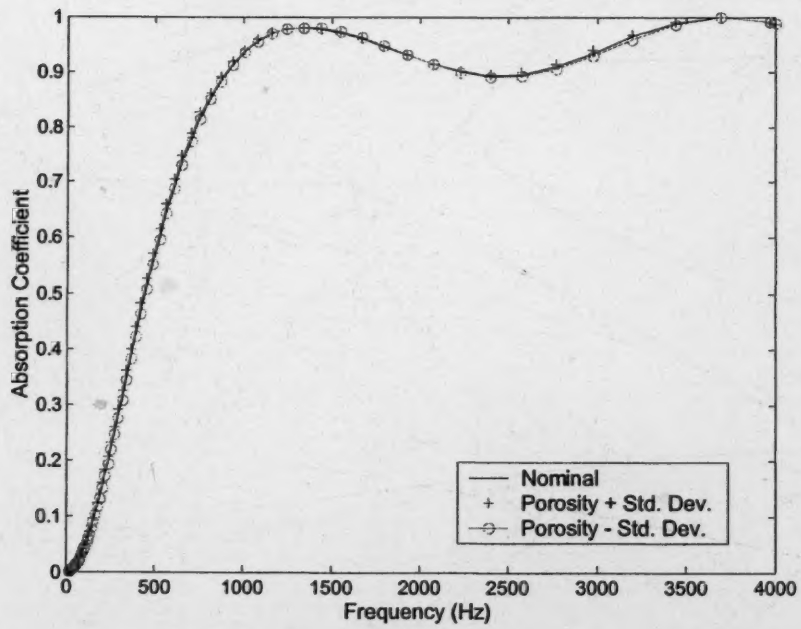

Figure 24. Modeled absorption coefficient of yellow fiberglass with varying porosity values

3.4.3.3 Structural Factor

It was noticed that as the structural factor increased, the absorption coefficient curve shifted to the left, and the number of oscillations in the curve increased until there was almost a sinusoidal pattern. It was observed that structural factor values beyond 1.3-1.5 resulted in very large differences between measured and numerical results. Figure 25 shows the effects of varying the structural factor between ± 10% for the yellow fiberglass specimen. This amount was chosen based on experience with the numerical models of the various samples. Note that small changes in structural factor resulted in small changes in the absorption coefficients.

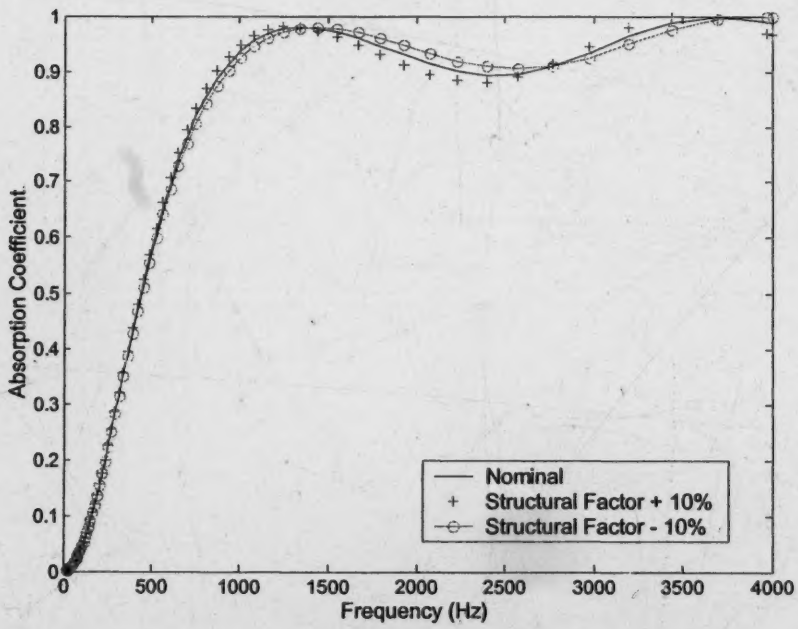

Figure 25. Modeled absorption coefficient of yellow fiberglass with varying structural factor values

3.4.3.4 Thickness

It was noticed that as the thickness of the material increased, the absorption coefficient increased, up to a point. Beyond this point, increasing the thickness did not result in an increase in the absorption coefficient values. This occurred because once the material has absorbed all it can, extra material will not absorb any more. As expected, this increase in absorption coefficient with increasing thickness occurred at the higher frequencies first, then filtered down to the lower frequencies as the thickness increased. Figure 26 shows the effects of varying the thickness between ± 10% for the yellow fiberglass specimen. Again this amount was chosen based on experience in using the actual impedance tube with the samples. Note that relatively small changes in thickness resulted in noticeable changes in the absorption coefficients obtained (the most noticeable changes of all of the parameters). This becomes important when considering the effects of modeling absorptive material in any situation. Thickness is a quantity that can vary from one installation to the next, and errors in measuring the thickness to include in the numerical model can cause noticeable errors.

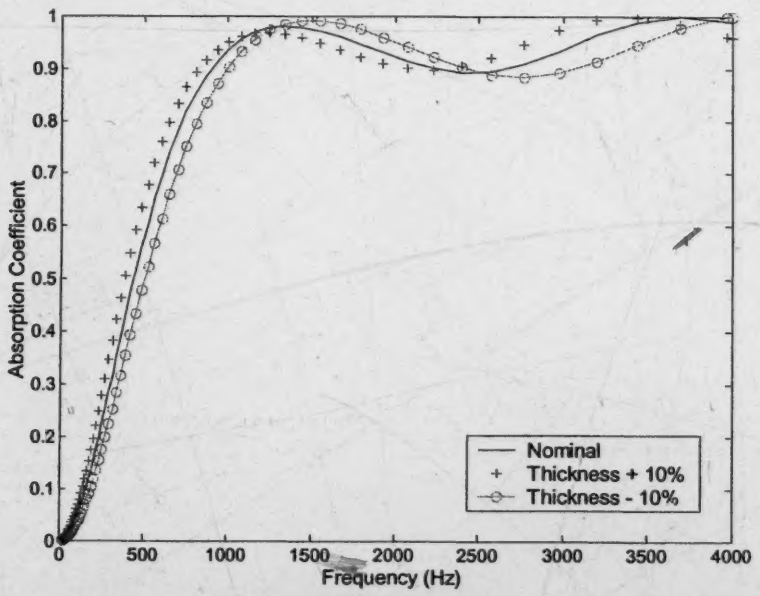

Figure 26. Modeled absorption coefficient of yellow fiberglass with varying thickness values

3.4.3.5 Various Materials

Figs. 27-31 display the measured and numerically calculated absorption coefficients for the various materials measured in the study and presented in Table 1. It can be seen that the results matched well for all materials tested. The only major exception was the Armstrong Mineral Fiber, which had a very high flow resistivity value (387,000 mks rayls/m), which essentially is beyond the generally acceptable limits of the flow resistivity test, and thus did not model well.

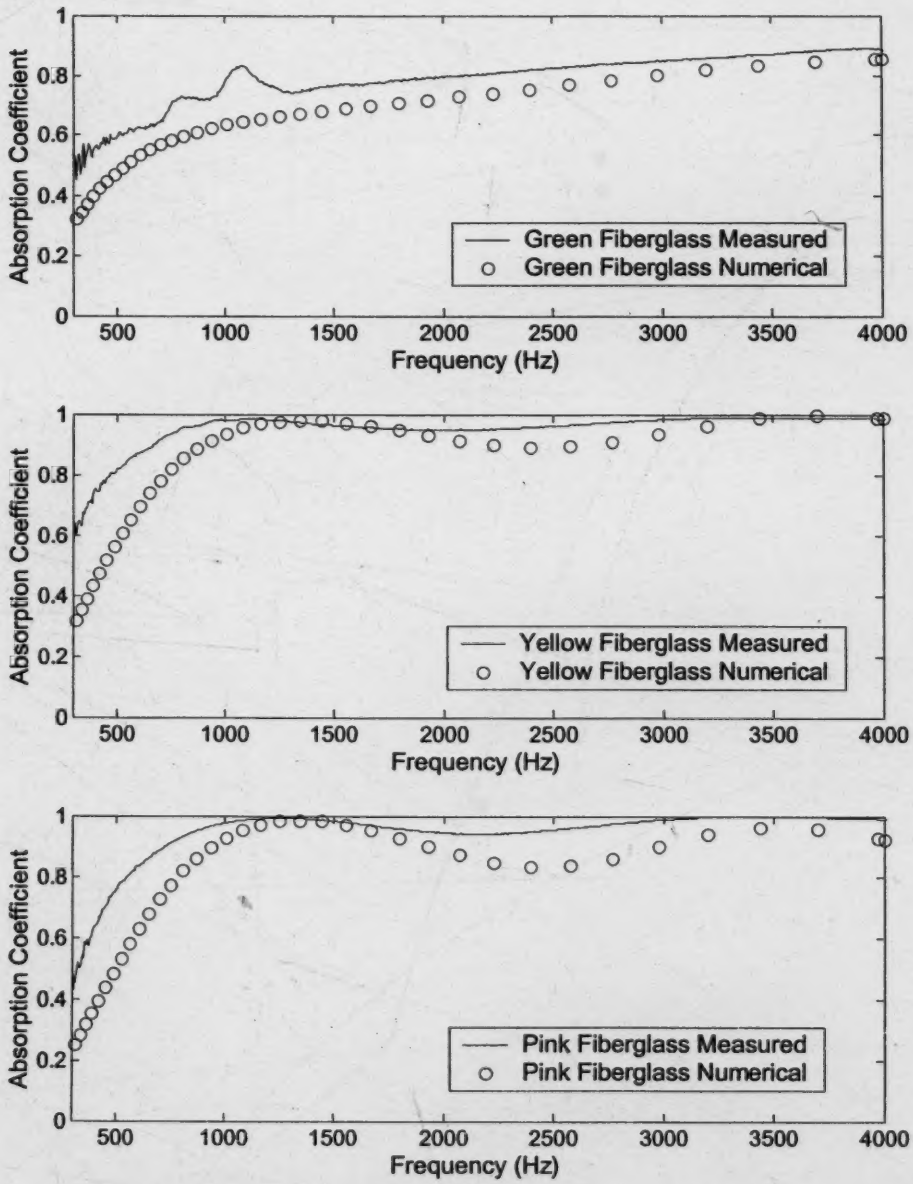

Figure 27. Measured and Modeled absorption coefficients of Green Fiberglass, Yellow Fiberglass, and Pink Fiberglass

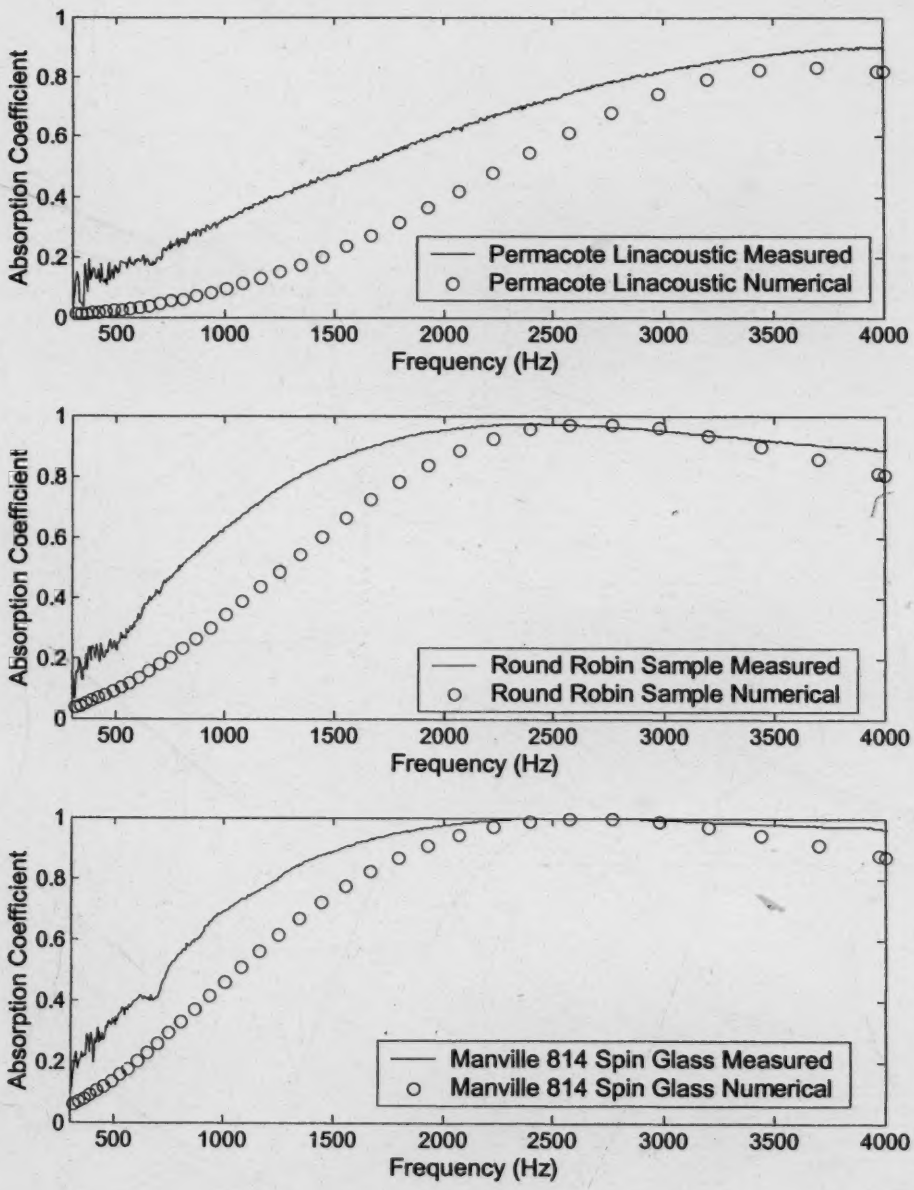

Figure 28. Measured and Modeled absorption coefficients of Permacote Grey Foam, ASTM Round Robin Sample, and Manville 814 Spin Glass

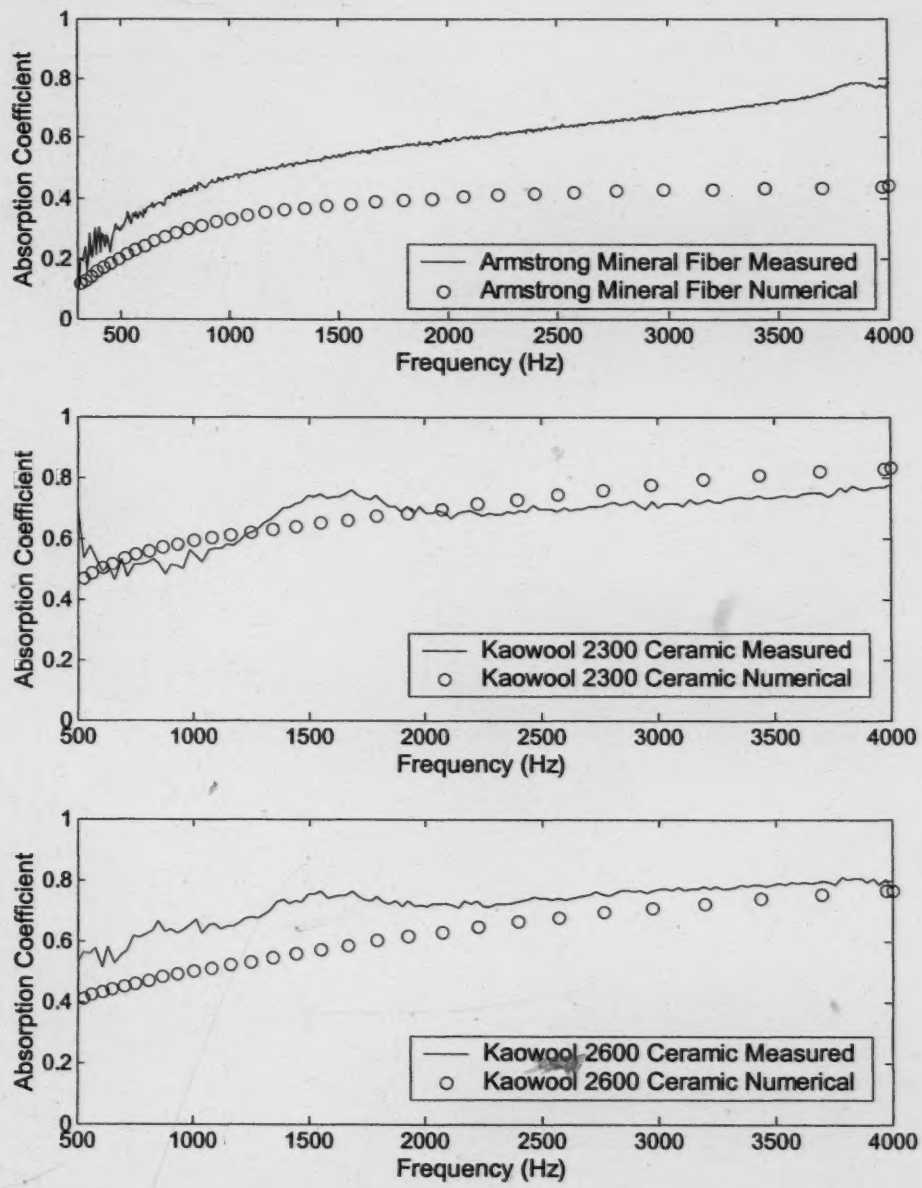

Figure 29. Measured and Modeled absorption coefficients of Armstrong Mineral Fiber, Kaowool 2300F Ceramic Fiber, and Kaowool 2600F Ceramic Fiber

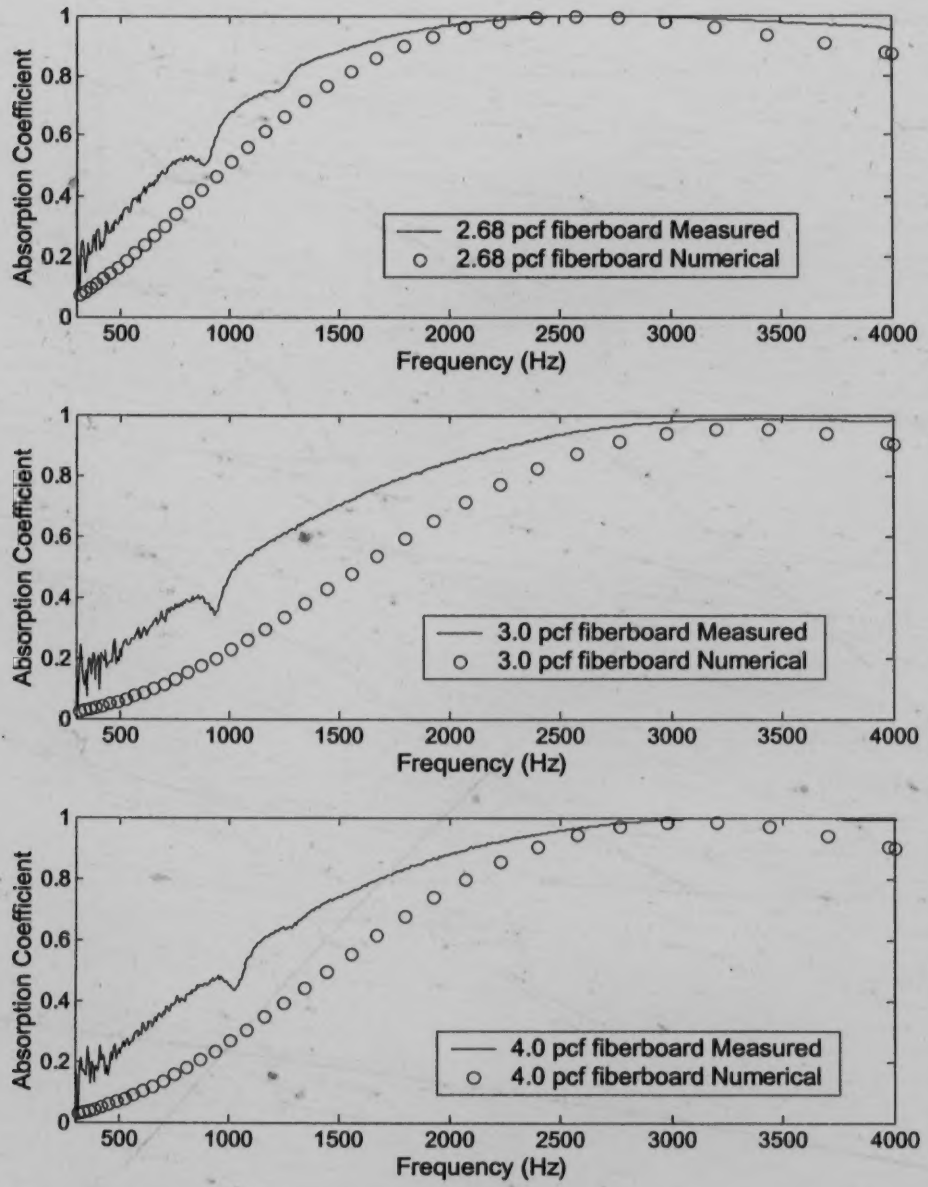

Figure 30. Measured and Modeled absorption coefficients of 2.68, 3.0 and 4.0 pcf Whispertone Wallboard.

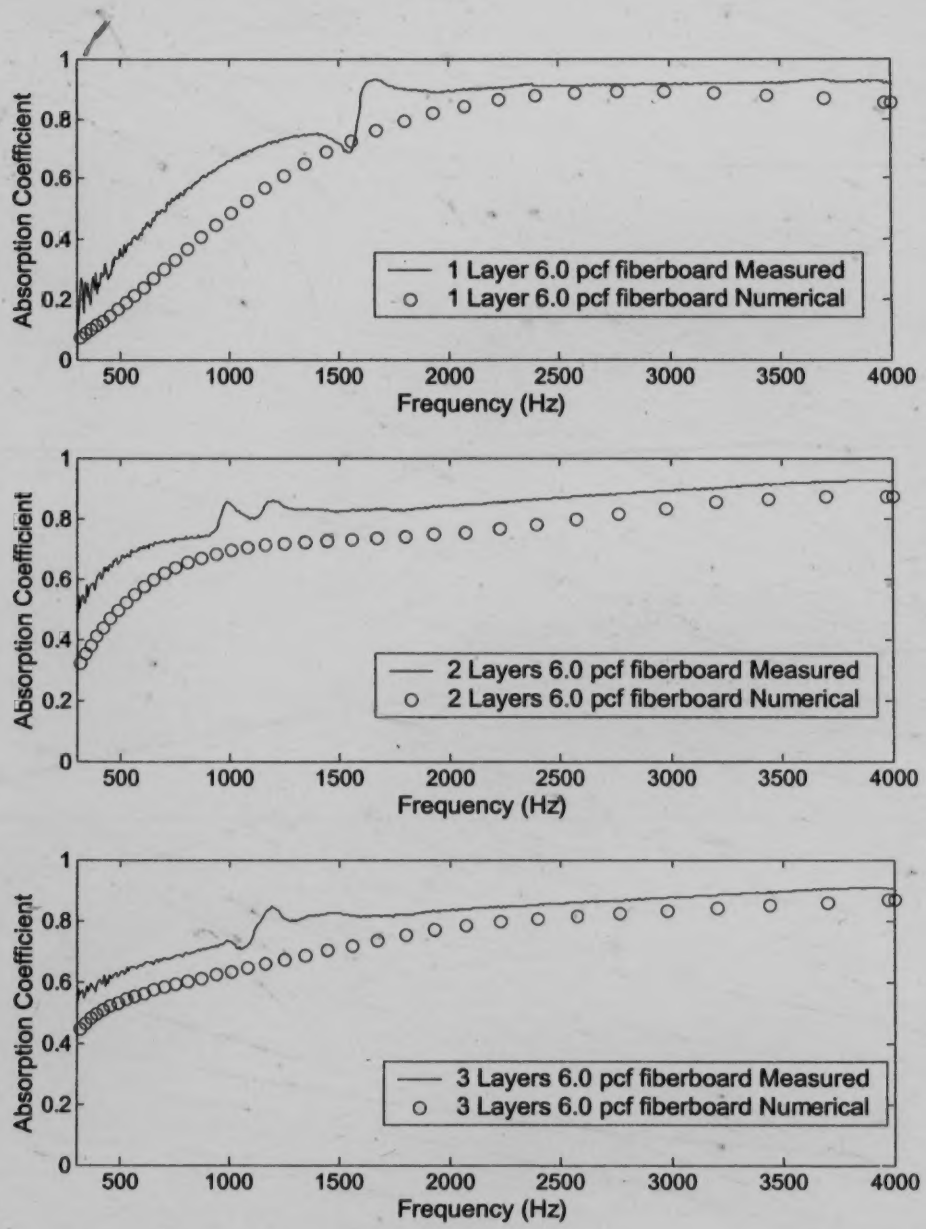
Absorption Coefficient
Frequency (Hz)
1 Layer 6.0 pcf fiberboard Measured
1 Layer 6.0 pcf fiberboard Numerical
2 Layers 6.0 pcf fiberboard Measured
2 Layers 6.0 pcf fiberboard Numerical
3 Layers 6.0 pcf fiberboard Measured
3 Layers 6.0 pcf fiberboard Numerical

Figure 31. Measured and Modeled absorption coefficients of 1, 2, and 3 layers of 6 pcf Whispertone Wallboard

It can be seen from Figs. 27-31 that the numerical results generally matched those obtained from the physical model. Differences between the two can be attributed to the assumptions made when deriving the numerical equations used, as outlined in Appendix D. These assumptions were made to simplify the geometry and the equations, but are not necessarily indicative of the physical system. For example, the assumptions that R is constant in all directions and that the solid is perfectly rigid and incompressible are not entirely correct, but these assumptions simplify things a great deal for the derivation. Also, the assumption that $\frac{\partial P}{\partial n} = 0$ at the boundary is only applicable for certain ideal situations and many circumstances (such as flow effects, and surface irregularities) exist where this assumption is not applicable. It is believed that the accuracy of the method is limited to the restrictions imposed due to these assumptions. In order to increase the ability of the numerical model to mimic the physical system, many of these assumptions will have to be removed or modified so that the equations can account for more complications than they currently are.

Having said all of this however, it is observed that the results are still very good, and the fact that the sound absorbing material cannot be modeled 100% accurately, should not be a deterrent for the rest of the work. The methods used for modeling the silencer systems as a whole are still valid, and a modified system for accounting for sound absorbing material could always be added in later.

3.5 Conclusions

The inclusion of sound absorbing materials in the numerical model is an important step in being able to predict the performance of parallel baffle, or lined duct silencer. The first step for including the materials in the numerical model was to identify the necessary bulk acoustic material properties, and the methods for obtaining their values. Once the flow resistivity, porosity, and structural factor are obtained, they can be included into the derived formulation and included into the model as an acoustic absorptive finite element. These elements can be coupled with the traditional acoustic finite elements derived in Chapter 2 to form the entire model for the acoustic system under investigation.

Numerical models of an acoustic impedance tube (used to obtain the normal incidence absorption coefficient, among other parameters), compared very well versus measured results. The results did not match exactly, which was noted to be attributed to the assumptions used to derive the acoustic material finite element. Again, the differences which arose were relatively small and have not deterred the work from continuing. Future updates to the formulations could be incorporated into the full models outlined in Chapter 5.

It is the opinion of the author that the more recent work mentioned in §1.4.2 could be utilized to improve the results of the numerical model. Incorporating these new acoustic material elements with their corresponding bulk properties into the methods already presented in the Thesis could improve the accuracy of the numerical model of acoustical silencers. Further study is required with comparison to physically obtained results.

4 Data Acquisition System

4.1 Introduction

One of the most important components of the physical model testing is the data acquisition system used to measure the various sound pressures required for the evaluation criteria. After much experimentation, the method used for all sound measurements (i.e. parallel baffle silencers, expansion chamber silencers, impedance tube) was to use a sound card inside a computer and custom code to handle the data. The advantage to the sound card is that it had dual 16 bit A/D converters (as most sound cards do) and was much cheaper than a dedicated data acquisition card. The program MATLAB [32], was used to control the sound card, read the data, and process it. In order to achieve this, the use of MATLAB in conjunction with the sound card as a data acquisition system had to be investigated. Areas such as accuracy, speed, input range, data collection settings and options had to be investigated before the main program could be written. Once completed, the results were verified with known input signals, and the program was checked against a known, calibrated instrument (B&K 2144 dual channel analyzer).

4.2 Equipment

The data acquisition system starts with a transducer that converts sound pressure waves into electrical signals in an analog format (microphone). As shown in Fig. 32, the microphone and pre-amplifier assembly send the signal to the amplifier where the level is boosted and sent on to the sound card in the computer.

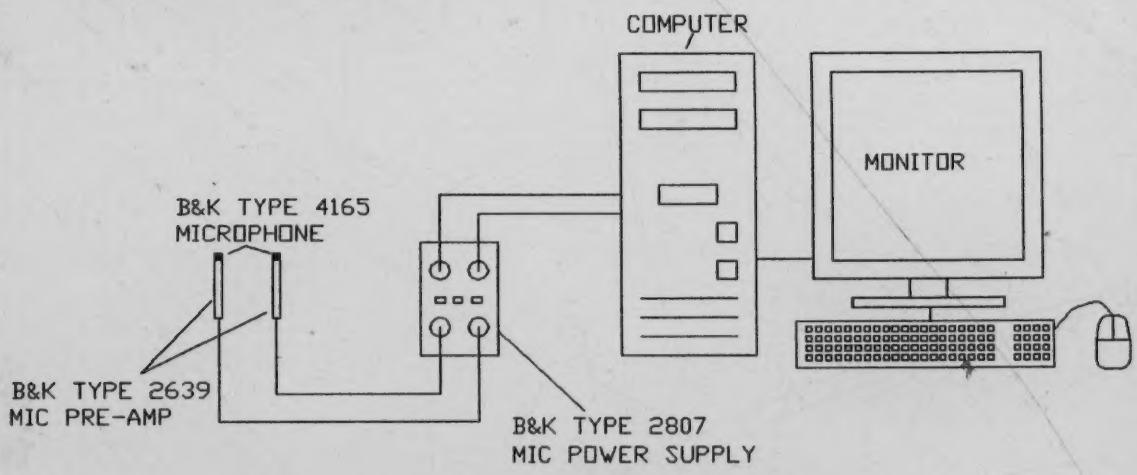

Figure 32. Diagram of Data Acquisition Equipment Used

The sound card used was a standard Creative Labs Sound Blaster PCI (WDM) 16 Bit, two channel unit. The amplitude range was pre-set to ±1V, with a sample rate range of 0-44100Hz. All of the analog to digital (A/D) conversion was performed on board at the sound card, and the resulting digital signal was then recorded by Matlab for future processing. Matlab also controlled the data acquisition parameters that could be modified with the sound card (such as sample rate, number of channels, and measurement duration). Note that since the sound card had a 16 Bit resolution, the dynamic range of the measurements was 96 dB.

Once the fully digital signal was obtained in Matlab, the data block was transformed from the time domain to the frequency domain with Matlab's built in FFT algorithm. This frequency domain data was then processed in a number of ways (depending on the program settings) to obtain the various output types set by the user.

All of the code for the program was written to operate with the graphical user interface (GUI) capabilities in Matlab. This gave the user the ability to change settings in real time without stopping the program, and acted as a perfect panel for displaying settings, and results of the data acquisition process (refer to Figs. 33 and 34 for images of the main screen).

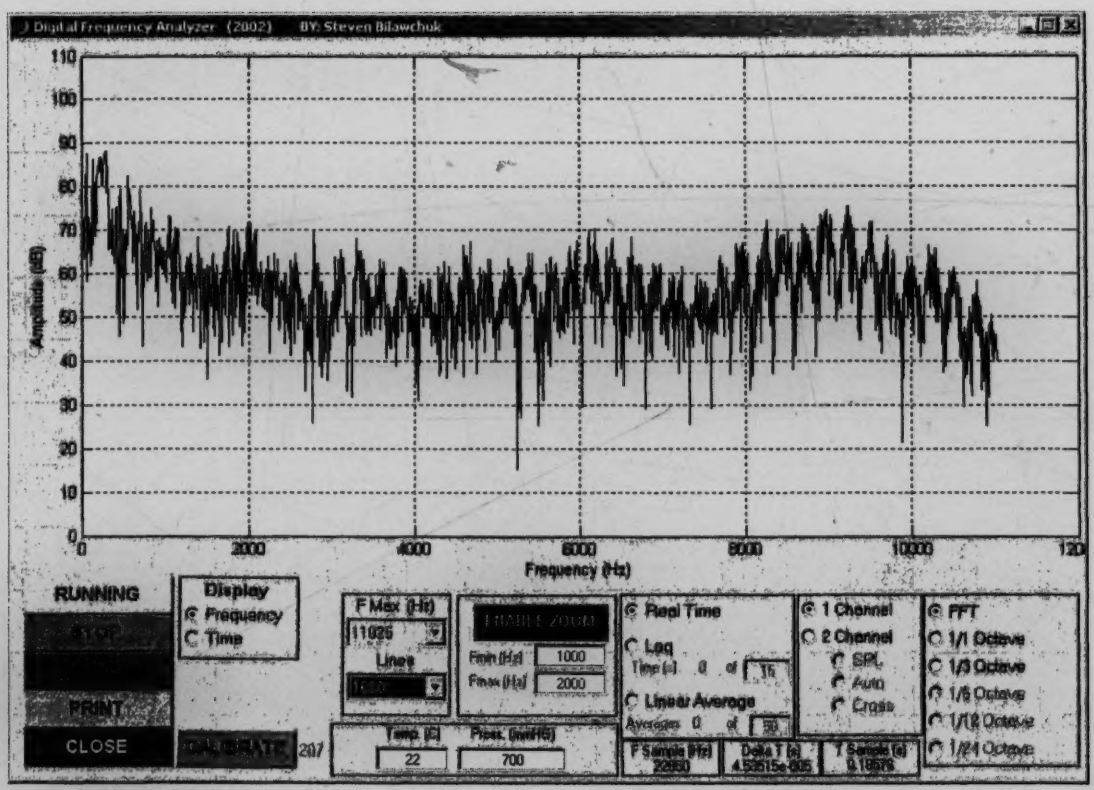

Figure 33. Data Acquisition Program with Single Channel FFT "Real Time" Data Collection

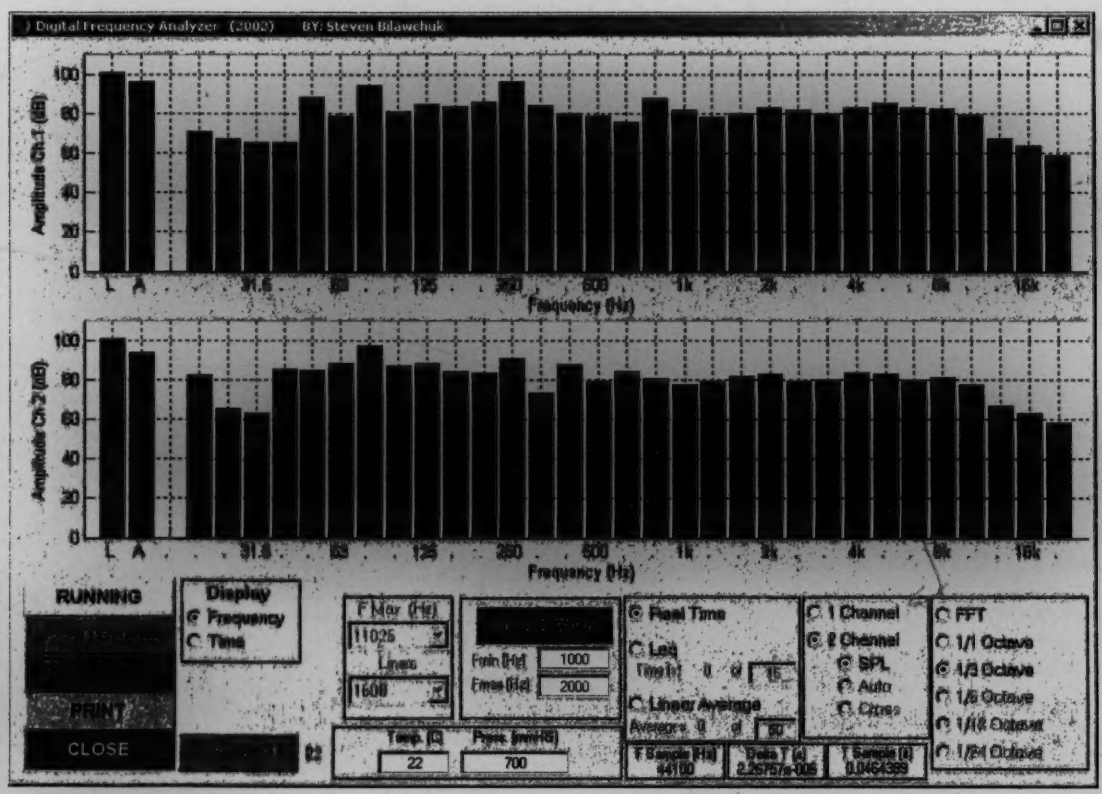

Figure 34. Data Acquisition Program with Dual Channel 1/3 Octave "Real Time" Data Collection

4.3 Theory

The theory behind the data acquisition parameters involves the relationships between sample frequency and sample duration and how these affect the acquired signal. The first, and most important criteria is that the sample frequency, f_s, must be at least twice the maximum, or critical, frequency f_c.

$$f_s \geq 2f_c \ , (Hz) \tag{27}$$

This is used to prevent aliasing of the signal. For acoustical measurements, however, the frequency content of the signal is not always known, or usually is greater than the frequency range of interest. Because of this, there will almost always be signals present that are beyond the critical frequency, and thus greater than ½ of f_s. The result is that there will almost always be some aliasing effects at the frequencies near f_c. This, coupled with the filter roll-off near f_c can cause the captured signal to be corrupted. In order to deal with this phenomena, the typical solution is to simply truncate the signal at some frequency lower than f_c. The factor of 400/512, is commonly used as the ratio of useable frequency content to captured content.

$$f_{useable} = \frac{400}{512} f_c \leq \frac{400}{512} \frac{f_s}{2} \ , (Hz) \tag{28}$$

For example, if a sample rate of 4096 Hz is used, the useable frequency limit is 1600 Hz.

With regards to sample duration, the two important factors are the frequency resolution required, and the speed of the FFT calculation. In order to greatly reduce the time required for the FFT calculation, it is recommended that the data block size (time domain signal) be a number of 2^n (known as radix 2). This yields block sizes of 2, 4, 8, 16, ..., 1024, 2048, 4096, etc... The data block size is determined from the sample rate, f_s, and the duration of the sample time, T.

$$Block\ Size = f_s T \tag{29}$$

Typically, the sample frequency is pre-set based on the input signal parameters, therefore, in order to obtain a data block size of radix 2, the duration of the signal is usually the parameter that is altered. The choice of data block size depends on how much discretization the user wants for the frequency domain signal. Usually, more is better in terms of information content, but the increase in resolution comes at the cost of greater computational time for the FFT calculation. The following example illustrates typical parameters used for the data acquisition of a sound signal.

> A maximum frequency of 1200 Hz is required and the user wants at least a 2 Hz resolution.
>
> Based on Eq. (28), the sample rate required is at least 3072 Hz. If a 2 Hz resolution is required, the data block size for 0-1200 Hz is 600. This number also needs to be multiplied by the factor used in Eq. (28) to give a data block size of 1536. The closest 2^n number to this value (without being undersized) is 2048. Therefore, 2048/3072 = 2/3 seconds. With a sample rate of 3072 Hz, and a duration of .666s, the resulting useable frequency range would be 0-1200 Hz with a resolution of 1.5 Hz.

Once the FFT of the signal has been calculated, the results are cut in half and doubled (to account for the complex conjugate frequency pairs) and the first value is divided by 2 to correct for the DC offset.

An important note relates to the sample rates capable by the sound card. It was determined that, although any sample rate up to 44100 Hz can be used, the sound card had certain pre-determined rates that were acceptable while others skewed the results. The sample rates of 8000 Hz, 11025Hz, 22050 Hz, and 44100 Hz, were pre-set values for the sound card to correctly collect the data.

Once the data had been collected, it could be displayed with the discrete frequency values calculated, or it could be further processed to obtain whole octave or 1/3 octave band values. These values correspond to a single number (at each of the whole or 1/3 octave center frequencies) that represents the total amount of energy contained within the frequency band surrounding the center frequency. In order to calculate this, all of the sound pressure levels within the band limits are added logarithmically and the resulting number represents the center frequency value. In all analyzers, these upper and lower band limits do not have infinite cut-off slopes, but rather roll-off at a prescribed rate. This rate (set by the ANSI S1.11 standard) [33] allows the levels at frequencies near the band limits to affect the neighboring band. For the purposes of the study, the roll-off values were set to ∞ dB/octave, which emulated a straight cut-off. This is not entirely correct (when compared to international standards) but provided a very close approximation.

In order to properly calculate the sound pressure level in decibels, a correction factor was included to relate the measured voltage with a calibrated voltage. To accomplish this, a standard B&K calibrator (type 4231) was used to provide a signal of 94 dB @ 1000 Hz. The signal was measured with the data acquisition system, and the resulting voltage at 1000 Hz was set equal to the voltage for 94dB. For future signals, the voltage was multiplied by this correction factor, and then the dB calculation was performed. After many tests, an average calibration factor was set as the default for the program, however, the calibration procedure was performed before each round of testing to reset the system. Once all of the coding had been completed, the results were verified with known input signals and vs. a standard calibrated instrument.

4.4 Verification

The first check that was performed was to verify that the frequencies calculated by the system matched those which were measured. In order to accomplish this, a function generator (Krohn-Hite model 5300 A) and frequency counter (Hewlett Packard model 5314 A) were used, in conjunction with a small amplifier and speaker, to generate specific tones at known frequencies. Table 2 contains the generated frequencies and the ones measured with the MATLAB data acquisition code.

Table 2. Evaluation of Frequency Accuracy of MATLAB Data Acquisition System

Generated Frequency (Hz)	Measured Frequency (Hz)
40	40
59	59
80	79
99	99
200	199
1000	299
2000	2000
4999	4999
9997	9996
15009	15007

Note that the frequency counter was not always stable, and the values displayed could easily be ±1 or ±2 Hz. From this it can be seen that the data acquisition system was able to measure and calculate the frequency content very accurately.

In order to check the response of the sound card, a test was conducted where frequencies ranging from 1 Hz to 30 kHz were generated with a Sony Tektronix AFG320 Arbitrary Function Generator. The generator was set to a constant output voltage of 0.1V and a sine function was generated at the various frequencies. Fig. 35 shows the response of the sound card over the tested range. Note that for the range of greatest interest (20 Hz – 20 kHz), the fluctuations were less than 1 dB. A difference this small is typically considered negligible for acoustic testing.

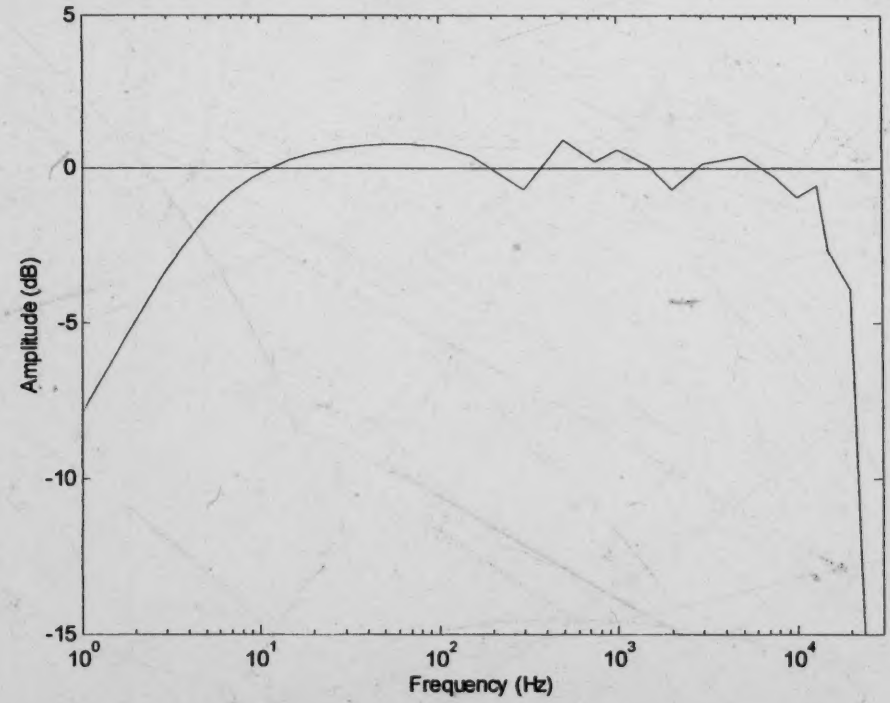

Figure 35. Frequency Response of Sound Card Used for Data Acquisition

The next verification step conducted was to compare the calibrated sound pressure level results, at various frequencies, measured by the MATLAB system to the results obtained from a B&K 2144 dual channel spectrum analyzer. Fig. 36 shows the difference between the whole and 1/3 octave sound pressure levels obtained with the B&K unit and MATLAB respectively. It can be seen that only at the very high and very low frequencies, did the results differ by more than 3dB and the differences were very small through most of the useful range. At the low end, this difference was probably due to the low frequency roll-off of the sound card, and the high end was probably due to aliasing problems (note that the 400/512 critical frequency ratio was not used for whole and 1/3 octave frequency analysis). Also, since the MATLAB code used ∞ dB/octave slopes, the values were bound to be slightly different.

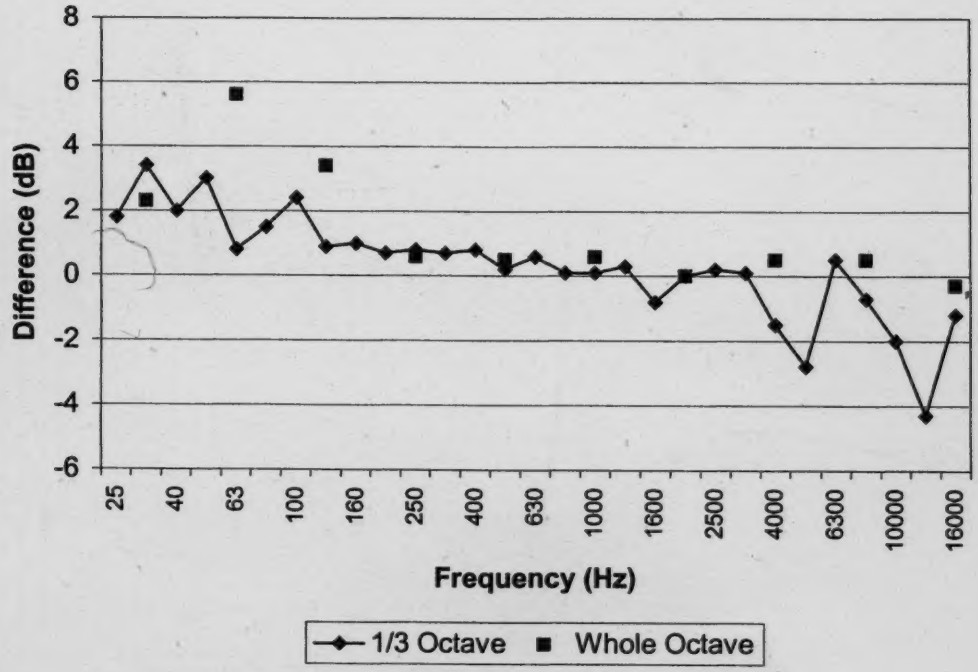

Figure 36. Whole and 1/3 Octave Sound Pressure Level Differences Between B&K 2144 and Matlab Data Acquisition System

The final verification step dealt with the dual channel data acquisition. For the calculation of the cross spectrum between the channels, it was important that the signals be collected simultaneously. To check this, a B&K dual channel calibrator unit (type 4228 Pistonphone and type 3541 dual microphone holder) was used as the source. The two microphones were inserted, and the signal was measured. The captured time domain signal was then plotted, as shown in Fig. 37, and the time difference between the two channels was evaluated. By taking the time difference of the x-axis crossings, a difference of .0000184 seconds was measured, which corresponds to a frequency of 54,347 Hz. This is beyond the maximum sample rate of the system, therefore, the time difference can be ignored and the two signals can be considered simultaneous.

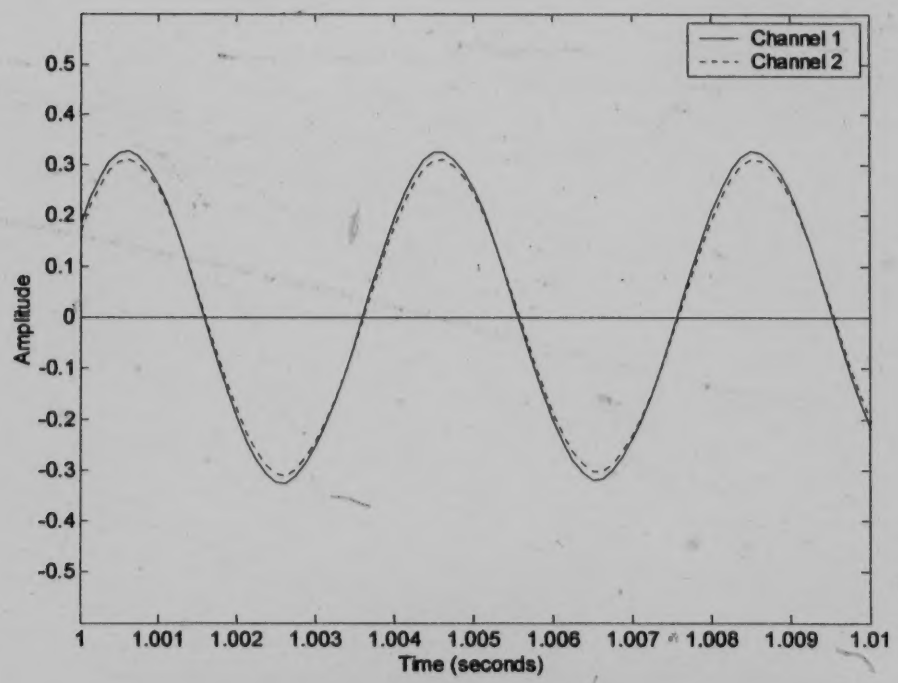

Figure 37. Dual Channel Data Acquisition with 250 Hz Signal

4.5 Conclusions

In order to obtain data from the physical systems used for the research work, a proper data acquisition system was required. The system had to be variable in its use in order to be able to handle various measurement scenarios, and had to be able to obtain dual simultaneous measurements. By using a standard sound card built into a personal computer, and the program MATLAB, a very accurate, easy to use data acquisition system was devised. This system was able to perform all of the necessary signal processing including FFT analysis, filtering, and whole octave and 1/3 octave band resolution.

Many verification steps were taken to ensure that the system would be accurate enough for all of the various measurements required. These tests involved comparison between known input signals and measured results, and between results measured with the MATLAB system and a certified dual channel FFT analyzer. Such tests as accuracy of frequency resolution, amplitude, and phase shift between the two channels were performed and the system was found to meet all of the minimum criteria for the research.

5 Scale Parallel Baffle Silencer Modeling

5.1 Introduction

The previous chapters dealt with the basic methods and formulations required for numerical finite element characterization of acoustic systems. The ability to handle various geometries, and sound absorbing materials was investigated and the results proved that the numerical models were able to describe a physical system with a good deal of accuracy compared to known results. This chapter pulls all of the methods together for use in the numerical modeling of a scale acoustic parallel baffle silencer. A physical model was constructed and tested with various material and geometrical configurations and the results were compared to those obtained in an equivalent numerical model.

5.2 Scale Model

In order to verify the numerical model's capability to model a parallel baffle silencer system, a scale model was constructed and the acoustic performance was measured for various configurations. Some of the physical considerations given at the design stage of the model related to variability of baffle configurations, the adaptability of future testing requirements (elbows, different test section dimensions, etc..) and the ease of use for numerous different tests. In terms of acoustical concerns, the model was required to be acoustically sealed from the outside, the construction material used needed to be strong and massive to avoid excessive vibrations, and there needed to be sufficient length between the source and the test section to assure planar propagation of the sound waves. Due to all of the above design considerations, the model was designed in three sections. Fig. 38 shows the side view of the model with the various sections and microphone and sound source locations.

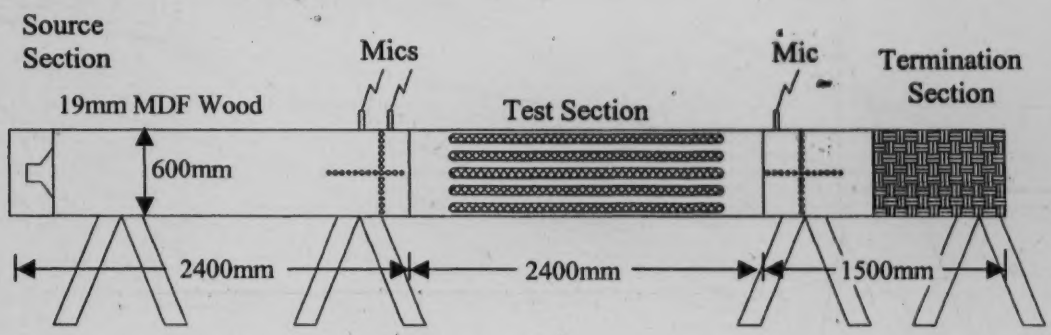

Figure 38. Scale Parallel Baffle Silencer Model

5.2.1 Geometry / Sections

The first section was built as a long straight section for the purpose of allowing the waves to propagate in a planar fashion from the sound source located at the far left side. Empirical results show that a minimum length of 3 equivalent section diameters is required in order for the waves to become planar (much like turbulent fluid flow becoming laminar). Because of this, the section was 600mm x 600mm square with a length of 2400mm, which gave 4 equivalent diameters. The 600mm dimensions were chosen to give the test section enough size to accommodate several baffle configurations, while keeping the overall size (mainly due to the required length) to a minimum. The entire section (and essentially the entire model) was constructed from 19mm (¾") MDF wood. It was chosen because it is very dense, inexpensive, and relatively easy to work with. The entire first section was un-lined except for the face where the drivers were located. This face was covered with 75mm of fiber-wool (holes were cut out for the drivers) to minimize reflections. Finally, the exit side was open to allow the sound to enter into the second section.

Located at the inlet side of the first section, was the sound source. It consisted of two 200mm and two 25mm PSB Speakers International drivers mounted in a sealed enclosure. The drivers were powered by (in the following order) a General Radio Company model 1382 Random Noise Generator producing white noise, a White Instruments Inc. Series 4000 1/3 octave equalizer, and a Bogen Flex-Pak

model CHS-20A amplifier. The equalizer was used to create a frequency response curve (upstream of the test section) that was "flat" or of equal sound pressure level in each of the 1/3 octave bands.

The second section was built as the test section. It is where the baffles were located. Similar to the first section, it was 600mm x 600mm x 2400mm (with the two ends open to allow passage of the sound waves) and was made from 19mm MDF. At the two ends of the vertical (side) faces, were slotted sections made of steel. These sections accommodated bolts, which could be manipulated up and down to adjust the location of the baffles. In addition, the top and front side panels opened (using hinges) for easy access to the baffles. For each of the four slotted sections, a door was made that could close and seal the opening of the slot. These doors, along with the edges around the top and side panels, were lined with a closed cell foam to provide an acoustical seal. The baffle sections themselves were supported by metal racks made from 25mm angle and thin wire mesh. Each rack was 2100mm long and allowed for support of a 600mm x 2100mm baffle. These racks were supported by the adjustable bolts at the four corners and allowed for the absorptive material to be placed upon them. Because of the complete variability of the system, an infinite number of configurations could be achieved, including different baffles lengths, spacing, thickness, and even staggered positions.

The third section was used as the termination section. Again, like the other two sections it was 600mm x 600mm and made from 19mm MDF, but it was only 1500mm long. Extra length of this section was not required since the waves simply terminated here. The inlet end of this section was open to connect with the second section, but the exit end was closed off with MDF. Inside at the far end was 600mm of pink fiberglass insulation. This was installed to provide an equivalent anechoic termination for the sound waves so that they would not reflect back into the test section. Testing was done to ensure that this 600mm amount was adequate for proper absorption of the waves. To accomplish this, a sound level measurement was taken at the inlet of the third section without any absorption in place. Then small amounts of absorption were installed, and the system was re-measured at the same location, until there was no difference noticed in the response of the system. This point was found

when the thickness was approximately 300mm, however there remained plenty of room, so the thickness was doubled to ensure that the termination was as absorptive as could be (given the material used).

At all of the joint locations for the sections, closed cell foam was placed along the mating surfaces. Once the closing latches (located around the perimeter of the mating surfaces) were secured, the foam acted as a barrier for the sound and sealed the entire unit. Finally, along the top and front faces of the first section (exit side) and third section (inlet side) holes were drilled for microphone locations. For each hole, a small plug was made for use when there was no microphone at that location. The entire unit measured approximately 6600mm long (with the driver enclosure installed) and was raised 900mm above the ground on wooden supports. Figures 39 and 40 are photographs of the model with the test section door closed and open respectively. Figure 41 is a close-up image of the adjustable baffle section.

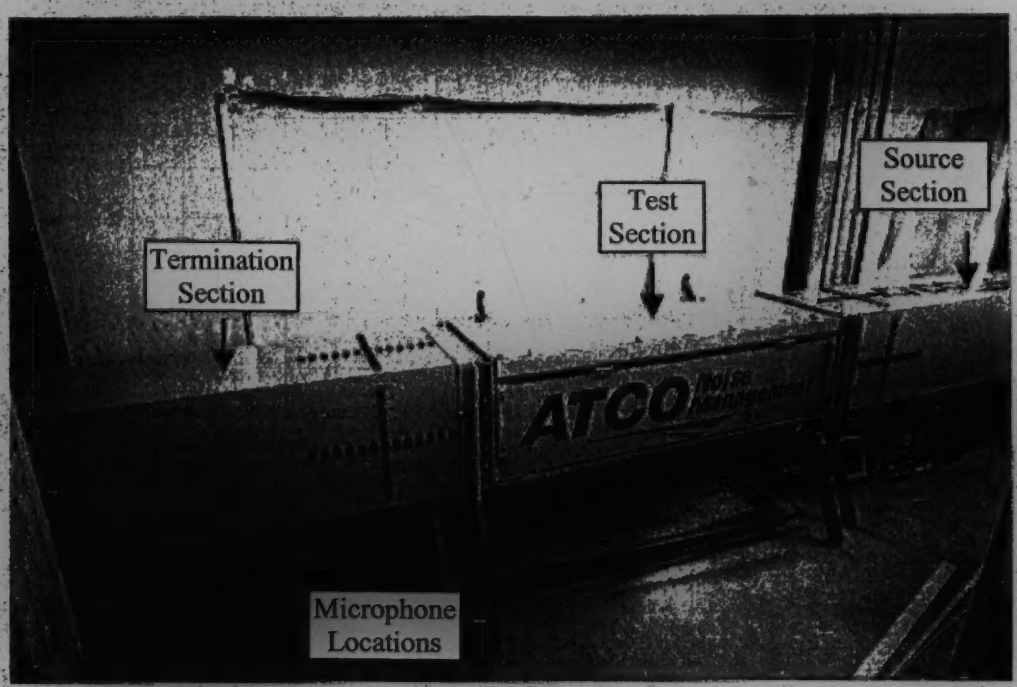

Figure 39. Physical Model with Test Section Door Closed

Figure 40. Physical Model with Test Section Door Open

Figure 41. Physical Model, Adjustable Baffle Detail

5.2.2 Limitations of Scale Model

Based on the geometry and construction materials used in the scale model, there were several limitations that required consideration when measuring *TL* for various configurations. For example, one limitation was the low frequency extension. Due to the 2400mm length of the inlet section, wavelengths beyond this length were unable to form properly. This means that frequencies below approximately 140Hz did not provide accurate results. Also, due to the 600mm cross section geometry, higher frequency modes could have been present to cause problems in the cross dimensions.

The main limitation of the model involved the difference in sound pressure levels measured before and after the test section, and the factors which affect this difference. All silencers have a practical limit for the *TL* they can achieve because of a phenomena known as "path flanking". The sound traveling down the duct of the silencer has three paths it can take to get to the receiver. The first path is directly through the fluid medium in which the originally generated sound is traveling (i.e. air in this case). The second path is through the material of the silencer walls (the wooden panel in this case). This occurs because the sound in the air upstream of the test section excites the panels of the silencer, the vibrations are transmitted through to the exit of the test section, and the vibrating panels then excite the air on the exit side. The third path (although much reduced in acoustic energy from the first two) is by sound radiating through the panels in the inlet section to the outside air, then re-entering the model at the exit side of the test section. These second and third paths are known as the flanking paths.

Because of the sound energy transmitted by the flanking paths, the silencer elements cannot create an infinite noise reduction. If the sound energy transmitted directly through the air on the inside of the model is eliminated, the flanking path energy will still exist. This limits most parallel baffle silencers to a maximum *TL* of approximately 50dB [16]. This amount varies slightly due to the construction techniques used in the silencers. Fig 42 shows the results of a test conducted where the entire test section was filled with pink fiberglass sound absorbing material and the

TL was measured. It can be seen that the maximum *TL* level attainable was about 45dB.

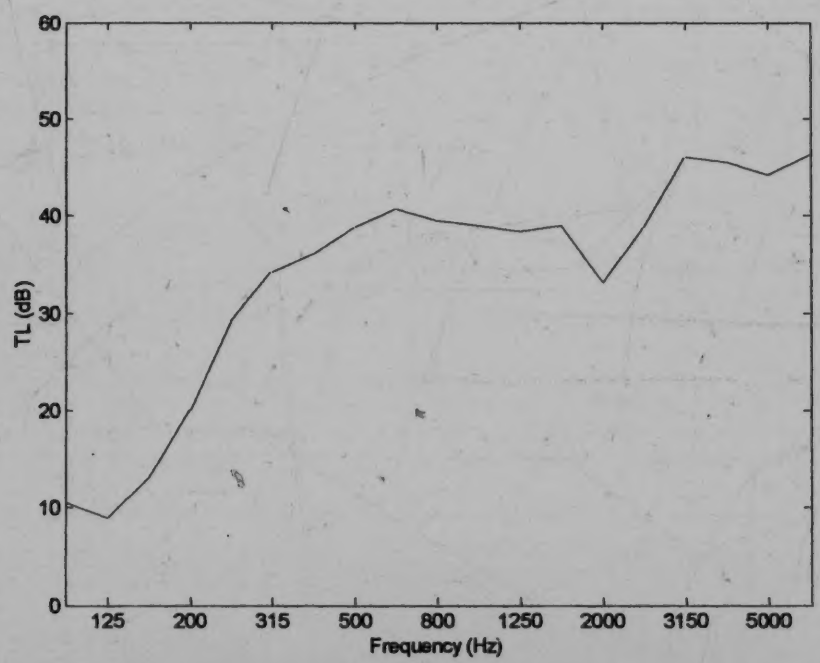

Figure 42. *TL* of Silencer Model with Full Test Section of Pink Fiberglass Insulation

Yet another factor contributing to the maximum *TL* attainable is the difference between the transmitted sound energy (through the silencer section) and the ambient background noise. Most measurement standards call for a difference between the measured noise and ambient noise of at least 10dB [9, 10, 22, 23]. If the difference is any less than 10dB, then the ambient noise can affect the results. For the physical model, the sound pressure level attainable at the source side of the test section was about 85dB. The ambient level measured at the termination section (with the sound source off) was approximately 40dB. This means that even if the silencer was able to reduce the transmitted sound level by more than 45dB, the transmitted sound would be equal to or less than the background noise. Therefore the maximum *TL* attainable would be approximately 45dB. In order to eliminate this issue, a louder source section (or correspondingly quieter ambient noise level) would be required.

The fact that these limitations exist is not detrimental to the use of the physical model for testing. The important thing to note is that these limitations do exist and results cannot be expected beyond those realistically attainable. Silencer manufacturers face these kinds of issues every day when designing.

5.3 Measurement of Transmission Loss

With the model constructed and the data acquisition system working, the next step was to begin to measure *TL* values in the silencer. As mentioned in §2.3, there are two main ways in which *TL* can be measured, namely the *traditional* method and the 3-point method. The *traditional* method follows the definition of *TL* exactly, and therefore is accepted as the standard method by which all others are to be compared. To that end, a comparison was performed to verify that the 3-point method (essentially new at the time of writing this Thesis) would give the same results as the *traditional* method. Before the 3-point method could be used, however, a different formulation was required.

5.3.1 Measured 3-point Method Theory

The formulation for the 3-point method was given in §2.3.3, where Eq. (17) can be re-written as:

$$TL = 20\log_{10}\left|\frac{p_1 - p_2 e^{-ik x_{12a}}}{p_3 - p_3 e^{-i2k x_{12a}}}\right|, \ (dB) \tag{30}$$

This is how the 3-point method is used theoretically, and when incorporating into a numerical modeling scheme such as the Finite Element Method. When using measurement equipment, the complex pressures are difficult to obtain, so a slightly different approach is taken [10, 18, 17, 34].

The following presents a derivation of the 3-point method that incorporates the auto and cross power spectrum obtained by most dual channel simultaneous

measurement systems. To begin with, start with the general solution to the 1-D wave equation for points 1 and 2 [26]:

$$P_1 = \left(P_i e^{-ikx_1} + P_r e^{ikx_1}\right) \tag{31a}$$

$$P_2 = \left(P_i e^{-ikx_2} + P_r e^{ikx_2}\right) \tag{31b}$$

where: $k = 2\pi f/c$ (wave number) (1/m)

ω = frequency (rad/s)

Fig. 5 (on page 2-9) illustrated the location of the 3 points used as well as the incident, P_i, reflected, P_r, and transmitted, P_t, pressure waves. As mentioned before, for transmission loss, only P_i is required from (31a) and (31b). This quantity cannot, however, be measured at a single point, since P_r will also be present. This is why there are two points measured (resulting in two equations and two unknowns). The difficulty is in the measurement of the complex values for P_1 and P_2. To solve this problem one can obtain the following auto and cross power spectrum from points 1 and 2 with a dual channel, simultaneous data acquisition system:

$$P_{11} = P_1 P_1^* \tag{32a}$$

$$P_{22} = P_2 P_2^* \tag{32b}$$

$$P_{12} = P_1 P_2^* \tag{32c}$$

where P_1^* and P_2^* denote the complex conjugates of P_1 and P_2 respectively. These quantities of P_{11}, P_{22}, and P_{12} (represented by capitals because they are vectors in the frequency domain) are readily measured.

Now (31a) and (31b) can be combined into (32a), (32b), and (32c) to obtain the following:

$$P_{11} = P_i P_i^* + P_r P_r^* + P_i P_r e^{2kx_1} \tag{33a}$$

$$P_{22} = P_i P_i^* + P_r P_r^* + P_i P_r e^{2kx_2} \tag{33b}$$

$$P_{12} = P_i P_i^* e^{-ik(x_1-x_2)} + P_r P_r^* e^{ik(x_1-x_2)} + P_i P_r e^{k(x_1+x_2)} \tag{33c}$$

Which can be written in the more common notation:

$$P_{11} = P_{ii} + P_{rr} + P_{ir} e^{2kx_1} \tag{34a}$$

$$P_{22} = P_{ii} + P_{rr} + P_{ir} e^{2kx_2} \tag{34b}$$

$$P_{12} = P_{ii} e^{-ik(x_1-x_2)} + P_{rr} e^{ik(x_1-x_2)} + P_{ir} e^{k(x_1+x_2)} \tag{34c}$$

It can be seen, that by measuring P_{11}, P_{22}, and P_{12}, and knowing x_1, x_2, and k, the system of equations can be solved for P_{ii}, P_{rr}, and P_{ir}. As mentioned previously, only P_{ii} is of interest for transmission loss, therefore, the system of equations can be solved for P_{ii} :

$$P_{ii} = \frac{P_{11}(E - DB) + P_{22}(DA - E) + P_{12}(B - A)}{(B - A)(C - D)} \tag{35}$$

where:

$$A = e^{2kx_1}\left(e^{-i} + e^{i}\right)$$

$$B = e^{2kx_2}\left(e^{-i} + e^{i}\right)$$

$$C = e^{-ik(x_1-x_2)}$$

$$D = e^{ik(x_1-x_2)}$$

$$E = e^{k(x_1+x_2)}\left(e^{-i} + e^{i}\right)$$

Once P_{ii} is known, the third point can be used to measure the transmitted sound pressure, P_{tt} where:

$$P_{tt} = P_t P_t^* \tag{36}$$

Finally, the transmission loss can be calculated by:

$$TL = 10\log_{10}\left|\frac{P_{ii}}{P_{it}}\right|, \quad (dB) \tag{37}$$

Again, the important thing to note is that the measurements at points 1 and 2 MUST be taken simultaneously. This is necessary in order to obtain the proper phase in the cross product between the two. Also, the numbers must be kept in complex form until the very end when the *TL* is actually calculated. If the absolute value of any complex number is taken before the final step, phase information will be lost and the results will not be precise.

5.3.2 Comparison of traditional and 3-point Methods

Actual implementation of the 3-point method is quite simple. All that is required is a dual channel simultaneous sound measurement system and the appropriate microphone locations (P_1, P_2, P_3).

The *traditional* method was used as the standard by which the 3-point method would be compared. To accomplish this, the incident sound pressure (P_i) was measured with the test section completely empty, and then baffles of sound absorbing material were installed for the transmitted sound pressure (P_t). This same baffle configuration was used for the three sound measurements used for the 3-point method (P_1, P_2, P_3). Figure 43 displays the results of the *traditional* and 3-point methods for a section with one 100mm thick baffle of yellow fiberglass insulation, along with the difference between the two. The values are presented using 1/3 octave analysis. Two dashed lines have been placed on the graph to illustrate a ± 3dB region. This region has been chosen as the range in which no perceptible difference between methods would be noticed by the end user, and as a region in which repeatable test results can be expected. It can be seen that for all of the useful frequency range, the differences between the two methods were very small, and follow the center (0dB difference) line very well. Similar to Fig. 43, Fig. 44 displays the results for two baffles of 50mm

thick green mineral rock insulation. Again, it can be seen that the differences between the *traditional* and 3-point methods were very small.

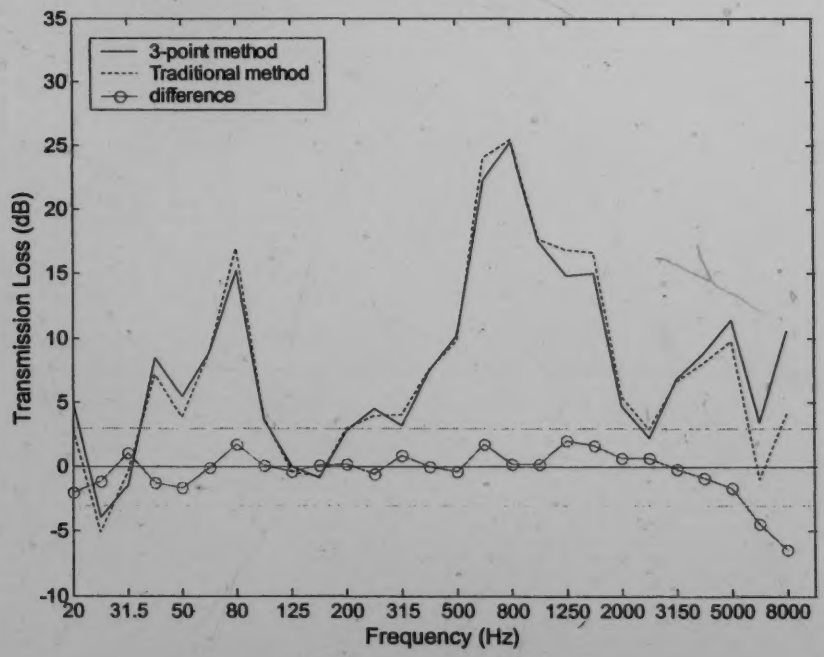

Figure 43. Transmission Loss Comparison of *Traditional* vs. 3-point Method for Single Baffle of 100mm Thick Yellow Fiberglass Insulation

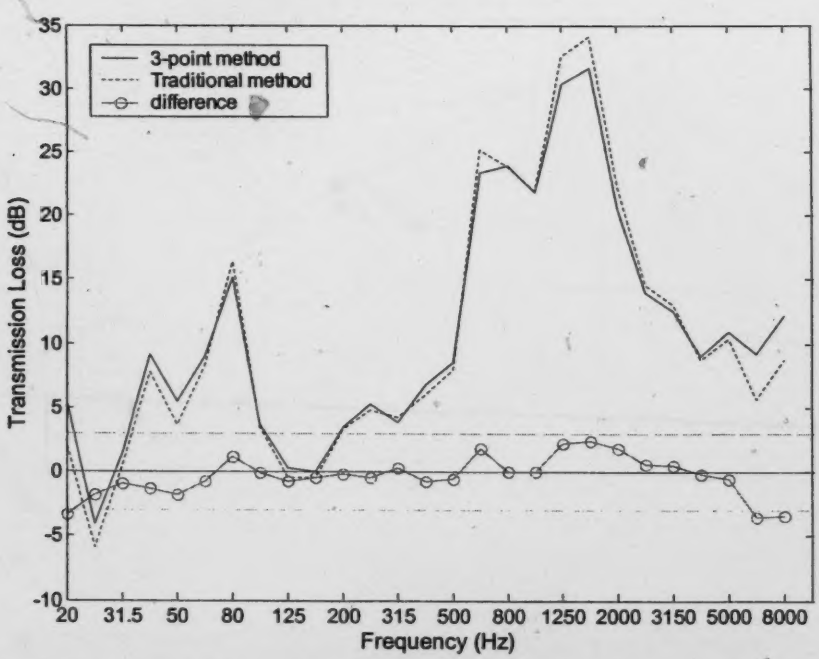

Figure 44. Transmission Loss Comparison of *Traditional* vs. 3-point Method for Two Baffles of 50mm Thick Green Mineral Rock Insulation

5.3.3 Practical Considerations / Measurement Concerns

During the testing and use of the 3-point method, different measurement parameters were investigated and evaluated. The first dealt with the center-to-center microphone spacing between locations 1 and 2. Fig. 45 shows the *TL* results for the same 2 baffles of green mineral rock insulation as in Fig. 44, with variances in the microphone spacing. It was found that for small microphone spacing (less than approximately 30mm for 13mm (½") microphones), the results were very repeatable. It was only at the very high frequencies (approximately greater than the 6300Hz 1/3 octave band) that there were any noticeable differences. Once the spacing began to increase, however, the results became less accurate and repeatable. It was observed experimentally, that with 13mm microphones, a center-to-center spacing of less than approximately 30mm gave the most consistent results.

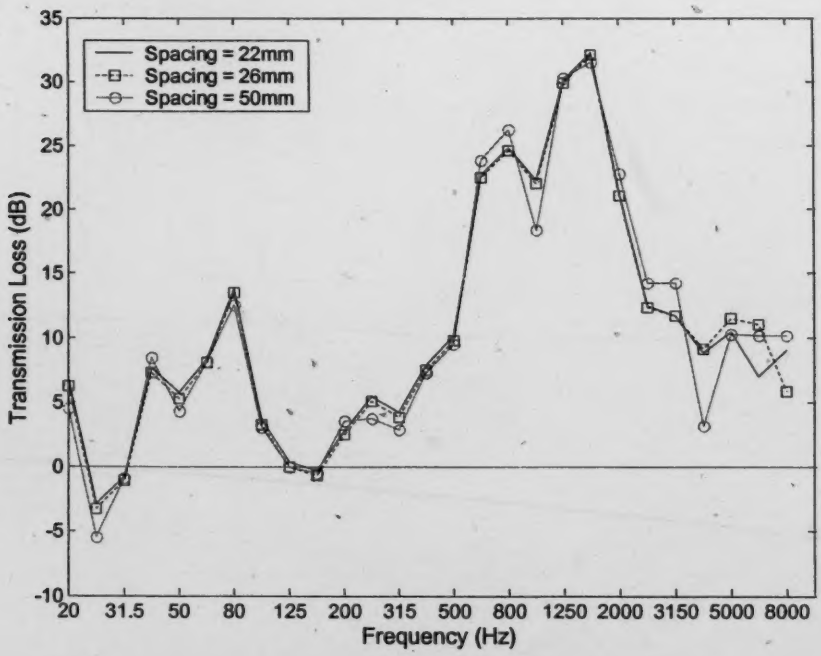

Figure 45. Transmission Loss with 3-point Method and Different Center-to-Center Microphone Spacing Between Points 1 & 2 for Two Baffles of 50mm Thick Green Mineral Rock Insulation

The next issue dealt with the location of the microphones relative to the test section. Several locations for points 1, 2, & 3 were evaluated. Various configurations such as side vs. top mounting and different distances from the test section were tried. Fig. 46 shows the *TL* results for 2 baffles of green mineral rock insulation with different positions for measurement point 3. For the most part, the results were close to each other, and followed the same general trend as seen in Fig 45. Similar results to those of Fig. 45 were obtained when the microphones were located on either the top or side of the model (for a rectangular section). The difference between the two is in how the baffles were oriented compared to the microphones (parallel vs. perpendicular). Fig. 47 shows the *TL* results when the microphones were placed on the top and side at equivalent locations. Again, the results were quite similar and both curves followed the same general trend. Finally, Fig. 48 shows the results when the microphone at point 3 was moved off of the

center-line of the model. Once again, the differences were small and the same general trends were observed for both curves.

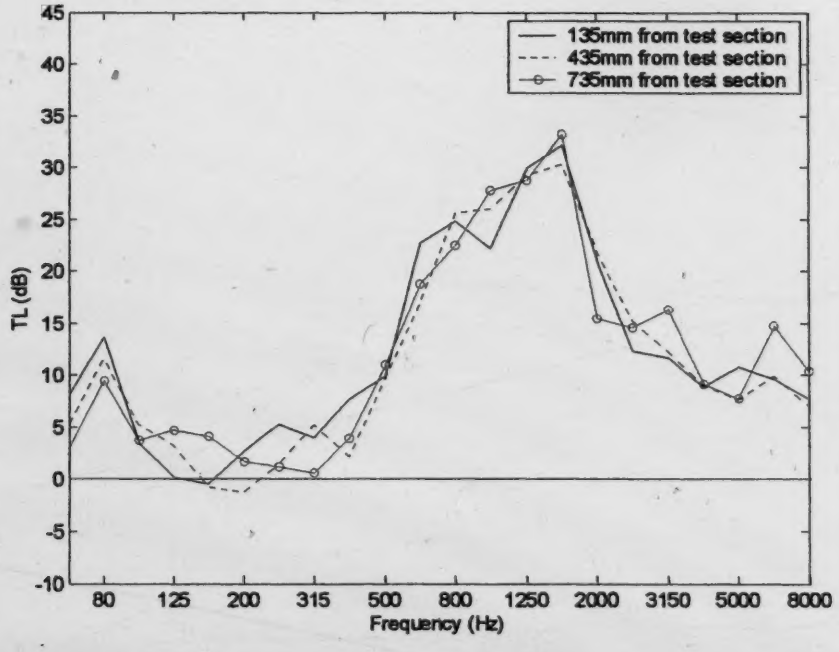

Figure 46. Transmission Loss with 3-point Method and Different Locations for Point 3 for Two Baffles of 50mm Thick Green Mineral Rock Insulation

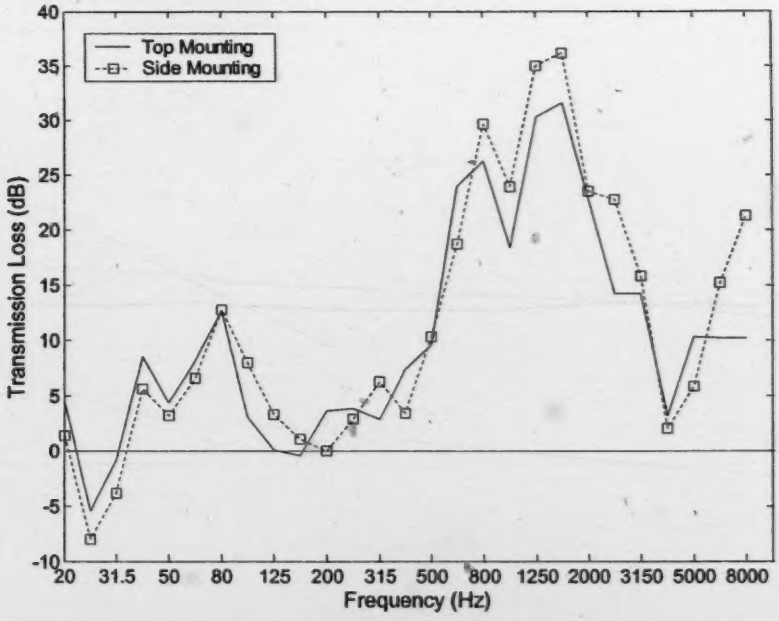

Figure 47. Transmission Loss with 3-point Method and Different Microphone Mounting for Two Baffles of 50mm Thick Green Mineral Rock Insulation

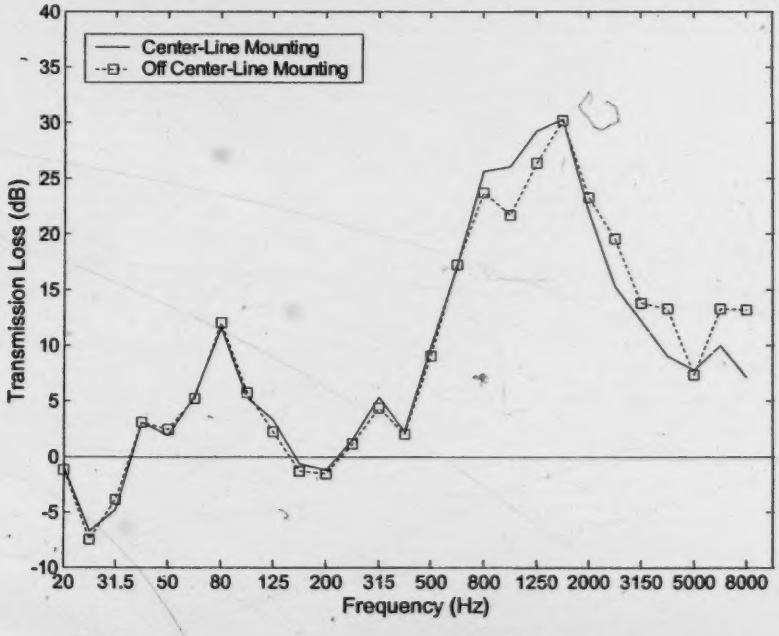

Figure 48. Transmission Loss with 3-point Method and Center-Line vs. Off Center-Line Microphone Mounting for Two Baffles of 50mm Thick Green Mineral Rock Insulation

In general, it is hypothesized that differences at specific frequencies were the result of multiple wave interference caused by reflections within the model. Preliminary data suggests that within a duct, small differences in downstream and upstream microphone locations did not affect the results appreciably. The closest match between the *traditional* and 3-point methods was obtained when the center-to-center microphone spacing was kept quite small (less than 30mm for 13mm microphones), the locations of all three points were kept quite close to the test section, and the three microphones were all aligned along the centerline of the particular side on which they were installed. Of course, each test situation will be different and subject to a variety of microphone location issues, however it has been observed that small geometric differences do not result in large *TL* differences.

With regards to the data acquisition system, most measurement systems allow for data acquisition and FFT analysis with several resolution settings (i.e. 400, 800, 1600 lines), and frequency range settings (i.e. 3200Hz, 6400Hz, 12.8kHz) as well as different averaging schemes. The choice for these settings is dependent on the requirements for the specific silencing element being tested. It is recommended that the resolution setting be as large as possible, and the measurements be averaged over such a time that convergence is observed.

5.4 Numerical vs. Measured Scale Model Results

With all of the measurement issues covered, the next step was to compare the results obtained for the numerical model to those obtained in the physical model. Various materials and baffle configurations were tested to verify the validity of the numerical model, and differences and limitations were identified. Figures. 49-51 show the *TL* results for 3 different materials (shown in Table 1) with 3 different baffle configurations. For each case, error bars were placed on the curves to illustrate the range of probable error with both the measured and numerical results. For the measured results error values, a range of ±3dB was chosen based on numerous tests and experience with the data acquisition system. For the numerical results error values, the statistical testing errors for each of the bulk acoustical properties were included in the model to get max/min *TL* values, along with the average value.

It should also be noted at this point, that the results are presented in 1/3 octave band frequency analysis. While the resolution of 1/3 octaves with the measured *TL* values is very straight forward, the conversion to 1/3 octaves with the numerical results is not. The data presented in each 1/3 octave band is a value that represents the total sound energy in that band. As stated in Appendix A, the numerical solution is solved at each specific frequency of interest. These frequencies can be considered as having a finite value with an infinitely small width, therefore there is no real energy associated with each value. Because of this, the frequencies solved in each 1/3 octave band cannot be summed together in an energy fashion necessary for the typical 1/3 octave representation. To deal with this several methods of converting the values to 1/3 octaves were investigated. The most accurate solution was an average of the resulting *TL* levels from the numerical solution for each of the 1/3 octave bands. This was determined by comparing the numerical *TL* solution for a simple model in 1/3 octave bands with the known solution for that given geometry.

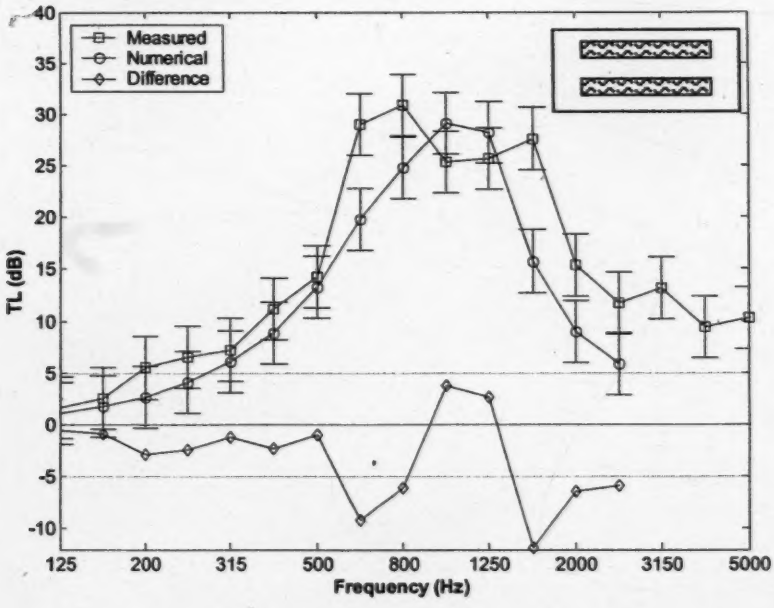

Figure 49. *TL* for Two 80mm Thick, 225mm Long Baffles of Pink Fiberglass Insulation

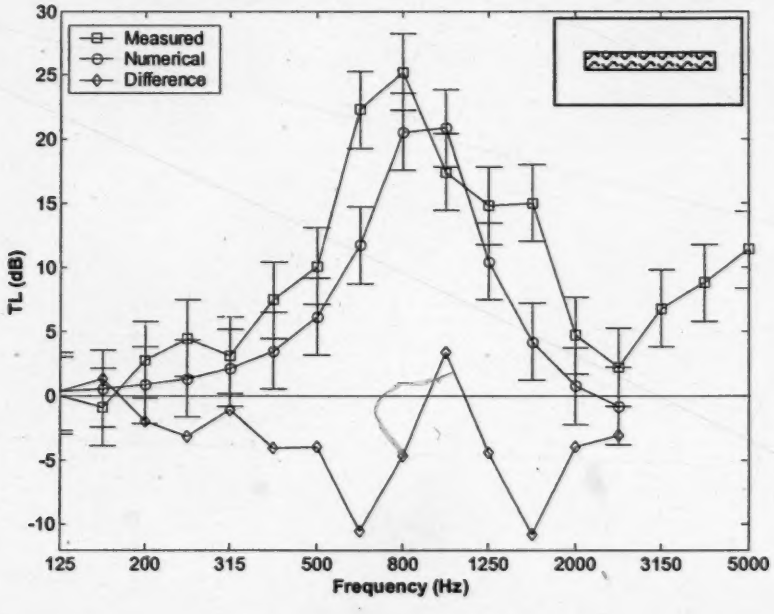

Figure 50. *TL* for a Single 73mm Thick, 225mm Long Baffle of Yellow Fiberglass Insulation

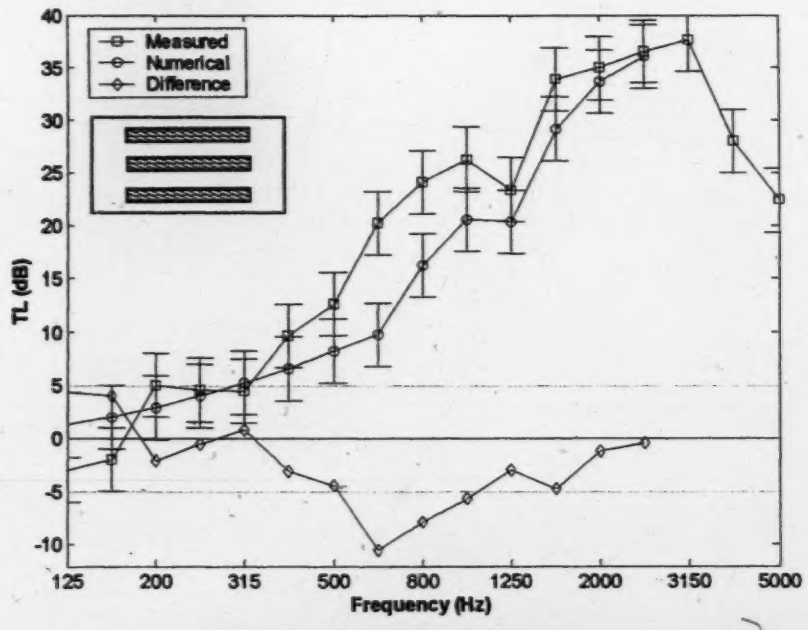

Figure 51. *TL* for Three Equally Spaced, 50mm Thick, 225mm Long Baffles of Kaowool 2600F Ceramic Fiber Insulation

It can be seen that the results match very well, especially within the error range for each respective method. Solid lines at ±5 dB represent the acceptable range for the difference between the two curves. This value was chosen based on experience with the measured data, and because differences of less than 5dB are considered acoustically small. A difference of 3 dB, for example, is the amount by which most humans will just begin to notice that there is even a difference, while a difference of 10 dB is considered to be a factor of 2 (half or double) from the original sound. For most of the useful frequency range, the difference between the measured and numerical curves does indeed lie in between this ±5 dB range.

5.4.1 Sources for Discrepancies

At this time, it is not entirely understood where the differences between the measured and numerical results come from. Since the purely reactive silencers modeled almost exactly, the most reasonable explanation is that the bulk parameters entered in for the sound absorbing material, although measured accurately, cannot account for all of the acoustical behavior of the material, as mentioned in §3.4.3.5. This was first noticed with the modeling of the normal incidence absorption coefficient. The numerically calculated values, while close, were not exact when compared to the measured values. It is surmised that in order to obtain more accurate *TL* predictions for absorptive silencers, the way in which the sound absorbing material is characterized and included in the numerical model will need further investigation.

The other main reason for the differences between the measured and numerical values is because of the sound path flanking discussed in §5.2.2. The numerical model did not have vibro-acoustical coupling included in the calculation, so no flanking was able to be modeled. Unfortunately, it is not known how much of an impact this would have caused, since there is no clear method for determining how much energy is radiated directly through the model, and how much is transmitted due to flanking.

Finally, at low frequencies, the thicknesses of the various materials used should have resulted in very low *TL* values (as predicted by the numerical and empirical models, and based on experience). Despite this, some large *TL* peaks were noticed at very low frequencies. This was likely due to the total model length (refer to §5.2.2). Standing waves could have resulted which would cause constructive or destructive interference at certain frequencies, resulting in uncharacteristic and unpredictable *TL* results at the low frequencies. The large differences in the 630 Hz band, for example, may have been the result of some cross modes due to the 600mm cross section dimensions.

Of course the issues mentioned above do not take away from the relative accuracy of the results with the current methods. It was observed that the numerical

results followed the measured results quite well for all of the varying geometries, and material compositions.

5.5 Numerical vs. Empirical Scale Model Results

One of the main reasons for using a numerical method is to have a more accurate tool for design. The currently available empirical methods involve extrapolation of previously gathered empirical data. That is, they are based on prior experiments that have been completed and use some sort of statistical analysis to extrapolate the data to non-tested cases. The major method investigated, as proposed by Munjal and Beranek, is the most common method used [4, 16]. It has been compiled from numerous tests performed on different baffle configurations, and material types. A set of standard curves has been published which can be used either graphically, or by using the numbers for an interpolation scheme in a computer program. The advantages to this method are that it is relatively easy to use and program into a spreadsheet, and for limited ranges of geometries, it is fairly accurate. The disadvantages, however, are more numerous.

The first disadvantage to the method proposed by Munjal and Beranek is that the geometries that it can handle are limited. The method is really designed to handle baffle sections with multiple whole baffles in the middle and half baffles on either side attached to the outer walls of the silencer. In all fairness, this is indeed the most common configuration, but if a deviation from this geometry is desired, the empirical formula is not able to deal with it. Also, curved sections, and staggered baffle orientations are not covered in this method, and the user is left to use some other empirical "guessing" schemes to extrapolate the standard results to the particular situation. Finally, the empirical models only allow for the inclusion of the absorptive material's flow resistivity values. Again, while this is the most important acoustic bulk material property, it is possible to have materials with similar flow resistivity values and different porosity and structural factor values, thus producing different sound absorption characteristics.

It was found through use and testing of this method, that the results generally agreed with those measured and obtained numerically. Fig. 52 shows the *TL* results for a single baffle and two half baffles of green mineral rock insulation with the measured, numerical, and empirical *TL* results. It can be seen that the results matched fairly well, especially at the lower frequencies where little absorption is occurring, but at the high frequencies, the results diverge. It was observed, through several examples, that the empirical method tended to over-predict the *TL* values at the peak frequencies. It is for this and all of the above reasons that a numerical model is preferred, since it can consider all of the design issues that the empirical model cannot.

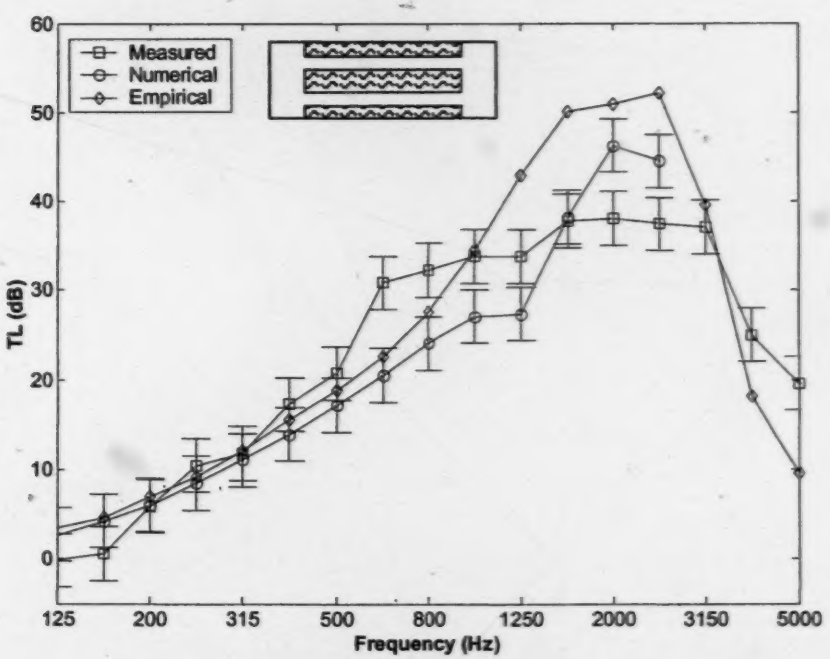

Figure 52. *TL* Results for a Single Baffle and Two Half Baffles of Green Mineral Rock Insulation

Yet another more recent method, is that proposed by Brandstatt [21]. It is essentially the same as that proposed by Munjal and Beranek, but much more detailed. A larger amount of data has been collected and a much more rigorous

statistical analysis has been completed to come up with better empirical data. This data and the method associated is available in a program called CompAS [21]. The results obtained from this program (although not evaluated by the author) appear to be much better than those obtained by the previous methods available (as indicated by the results presented in the paper). It is important to remember, however, that this is still an empirical formula and falls prey to the same design issues that its predecessor has.

5.6 Comprehensive Parametric Study

Once confidence in the numerical results compared to the measured values, was obtained, many of the geometric, bulk material, and environmental parameters were studied separately to see their effect on the *TL* of the system. The following sections were obtained from results of the numerical model of the scale silencer model. Unless otherwise noted, the cross section of the duct modeled was 600mm x 600mm and the length of the baffles was 2250mm.

5.6.1 Baffle Length

The geometrical parameter that has the greatest impact on the overall *TL* of a silencer system is the length of the baffles. In most situations, it is advantageous to make the baffles as long as possible (given the space limitations) if a large amount of *TL* is desired. For the tests, a system of one single baffle in the middle (10cm thick) along with one half baffle at the top and bottom (5cm thick) was modeled. The R, Ω, and K_s values used were 20,000 mks rayls/m, 0.8, and 1.0 respectively, and the temperature and pressure were 23°C and 700 mmHg. Baffle lengths were varied between 10cm and 3m.

Figs. 53 and 54 show the *TL* results with several of the different baffle lengths tested. It can be seen that, in general, as the length increases, the *TL* increases. This effect is frequency dependent and has less of an impact at the very high frequencies because the high frequency sound is mostly absorbed in the first part of the baffles,

and longer lengths will not add much to the absorption. At low frequencies, however, there is a definite gain by increasing the length.

Fig. 55 shows the dB ratio of *TL* for different baffle lengths. As a general rule, it can be said that as the length changes by a factor of 2, so does the *TL*. Similarly, factors of 3 and 4 (not shown) were also observed to have a similar effect. It was observed that this only started to become valid when the shorter of the 2 baffle lengths was at least as long as the larg est cross sectional dimension of the duct (i.e. width or height).

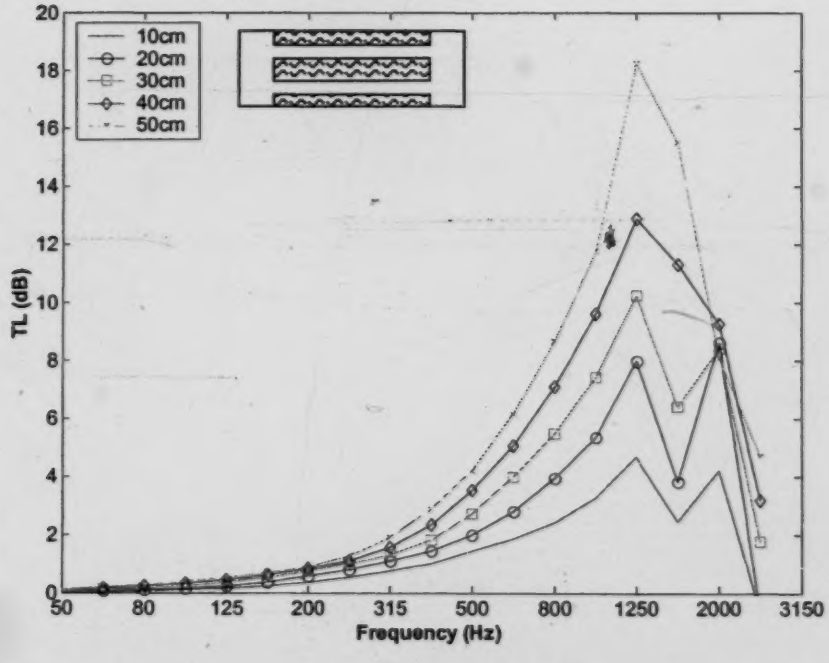

Figure 53. *TL* with Varying Baffle Length (10cm – 50cm)

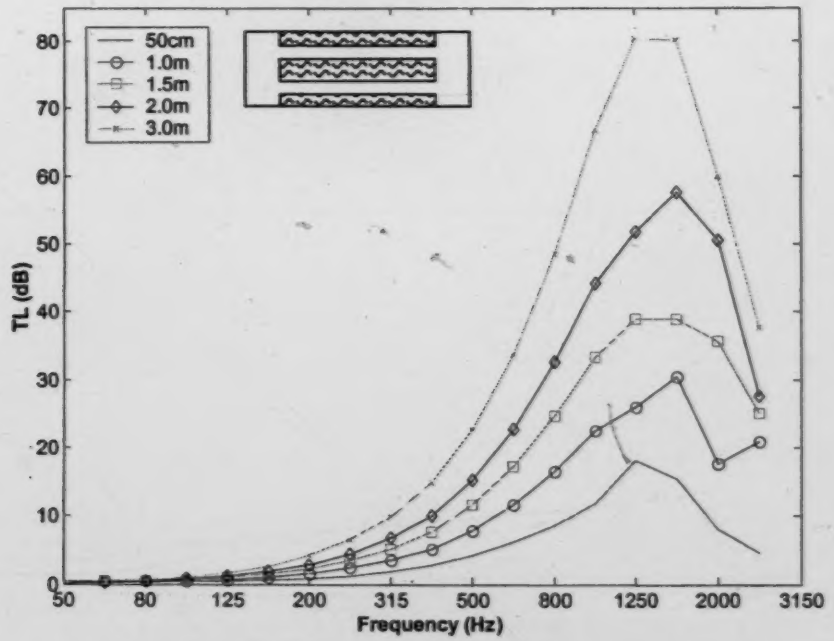

Figure 54. *TL* with Varying Baffle Length (50cm – 3.0m)

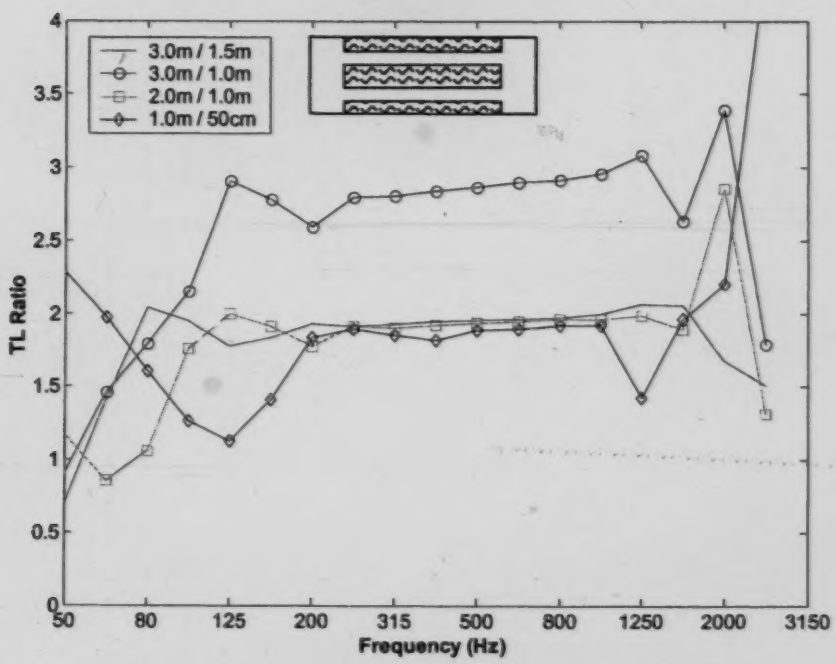

Figure 55. *TL* Ratio with Varying Baffle Length

5.6.2 Baffle Thickness

Similar to changes in length, an increase in the baffle thickness generally increases the *TL* values. The difference is with regards to the frequency dependency of the increase. It should be noted that the data presented was obtained by increasing the baffle thickness while maintaining the overall cross sectional dimensions and the baffle spacing constant. The result of this is that the percentage of open area decreased as the baffle thickness increased. This was done to eliminate the effects of baffle spacing on the study. The environmental variables and absorptive material properties, along with the overall silencer dimensions are the same as those mentioned in the previous section, and the baffle length was set to the default value of 2.25m.

Figs. 56 and 57 show the results of modifying the baffle thickness. It can be seen that as the thickness increased, the *TL* values increased. The effects are more pronounced at the higher frequencies first, and then start to move down to the lower frequencies. This is expected since attenuation at higher frequencies is easier to obtain than at lower frequencies. The thickness of any absorptive material needs to be quite substantial before any appreciable gains in low frequency absorption are realized. Another result that can be seen in the figures relates to the maximum attenuation possible. Once all of the energy is essentially absorbed, an increase in baffle thickness will not improve the *TL* values. Again, this happens at the higher frequencies first and then starts to filter down to the lower frequencies.

One final important note is with regard to the *TL* levels. The figures display very high values. This is due to the fact that the numerical model is not taking noise flanking into account. Therefore the theoretical maximum *TL* values are almost limitless. In reality this is not the case and most silencers are only capable of maximum *TL* values of about 50dB. The important thing is the relative difference between the various curves, and not so much what the amplitudes are.

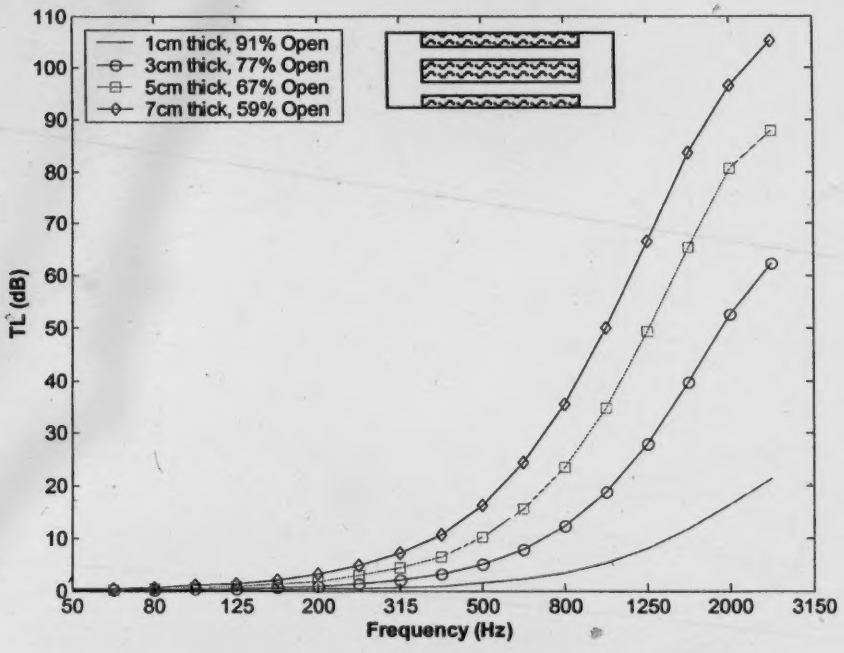

Figure 56. *TL* Values with Varying Baffle Thickness (1cm-7cm)

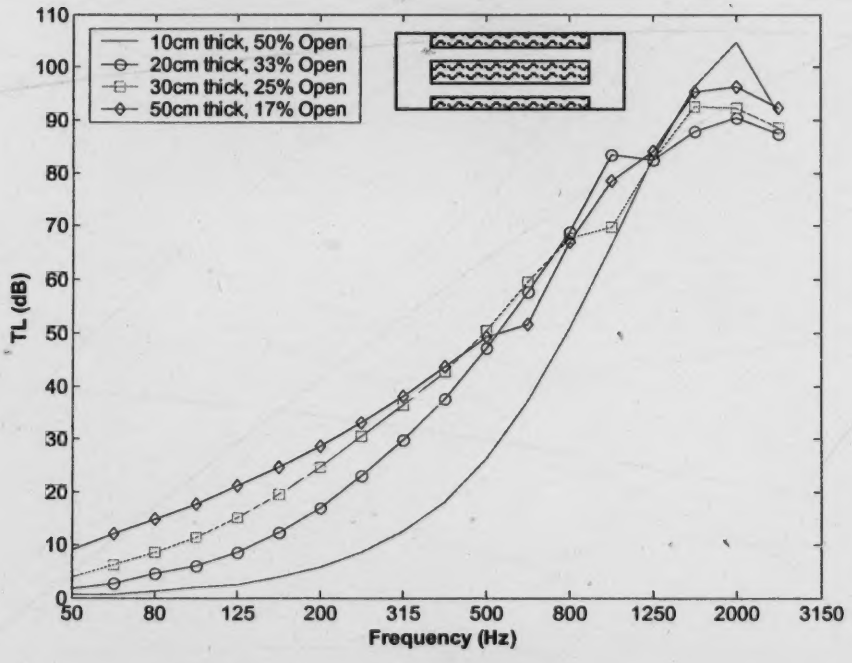

Figure 57. *TL* Values with Varying Baffle Thickness (10cm-50cm)

5.6.3 Baffle Spacing

The effect of changing the baffle spacing is an inverse one to that of changing the baffle thickness. As the baffle spacing increases, the *TL* generally decreases. In order to eliminate the baffle thickness effects, the thickness was kept constant at 10cm. Therefore to change the spacing, while keeping the thickness the same, the total height of the silencer was modified and, as a result, so was the percent open area. The environmental conditions and the absorptive material properties were set to the same as the previous sections, and the total length of the baffles was set to 2.25m.

Figs. 58 and 59 show the effects of changing the baffle spacing and, as a result, the percent open area. Again, similar to the baffle thickness study, it is important to note that the *TL* amplitudes are not necessarily important on their own and that it is the relative changes that are of concern. It can be seen that as the baffle spacing increased, the *TL* values decreased. Also, at higher spacing values, the *TL* values behave normally below a certain frequency range and then drop off sharply beyond this point. This occurs because after this region, the spacing is so large, that the sound waves can pass through essentially un-impeded.

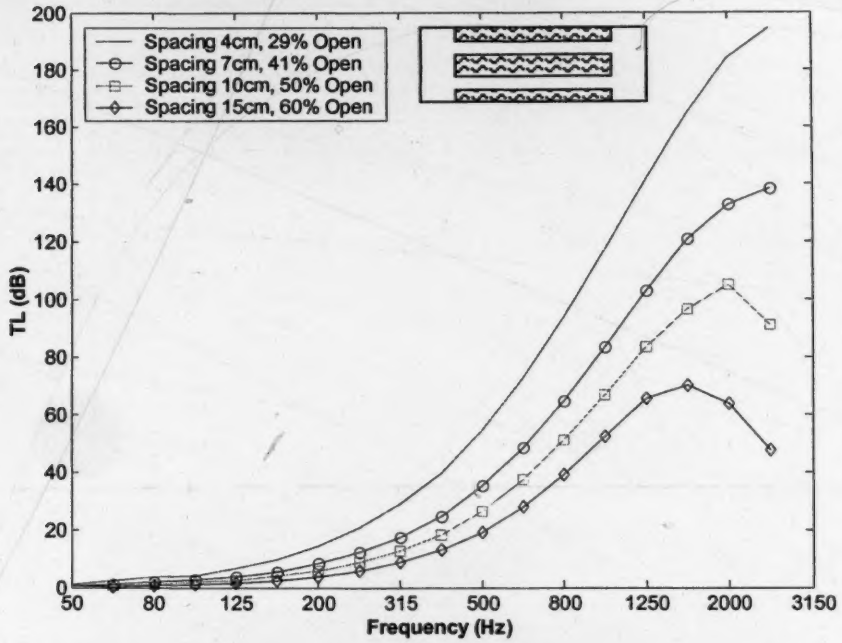

Figure 58. *TL* Values with Varying Baffle Spacing (4cm-15cm)

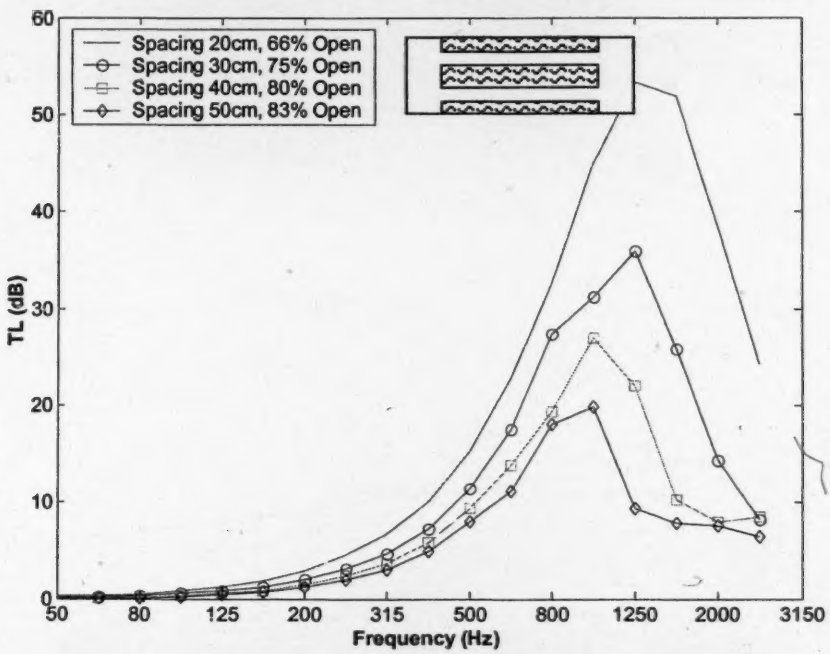

Figure 59. *TL* Values with Varying Baffle Spacing (20cm-50cm)

5.6.4 Percent Open Area

There was no specific study done to see the effects of changing the percent open area, since this parameter could not be changed while keeping both the baffle spacing and thickness constant. Since both of the previous two sections dealt with modified percent open area, conclusions will be drawn based on their data.

It is apparent, from Figs. 56-59, that as the percent open area increases, the *TL* decreases. This is very analogous to the sound transmission through a solid wall section where the amount of open area (compared to the wall area) has a large impact on the total sound reduction. The main difference is that with sound transmission through a wall, there is a large difference for a small change in percent open area at first, and then the differences reduce as the hole opens up. The same general trend was not observed with the calculated parallel baffle silencer *TL* values. It appears that, while the relationship is not linear, there is a fairly constant progression in decreasing *TL* with increasing percent open area.

5.6.5 Staggered Baffles

A common practice in silencer design is to have multiple sections of baffles oriented in a staggered fashion, as illustrated in Fig. 60.

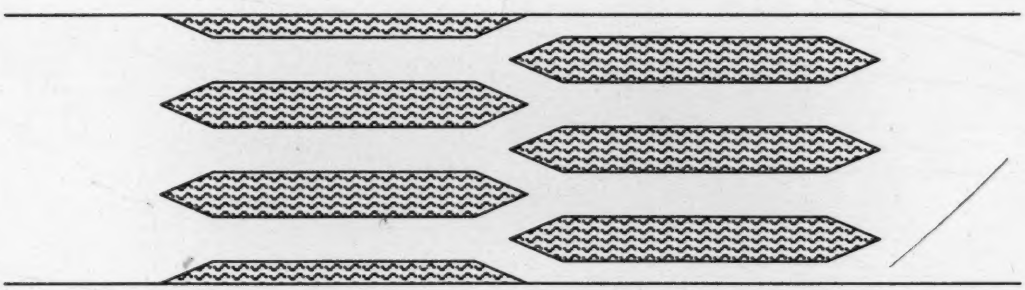

Figure 60. Parallel Baffle Silencer with 2 Staggered Baffle Columns

The reason this is done is to eliminate the line of sight through the silencer. This has a large impact on the high frequency *TL* characteristics of the silencer. Fig. 61 shows the results of staggering vs. non-staggering for a similar model to that shown in Fig. 60. The two versions modeled had the same baffle thickness, spacing and absorptive material composition. The total baffle area was essentially the same and the total length of the system was unchanged. The difference between the two is that the non-staggered model had one column of 2 full and 2 half baffles along the entire length of the silencer. The staggered model had 2 columns. The first column was similar in composition to the non-staggered model with the exception that the baffles were essentially half as long (similar to the illustration in Fig. 60). The second column was composed of 3 full baffles, again approximately half as long as the full length baffles. It can be seen that at the lower frequencies, there is little to be gained by staggering the baffles. At the higher frequencies, however, the increase in *TL* is quite substantial. The frequency peak at which the largest increase in *TL* was realized, corresponds to the half wavelength of the baffle spacing. It cannot, however, be concluded at this time if this is a general rule. Further study into staggered geometries is required before any substantial conclusions can be drawn. Several different baffle configurations with variable spacing would be required, which would require a large physical model (larger than the current one) for verification.

In general, the price paid for this increase in *TL* is an increase in pressure drop across the silencer (the flow path becomes more difficult), but there are many applications where this increase in pressure drop is a worthy price to pay for the increase in *TL*. For more on the pressure drop across the silencer, refer to §6.4.

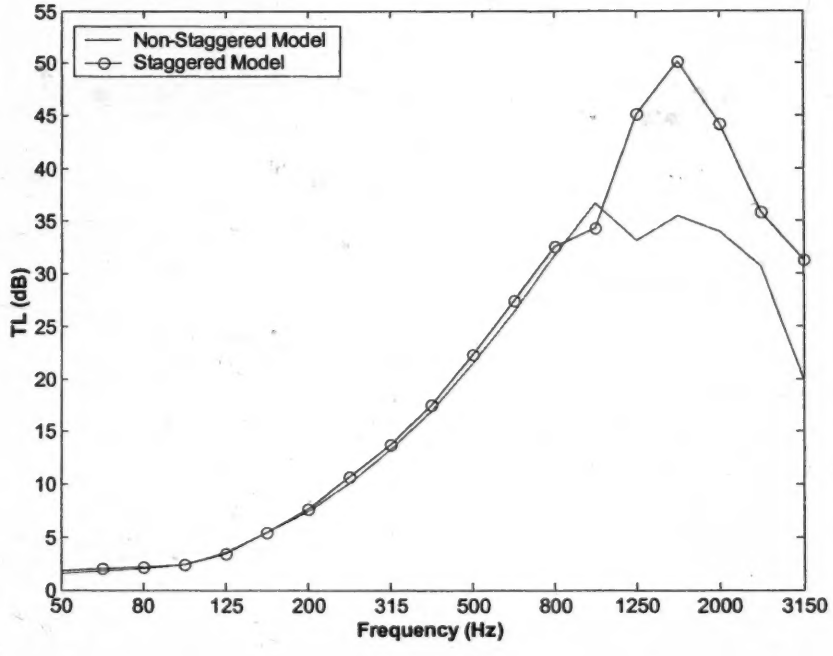

Figure 61. *TL* with Equivalent Staggered and Non-Staggered Baffle Models

5.6.6 Flow Resistivity Values

With the geometrical concerns addressed, the attention was then turned to the bulk acoustical absorptive material properties. As stated earlier, the most important bulk material property is the flow resistivity, *R*. It is a value that quantifies the material's resistance to a fluid flowing through its pores. It is also the quantity that most directly relates to the material's ability to absorb sound. A numerical model was created with a single full baffle in the middle and 2 half baffles at the walls. The total length of the baffles was 1.0m with a thickness of 15cm, and a percent open area of 50%. This geometry was used for the porosity and structural factor sections as well as temperature and pressure effects. For this model, the structural factor was held at 1.0 and the porosity was set to 0.8. As before, the air temperature and pressure were set to 23°C and 700 mmHg respectively.

Figs. 62 and 63 show the effects of changing *R*. It can be seen that for high frequencies as *R* increases, the *TL* increases. At low frequencies the opposite happens and as *R* increases, the *TL* decreases. It is not known why the low frequency attenuation behaves in this fashion, however, the *TL* differences at these low frequencies for various *R* values, were quite small and are essentially negligible. The other important result seen on the figures is that the *TL* values increase with increasing *R* up to a certain point, and then they decrease with increasing *R*. This is expected, because increasing *R* is the result of a more densely packed volume of material. After a certain point, this material will become so densely packed that its absorption will reduce and it will begin to reflect more of the sound energy than it had before. The *R*-value of 200,000 mks rayls/m (which is much higher than practical for effective sound absorption) illustrates this fact very well. The *R*-value at which the maximum attenuation is reached, is different for every situation. Depending on the baffle geometry, the porosity, and the atmospheric conditions, etc… this value will change. The problem then becomes one of optimization. For this particular geometry, the optimal *R*-value was approximately 20,000 mks rayls/m.

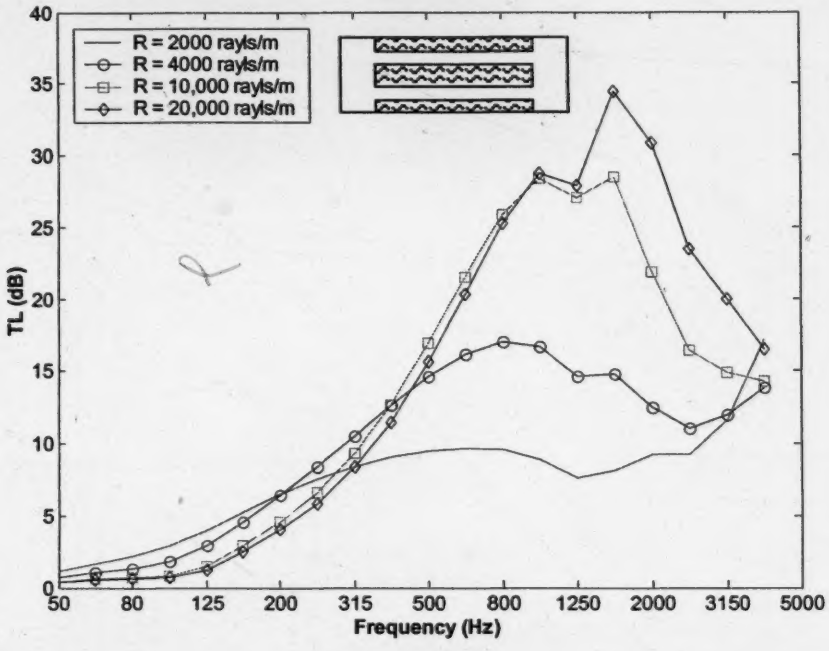

Figure 62. *TL* Values with Varying Flow Resistivity (2,000 – 20,000 mks rayls/m)

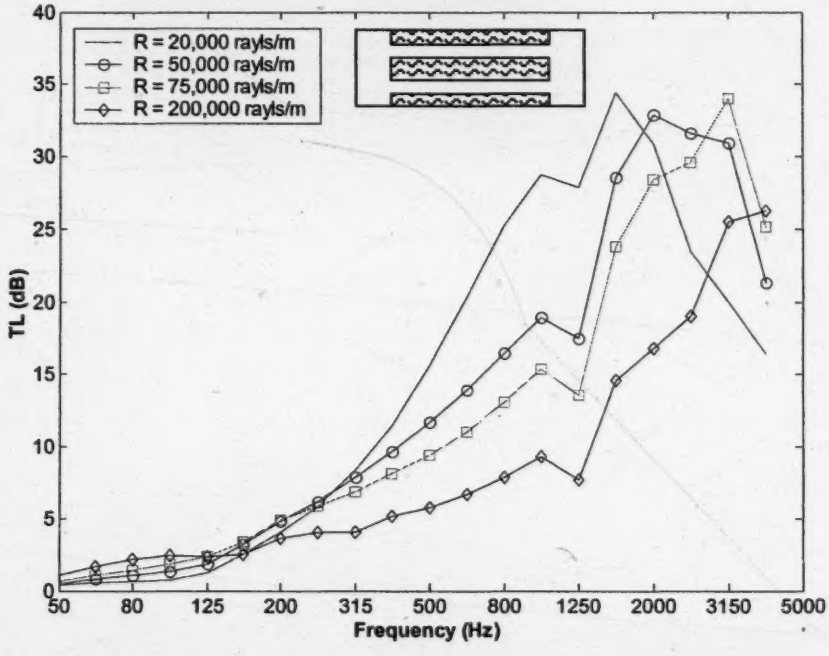

Figure 63. *TL* Values with Varying Flow Resistivity (20,000 – 200,000 mks rayls/m)

5.6.7 Porosity Values

The other major bulk acoustical material property is the porosity, Ω. This is the quantity that describes the ratio of open volume to the total volume (i.e. porosity for air = 1.0). Again, as in the case of R, a numerical model was created in which various Ω values were tested. The geometry was the same as in the §5.6.6, as well as the environmental properties and the structural factor. The R-value used was 20,000 mks rayls/m.

Fig. 64 shows the effects on TL of varying Ω through a large range of values. It can be seen that there is very little dependence of TL on Ω. At the very low and very high frequencies, the differences are negligible, and at the middle frequencies (where the largest differences occur) there was a very consistent shift of 1dB for every 0.05 change in Ω. Even at an extremely low Ω value of 0.2, the TL curve was very consistent with the others and its results were predictable. Testing indicated that the values of Ω are easily attainable to within ±0.05, which would result in very negligible variance in predicted TL values.

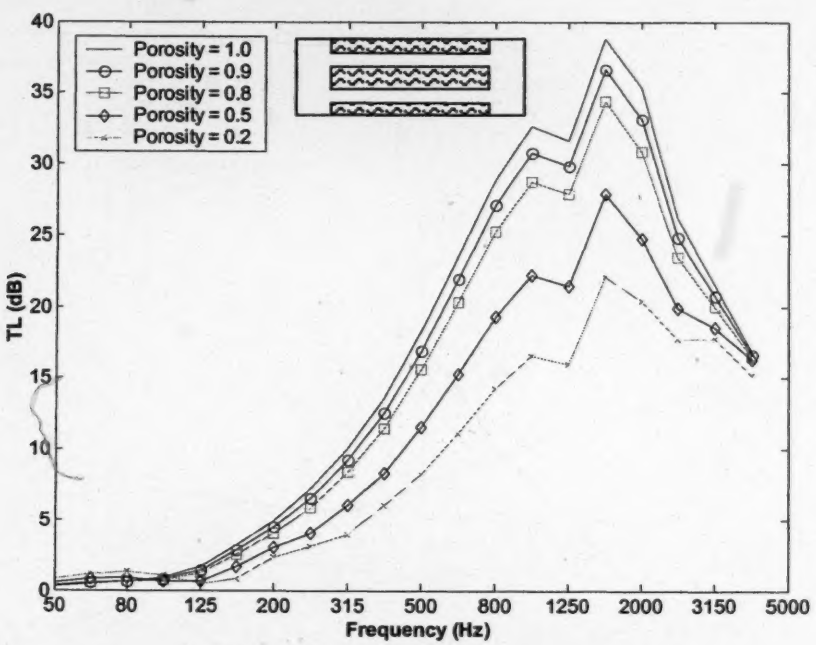

Figure 64. TL Values with Varying Porosity (1.0 – 0.2)

5.6.8 Structural Factor Values

The final bulk acoustical material property is the Structural Factor, K_s. This is a value that takes into account the viscous effects of the path traveled by the sound wave as it propagates through the material. Again, the geometry, and environmental conditions used were the same as §5.6.6. The R and Ω values used were 20,000 mks rayls/m and 0.8 respectively.

Fig. 65 shows the TL results with K_s varied from 1.0 to 5.0. It can be seen that, similar to the porosity data (Fig. 64), at the very low and very high frequencies, large changes in K_s resulted in negligible changes in TL. At the mid-frequencies, there was a very noticeable change in TL with changes in K_s. Typical accuracy for K_s fell in a range of ±0.2, which would result in a maximum change of approximately 2dB (based on the model used, this value could change slightly for other geometries). It can be seen, however, that the TL results are much less dependent on K_s than they are on R.

The other important result seen on Fig. 65 is what happens when K_s is increased to a very large value. It was observed that at values above $K_s = 3.0$, the TL curve began to exhibit a sinusoidal response. This can be seen starting to take shape with $K_s = 3.0$ and becoming very pronounced with the value of $K_s = 5.0$. Of course, this result is specific to the given geometry and remaining bulk material parameters, but the same general trend was observed with other configurations. This serves as additional evidence that the value of K_s should be kept as small as possible, (ideally under 2.0) and should rarely exceed a value of approximately 4.0 (based on test observations).

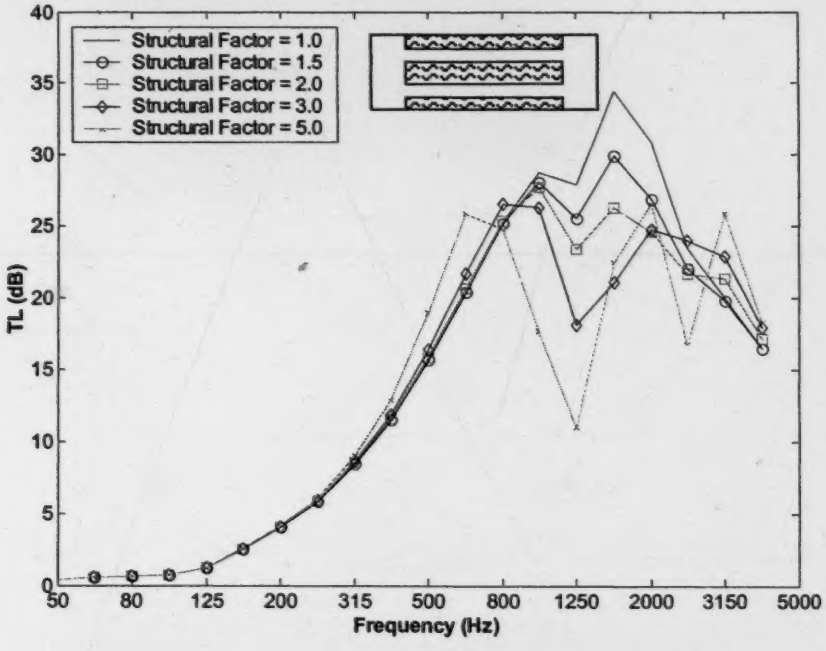

Figure 65. *TL* Values with Varying Structural Factor (1.0 – 5.0)

5.6.9 System Temperature

One of the main advantages of the use of a numerical model is that a wide range of environmental conditions can be imposed which might otherwise be very difficult to simulate in a laboratory environment. Using this advantage, several air temperatures were imposed ranging from –100°C to 2000°C. The geometry used for the models was similar to that outlined in section §5.6.6 and R, Ω, and K_s values were 20,000 mks rayls/m, 0.8, and 1.0 respectively. In addition an atmospheric pressure of 700 mmHg was used.

Figs. 66 and 67 show the *TL* results for the wide range of temperatures used in the model. It can be seen that as the temperature increases, the *TL* curve shifts to the right (higher frequencies) and the *TL* drops at frequencies lower than the peak. This result is supported by Beranek [16] in which an explanation is stated as:

> "...due to the increase in the propagation speed of sound with increasing temperature. In addition, one also observes distortion in the shape of the attenuation-versus-frequency curve. This is caused by the increase in the flow resistivity of the porous material, which in turn is due to the increasing viscosity with increasing temperature."

By this, it is apparent that that the operating temperature of the system is an important factor in the design. However, small differences in temperature do not affect the results by an appreciable amount, as illustrated by the 0°C and 50°C curves.

It should also be noted that using the numerical model, it is possible to assign different temperature values to various regions of the model. This would be useful if there is a large temperature gradient from the inlet to the exhaust of the silencer. Again, by using the numerical analysis, various temperature gradients could be tested.

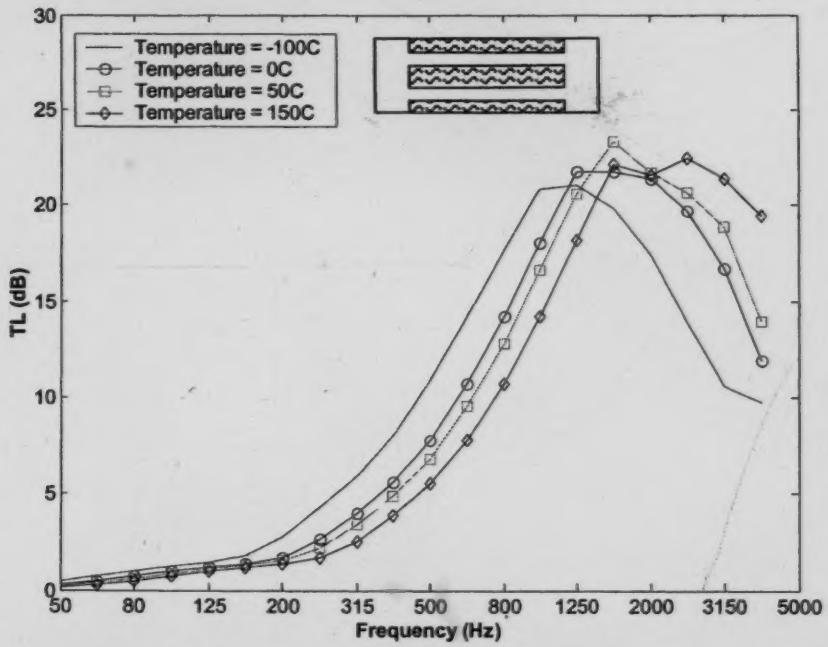

Figure 66. *TL* Results with Various Air Temperatures (-100°C – 150°C)

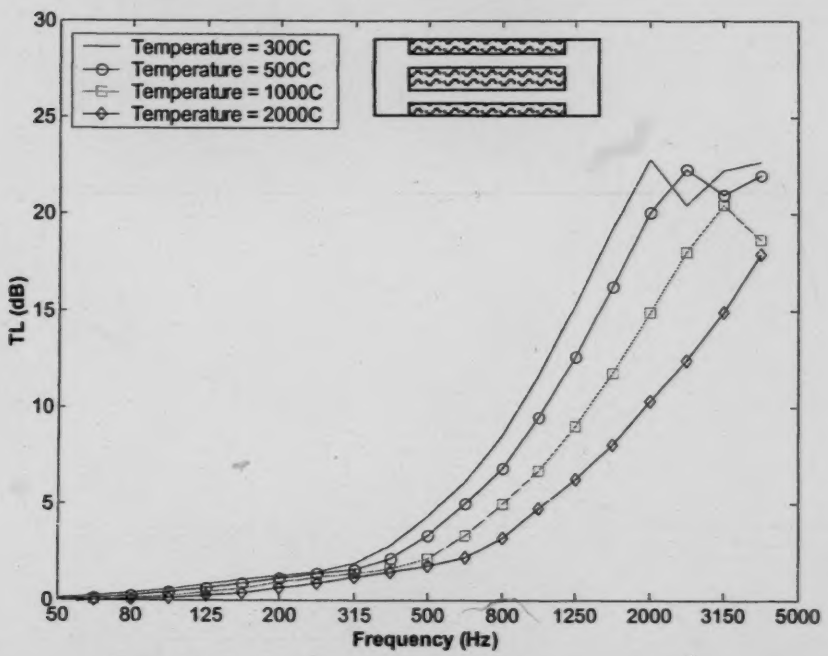

Figure 67. *TL* Results with Various Air Temperatures (300°C – 2,000°C)

5.6.10 System Pressure

Very much like the operating temperatures in a silencer system, various operating pressures can be modeled numerically much easier than recreating them in a laboratory situation. Various pressure values were modeled ranging from 690 mmHg to 770 mmHg. All geometrical and absorptive conditions were the same as in the previous section, and a temperature of 20°C was used.

Fig 68 shows the *TL* results for the various system pressures tested. It can be seen that the effects of a wide range of pressure values are negligible over the entire frequency range tested. This is not a surprise since the sound pressure level measurements are taken relative to the ambient pressure, so the effects of the variable ambient pressure should not be a factor, especially over such short distances.

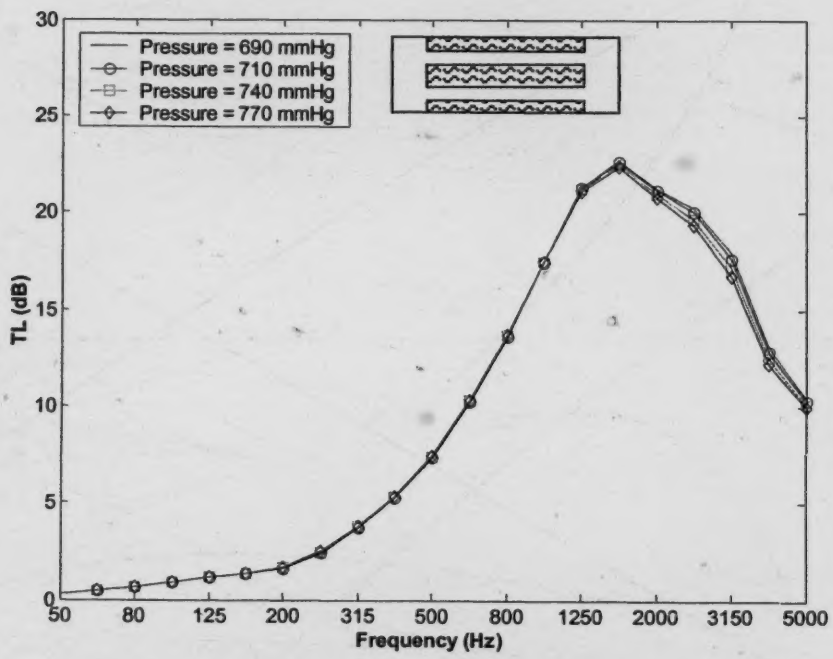

Figure 68. *TL* Results with Varying Atmospheric Pressure

5.7 Conclusions

Several important steps in the research work were discussed in this chapter. First, the construction of the physical model was presented, along with the various factors and limitations to consider while testing. Next, the *traditional* and 3-point measurement methods for *TL* were compared and it was found that the 3-point method, with a slightly different derivation (required because of the difficulties in obtaining complex pressures with the data acquisition equipment) gave similar results to the *traditional* method (accepted as the standard to which all other methods are compared).

With all of the numerical model and physical model methods taken care of, the *TL* results obtained from each method were compared for various geometrical and absorptive material configurations. It was shown that the results matched very well, with the majority of the discrepancies associated with the bulk material property characterization in the numerical model. Also, the results obtained using current empirical methods were compared to those obtained with the numerical models, and shown to be generally comparable. These empirical methods, however, are not able to handle the wide range of geometrical and environmental configurations that a numerical method deal with.

Finally, a comprehensive parametric study was conducted where various geometrical, material, and environmental properties were examined separately to see how each affected the *TL* results obtained in the numerical model. Table 3 outlines a summary of each of the parameters, and what their effect was.

Table 3. Summary of Effects of Various Parameters on Transmission Loss

Parameter	Effect on Transmission Loss (TL)
Baffle Length	As length increases, *TL* increases. In general changing length results in a linear change in *TL*.
Baffle Thickness	As thickness increases, *TL* increases, up until the point of maximum absorption where no more sound reduction is possible. These results are frequency dependent with higher frequencies being reduced first, then lower frequencies. Note that at very low frequencies, a large amount of material is required for sound absorption.
Baffle Spacing	As baffle spacing increases, *TL* decreases. At high enough frequencies, the spacing allows the sound waves to essentially pass un-impeded, which means that as the spacing increases, this frequency decreases.
% Open Area	As % open area increases, *TL* decreases. As in baffle thickness and spacing, the results are frequency dependent based on the thickness of the material and the spacing between baffles.
Staggered Baffles	Keeping all other parameters the same (i.e. total baffle volume, and material type), staggered baffles will yield higher *TL* values than the equivalent non-staggered orientation. This increase in *TL* is predominant at higher frequencies due to the loss of line-of-sight through the silencer. Low Frequencies simply pass through as they would without the staggering.
Flow Resistivity	As flow resistivity increases, *TL* increases up to a maximum point where the material starts to act less as an absorber and more as a reflector. This maximum point is different for each material.
Porosity	As porosity decreases, *TL* decreases, however, small changes in porosity (i.e. 0.1) result in negligeable changes in *TL (2 dB)*.
Structural Factor	*TL* is not as dependent on structural factor as on resistivity. Only at middle frequencies does any effect of changing the structural factor appear. Beyond values of 3, the *TL* results start to exhibit sinusoidal results. The value of structural factor should idealy be kept under 2.0.
Temperature	As temperature increases, the *TL* curve shifts to the right (higher frequencies), and the *TL* drops at frequencies lower than the peak. However, small changes in temperature result in negligible changes in *TL* (a change of 50 degrees C, results in a TL change of less than 1 dB).
Pressure	Large changes in pressure result in negligible changes in *TL*. A range of 690 mmHG to 770mmHG resulted in a maximum of 1dB change.

6 Design Considerations

6.1 Introduction

The previous chapters dealt with the fundamental issues concerned with using a numerical method to characterize an acoustical silencer. Factors such as geometry, sound absorbing material, and environmental concerns were addressed and quantified. This chapter deals with some of the other design concerns which will have an effect on the design process.

6.2 Computational Effort

One of the main concerns with the use of a numerical method is the time involved in setting up and solving the system of equations required to describe the system being evaluated. Even with the speed of modern computers, it is very easy to have a system that may take many hours or days to solve.

The factor that directly affects the number of equations, and therefore the time required, is the number of elements in the model. Obviously, it can be seen that as the model grows physically, the number of elements will increase. Another factor that affects the number of elements is the size of each element. The smaller the element, the more of them are required to fill the model. Finally, the element type effects the number of elements based on the number of nodes per element. For example, more linear elements would be required than quadratic or cubic elements because the higher order elements contain more nodes. The element size has a direct relation to the frequency range that can be accurately modeled by the system. In order to accurately interpolate the sinusoidal nature of sound waves, a minimum of 6 nodes per wavelength are required. With this constraint, it can be seen that as the wavelength decreases (or in other words, as the frequency increases) the element size needs to be made smaller to properly solve the system at the small wavelengths (or high frequencies).

It is also important to realize the nature of how the equations themselves are set up in order to appreciate the effect of increasing/decreasing the number of elements. For example: with a two-dimensional model, cutting the element size in half (in order to double the maximum frequency attainable) results in an increase of 4-times the number of elements. Since, the equations are in a matrix format, this makes the matrix 4x4-times larger for an increase of 16-times. Suddenly, the number of equations that need to be solved has grown dramatically. It would, therefore, be beneficial to have methods to simplify the model to decrease the number of equations. While there are potentially many ways in which this can be accomplished, the three with the greatest impact will be discussed.

6.2.1 2-Dimensional vs. 3-Dimensional

The first and best way to realize a time savings is by using 2-D models instead of 3-D models, if the geometry permits. For example, with the case of the parallel baffle silencer model used for the research, the cross section is the same throughout the entire depth of the model. In a case like this, a simple 2-D cross section numerical model can be used to predict the same results as the full 3-D model. The advantage to this is in the number of elements required for the discretization of the area vs. the volume. As previously discussed, increasing the number of elements increases the time in an exponential fashion, therefore the jump from 2-D to 3-D has a very large impact on the time required.

The concern with this method is that it only works if the sectional view is the same throughout the entire depth. Models of round silencers, or square ducts with irregular sound absorbing material will not transfer from 3-D to 2-D directly. The best way to deal with these types of geometries is to take advantage of lines of symmetry, as discussed in the next section.

6.2.2 Symmetry

The other time saving method is to exploit any geometrical symmetry's in the model. By simply cutting the model in half, as shown in Fig. 69, the time can be cut in half (approximately).

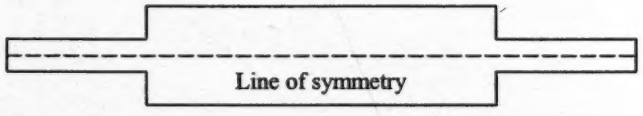

Figure 69. Planar Symmetry for Single Expansion Chamber

For circular shapes with a plane of axi-symmetry, the three-dimensional tube section can be modeled as an area and then numerically revolved around an axis to form the whole volume, as shown in Fig. 70. This can reduce the number of equations down from those required for a three-dimensional object to those required for a two-dimensional object (approximately).

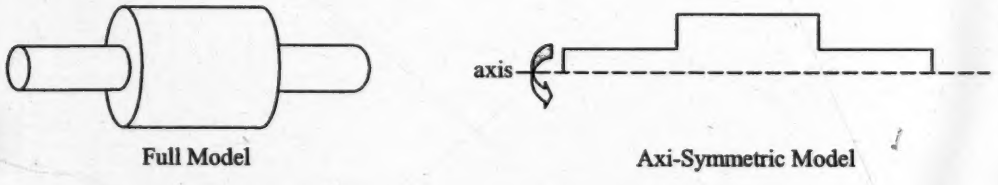

Figure 70. Axi-Symmetry for Three-Dimensional Single Expansion Chamber

In order to verify the use of symmetry in the numerical model, the full 3-D expansion chamber from §2.5.2 was modeled as a full model, a half model, and an axi-symmetric model. Figure 71 shows that the full, half, and axi-symmetric models matched exactly with each other. Utilizing lines of symmetry could be applied to more complicated geometry's to greatly reduce the time required and to simplify the model.

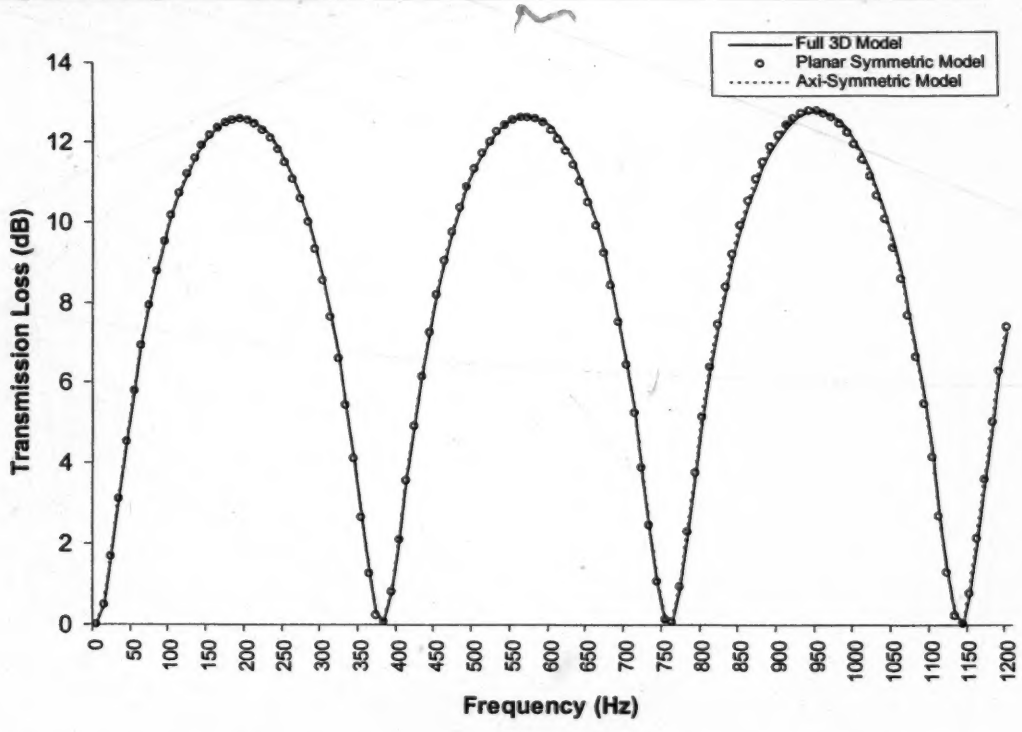

Figure 71. Transmission Loss for Silencer with Full 3-D, Planer Symmetric, and Axi-Symmetric Numerical Models

With regard to a parallel baffle silencer, the multiple symmetries in the model can be used to reduce a large problem into a much smaller one. If the silencer is simply composed of several equally spaced baffles, the system can be approximated by a single section representation. Fig. 72 shows an example of a parallel baffle silencer with 2 full baffles and 2 half baffles, and how it can be reduced to a system with just 2 half baffles.

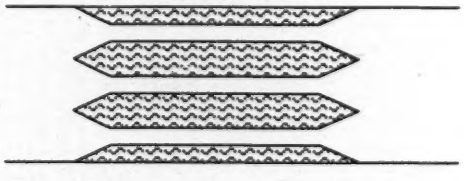

Full Section with 2 full and 2 half baffles

Symmetrical model with 2 half baffles

Figure 72. Parallel Baffle Symmetry Example

Various tests were performed with several different configurations of baffle numbers and reductions to planar symmetric and single section representations, and there was no difference in the *TL* results for the full system or any of the symmetrical reductions of that system. Fig. 73 shows the results obtained for a full model with 3 full and 2 half baffles, the half model with 1 full and 2 half baffles and the minimum model with 2 half baffles.

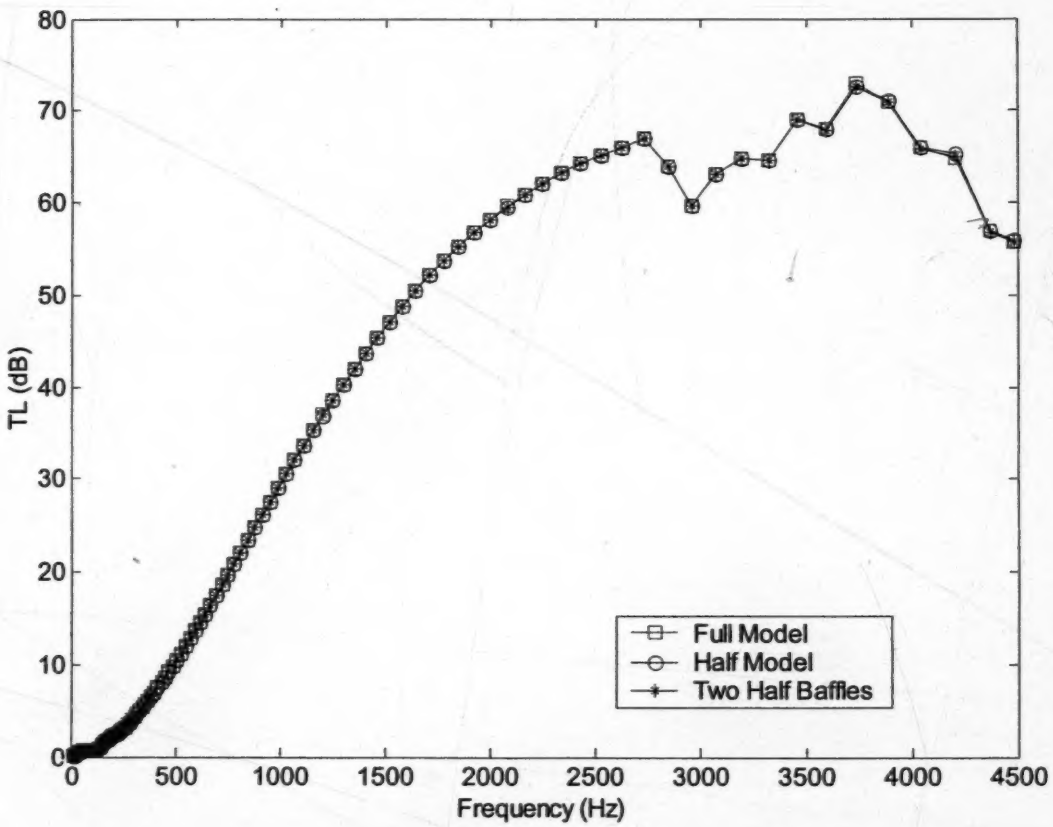

Figure 73. Full Model, Half Model, and Two Half Baffle Model *TL* Results

The reason why a full baffle can be represented as two half baffles along the wall is due to the path the sound wave takes while traveling through the baffles. For the full baffles, as shown in Fig. 74, the wave passes through the entire baffle and its

energy is reduced along the way. When passing through the half baffles along the walls, the total path is composed of the passage through the baffle to the wall (which is modeled as completely reflective) and then the reflected wave passage back through the baffle into the open area of the silencer. Thus the total path length is equal to that of the full baffle, and the amount of energy absorbed will be equal.

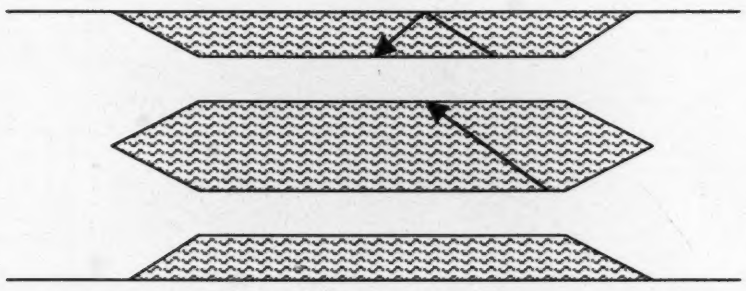

Figure 74. Sound Wave Paths Through Baffles in Silencer

By employing these geometrical symmetries, great time-savings can be obtained. It is therefore advantageous for any model to take advantage such symmetry's before any other time saving technique is applied.

6.2.3 Multiple Models

One other time reduction technique involves dividing the solution scheme into models with different element sizes. The reason this is beneficial, is that for the lower frequencies, it is possible to have a much coarser mesh. Due to the nature of human hearing (based approximately on a percentage scale), most of the frequencies that need to be calculated for a whole octave or 1/3 octave analysis are at the lower frequencies (less than 1000 Hz). Using a finer meshed model to calculate these lower frequencies is unnecessary and will simply be a waste of time.

For example: using 1/3-octaves between 20-8000Hz, there would be a total of 27 center frequencies to be calculated. One can model the geometry with an element

size that calculates the 20-4000Hz range (for 24 out of the 27 center frequencies), and then another finer meshed model to get the remaining 3 center frequencies, as shown in Fig 75. By doing this, the mesh size can be cut in half (resulting in a matrix that is 1/16 the size as that required for the 8000Hz frequency) for 89% of the calculations. When applied to a particular simple two-dimensional system, a reduction in time of 13-times was achieved (compared to performing all the calculations with the high density mesh). Of course this time reduction is case specific but similar results should be attainable in most situations.

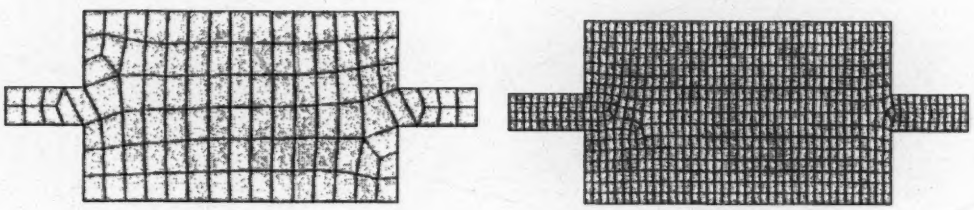

Figure 75. Fine and Coarse Mesh Sizes for Similar Geometry

It is this kind of time saving technique that would lend itself well to an optimization scheme. Due to the fact that additional meshed models are required, the time will increase. However, as discussed in the previous paragraph, by separating the solution into different frequency ranges, great time savings can be achieved. Depending on the geometry and frequency range of interest having more than 2 different element sizes may result in even faster solution times. On the other hand the most efficient solution may result from only one element size. Further investigation is required to determine which would be the best method for solution.

6.3 Perforated Material

Typically, acoustic silencers which employ the use of sound absorbing materials also use some sort of perforated liner material (usually, perforated mesh metal) as a protective cover. This perforated metal is used as a barrier to contain the absorptive material and keep it from blowing out of the silencer system. Because the perforated metal is installed in between the sound absorbing material and the open passage, its acoustical effects are very important. Fortunately, there has been extensive work done in this field. In his book, Schultz [20] describes the many acoustical uses and implications for perforated metal material. The proposed value for rating the acoustic transparency of the perforated material is the transparency index (*TI*). This index is calculated by the following:

$$TI = \frac{nd^2}{ta^2} = \frac{0.04P}{\pi ta^2} \tag{38}$$

Where:

n = number of perforations per square inch

d = perforation diameter (in)

t = sheet thickness (in)

a = shortest distance between holes (in)

P = percent (not fractional) open area of sheet.

Once the *TI* is calculated, Fig. 76 can be used to determine the frequency dependent sound attenuation caused by the perforated metal. It is apparent that as the *TI* increases, the amount of attenuation by the perforated metal decreases. Also, as the frequency decreases, the attenuation decreases. The ideal case is to have zero attenuation, which would indicate a completely acoustically transparent material. What is important to note from Eq. 38, and Fig. 76, is that it is possible to have two perforated materials with the same percent open area, and different perforation orientation (different n,d and a values) which would result in different levels of acoustic transparency. In general, as the percent open area increases, so does the *TI* value, but it is stressed that this is not always the case.

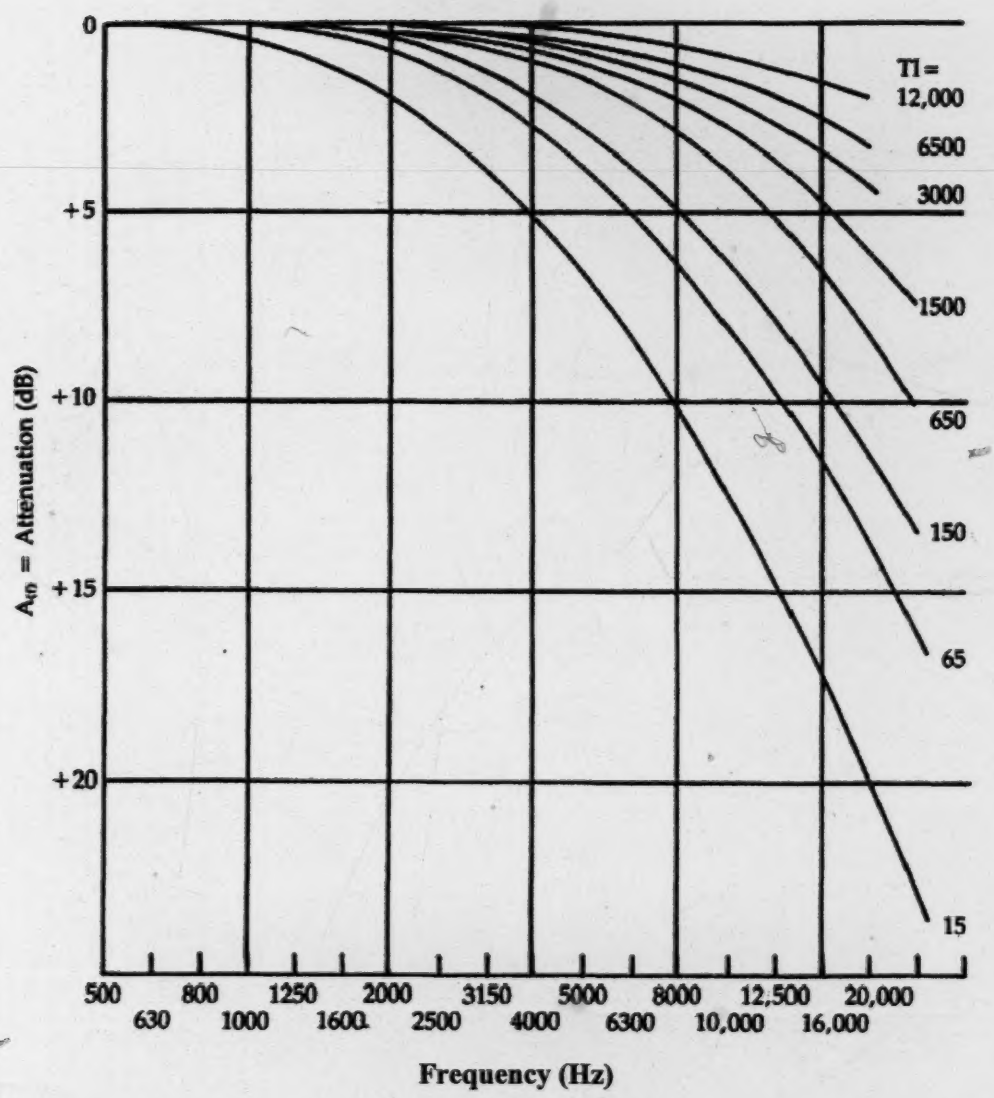

Figure 76. Perforated Material Attenuation with Various Transparency Index Values
(Obtained from Acoustical Uses for Perforated Materials: Principles and Applications, by Theodore J. Schultz, Ph.D.[20])

In order to confirm the use of Eq. (38) and Fig. 76, a tests were conducted in the physical silencer model with and without perforated material. An installation of one full baffle and two half baffles of green mineral rock insulation was used with and without the inclusion of the perforated metal mesh. The metal mesh had the following geometrical parameters (d = 0.1 in, b = 0.188 in, t = 0.03 in, n = 33 holes/in^2, P = 25.9%, a = 0.088 in). Fig. 77 shows the *TL* results for the two configurations tested.

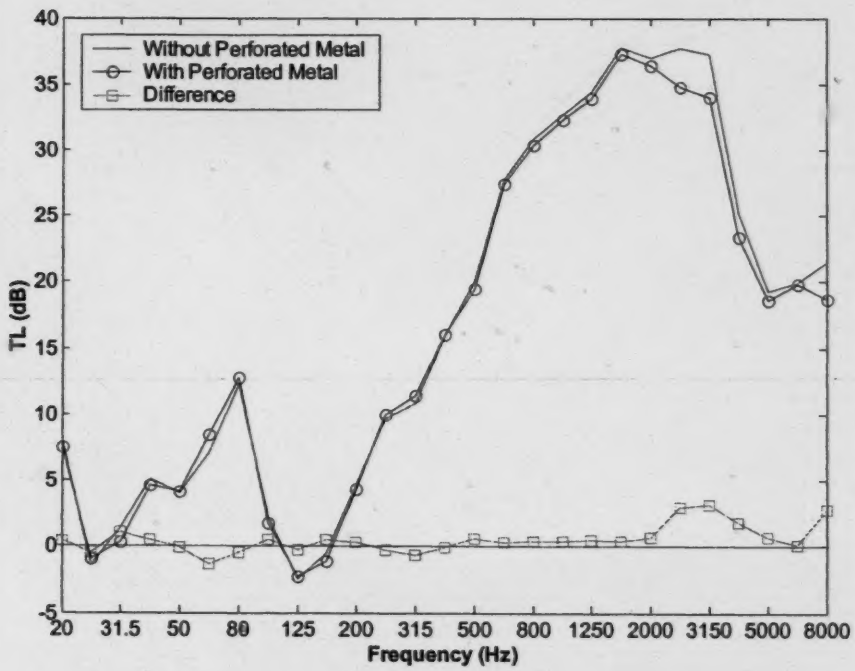

Figure 77. TL Results With and Without Perforated Metal Mesh

It can be seen by Fig. 77, that there was essentially no difference between the results with and without perforated material. The calculated transmission index (using Eq. 38) was 1420. Using Fig. 76, the corresponding attenuation values at some of the whole octave center frequencies were calculated, as shown in Table 4.

Table 4. Predicted Perforated Material Attenuation

Frequency (Hz)	1000	2000	4000	8000
Attenuation (dB)	0	0.5	1.5	2

Obviously, the predicted attenuation is very low across most of the useful frequency range. Also, the fact that the attenuation increases at the higher frequencies, matches the results shown in Fig. 77, where the two curves start to deviate from each other more at the high frequencies. It can, therefore, be concluded that by using Eq. (38), and Fig. 76, the effect of the perforated material on the acoustic performance of the system can be predicted. Note also that this method could easily be incorporated into a simple program which would accept the initial variables and produce a chart of attenuation values, similar to Table 4.

The main advantage in knowing that the formulations presented in this section can be used to predict the performance of the perforated material deals with the numerical model. For most cases, it is not always necessary to include the perforated material in the numerical model, since it is easy to add in the effects after the model has been solved. Including the perforated material increases the time required for the numerical mesh generation, and requires a finer element size to properly account for the perforations. This can become a large problem when the size of the perforations is very small (materials can easily have 3mm – 5mm perforation diameters). The numerical mesh size required to properly model geometries of this scale is very small which would result in a very high element count for the model.

6.4 Pressure Drop

One of the most important design considerations is how the silencer is going to affect the rest of the mechanical system in which it is installed. The biggest concern deals with the effective pressure drop across the silencer. In almost all design cases, there are limits set for the total pressure drop that the silencer is allowed to have. The problem is that the design factors which provide good acoustical performance also tend to increase the total pressure drop. Because of this, the final

design is usually a balance between what the acoustical goals are, and what the mechanical system limitations are. Fortunately, the parallel baffle design typically results in smaller pressure drops than that of reactive silencers such as expansion chambers. It is for this reason that parallel baffle silencers are typically chosen for applications where the total pressure drop is of great concern.

In order to calculate the total pressure drop across the silencer, the geometry and the fluid flow conditions are required. The following equation, outlined by Beranek, [16] can be used to calculate the pressure drop:

$$\Delta P_T = \frac{\rho v_p^2}{2}\left(K_{entrance} + K_{exit} + \frac{PLK_f}{A}\right) \tag{39}$$

Where:

ΔP_T = total pressure drop (Pa)

ρ = density of fluid (kg/m^3)

v_p = silencer passage velocity (m/s)

$K_{entrance}$ = entrance loss factor

K_{exit} = exit loss factor

K_f = friction loss factor along baffle length

P = wetted perimeter (m)

A = total open area (m^2)

L = total length of baffles (m)

The loss factors are determined from a table of values that has several groups of geometry types. As shown in Fig. 78, the entrance and exit loss factors depend on the shape and dimensions of the inlet and outlet sections of the baffles (round, square, tapered, etc), while the friction loss factor depends on the length of the baffles and the baffle spacing.

Geometry	Loss Coefficient
Square Edge Nose 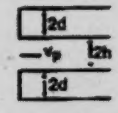	$K_{ENT} = \frac{0.5}{1 + h/d}$
Rounded Nose 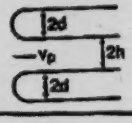	$K_{ENT} \simeq \frac{0.05}{1 + h/d}$
Typical Perforated Metal Facing 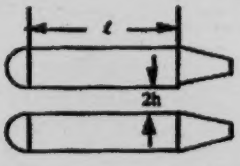	$K_F \simeq 0.0125 \frac{\ell}{h}$ ℓ = baffle length, tail and nose not included
Square Tail 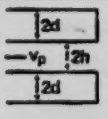	$K_{EX} = \left(\frac{1}{1 + h/d}\right)^2$
Rounded Tail 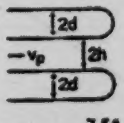	$K_{EX} = 0.7\left(\frac{1}{1 + h/d}\right)^2$
Faired Tail 7.5° 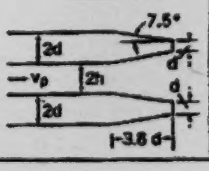	$K_{EX} = 0.6\left(\frac{1}{1 + h/d}\right)^2$

Figure 78. Entrance, Exit, and Friction Loss Factors for Various Geometries
(Obtained from Noise and Vibration Control Engineering, L. Beranek [16])

These tables are provided in the book by Beranek [16], and can be found in almost any fluid mechanics or HVAC design textbook. In addition, a detailed process for calculating the entrance and exit losses has been presented by Idel'chik [19]. One of the assumptions made for Eq. (39) is that the flow through the material is negligible. Based on how much more difficult the path through the material is compared to the path along the edge and the fact that the pressure is the same on each side, this assumption is not hard to accept.

The use of Eq. (39) is an iterative process due to the inclusion of the passage velocity. As the total open area changes, so does the passage velocity, so several iterations through the formula are required to obtain the minimal pressure drop given the acoustical design constraints. Work was done with Eq. (39) to see the effects between entrance, exit, and friction losses, however, each silencer design will have a unique geometry, so direct comparisons/conclusions cannot be made. Once again, by using the numerical methods outlined in the previous chapters, and then calculating the pressure drop, an iterative process could be programmed to produce the optimal design given the initial constraints for pressure and geometry.

6.5 Conclusions

The considerations presented in this chapter had some relation to the numerical methods discussed in previous chapters. The time saving techniques presented can be used to reduce the numerical effort required for solution. For small single run models, these savings might not have a large impact, but for the larger geometries and for models in which optimization schemes will require multiple solution runs, the time savings could be quite large. The greatest impact resulted from the use of multiple symmetry in full parallel baffle silencers, where it was proven how the full model could be reduced to a single set of baffles.

It was shown that the acoustic effects of perforated materials (used for containment of the sound absorbing materials) can be predicted relatively easily by simple calculations. For most materials, inclusion in the numerical model is not required, as this could slow down the computational process a great deal. Finally, the

pressure drop across the silencer unit was discussed and some formulations were presented. The calculations themselves were quite simple, and would lend themselves very well to a small computer program. Due to the iterative nature of the methods used for pressure drop, the design process of the acoustical performance and the pressure performance would also lend themselves very well to an optimization scheme for the total silencer system design.

7 Conclusions and Future Considerations

7.1 Thesis Contributions

The major information presented in the Thesis involves the comparisons between the various numerical methods outlined, and the results obtained through physical testing. Most of the numerical models were based upon physical systems and factors such as geometry and material properties were kept constant between the physical and numerical models. This is one of the major contributions of the Thesis since most of the papers written on the subject do not compare the numerical results to physically obtained results. Various considerations and idiosyncrasies were covered and limitations for the various methods were discussed.

It was found that the method best suited for modeling of transmission loss was Finite Element Method with the 3-point method. This method was the fastest, most accurate, and easiest to implement. With the above mentioned method for solution, it was found that purely reactive type silencers could be modeled to essentially match with what is expected empirically and experimentally. Once absorption was included in the model, the results were found to match reasonably well. This was attributed to the methods used to include the bulk material properties into the numerical scheme. A review of more recent papers revealed some newer techniques for inclusion of sound absorbing materials, and it is believed that these methods can be included into the methods presented in the Thesis (for the model as a whole) to obtain an even more accurate solution.

In addition to the numerical methods presented, a modified 3-point method for measuring Transmission Loss was presented. This method requires three (3) measurement points, and enables the test to be conducted with the silencer installed (which is the greatest advantage resulting from the new method). Previous methods required that two separate test be conducted; one with the silencer removed and one with the silencer in place. A comprehensive set of comparisons was performed to verify the accuracy of the new method, along with the limitations of use. One of the

other advantages to the new method is that it follows along with the numerical solution method. With this, a direct comparison can be made between the physical and numerical results obtained.

Another major contribution of the Thesis dealt with the issues surrounding the numerical solution times. Methods for reducing the model size, and increasing the efficiency of the numerical solution were presented and it was shown that using some simple techniques can dramatically reduce the computational effort required (and hence the time required) while maintaining the accuracy of the solution.

7.2 Future Considerations

It has been shown that the numerical model is able to predict the transmission loss performance of both reactive and absorptive silencers very well. The design concerns presented in the previous chapter are of great importance to the overall performance of the silencer system, however, there are other considerations that must also be addressed if a true, all encompassing, design package is to be obtained. If higher accuracy is desired, then some of the following concerns need to be addressed.

7.2.1 Insertion Loss Calculation

Throughout the study, the performance parameter that was used was transmission loss (*TL*). Ultimately, the insertion loss (*IL*) values would be desired, since these numbers are used most commonly by industry. The prediction of *IL* is more difficult to obtain than *TL* because of the methods required. For the *TL* calculations, only the interior of the silencer system was considered, which led to the use of the Finite Element Method (FEM) and the 3-point measurement method. For *IL* calculations, however, the sound pressure levels need to be obtained outside of the silencer section (at some arbitrary distance from the exhaust). In order to do this numerically, there are two choices.

The first option is to use the Boundary Element Method (BEM) to model the exterior surface of the silencer and calculate the internal and external effects at the same time. Preliminary tests conducted on purely reactive silencers with the BEM

show that it can calculate *TL* values very well when using the 3-point method. Extrapolation to the calculation of *IL* would involve some work to make sure the correct calculations are being performed. The biggest problem with this method, as mentioned in §2.4.2, is that the BEM cannot account for bulk acoustical absorption properties and can only model acoustical impedances at the surface. A method which can include these bulk properties is desired.

The second option for *IL* calculations is by using the FEM inside the silencer, coupled with Infinite Elements [27] outside the silencer. By using this method, the bulk acoustical material properties can be included in the model, and the Infinite Elements can be used to calculate the external pressure values. An added feature is that it would be possible to calculate both the *TL* and *IL* at the same time.

7.2.2 Flow Noise

The most important factor present in practically all silencer systems, which was not included in the study, is fluid flow. Whether it is from an automobile exhaust, or from a gas turbine exhaust, the acoustical effects of flow must be considered. The noise generated by flow can take on many forms. First, the flow at the silencer exhaust can cause large amounts of noise (called self-generated noise), which can turn out to be the limiting factor in the overall silencer performance. In addition, turbulent effects inside the silencer, as the fluid flows over and around the baffles, can possibly have a substantial impact. Currently, empirical methods (such as those proposed by Ver [35]) exist for prediction of flow generated noise.

Future work would include the effects of turbulent flow in the numerical model, and use the resulting character of the flow to try to predict the addition of noise to the system. Also, once the issues regarding the calculation of *IL* have been addressed, the self-generated noise could be included into the calculation. This would be the most difficult of the proposed steps for increased accuracy in silencer performance predictions.

7.2.3 Break-Out Noise

Another phenomenon that could be included once the *IL* calculation issue has been solved, is the inclusion of break-out noise. This is the noise that radiates through the walls of the silencer and ducting to the outside. Depending on the quality of construction, this noise can be of great concern to the overall *IL* performance. In order to include the break out noise, the wall of the silencer would have to be modeled as a structure (with structural material properties) and coupled to both the interior and exterior regions. The model would account for the vibration excitation, transmission, and noise emission of this structural component. Similar to flow noise, this phenomena is required if a more accurate prediction of *IL* is desired.

7.2.4 Absorptive Materials

Much work has already been done to define and measure some of the acoustic properties that are associated with sound absorbing materials. Based on the results obtained thus far, it is believed that there is still work to be done in this area. The modeled results for purely reactive silencers, indicate that the numerical model is able to account for the geometrical and propagation concerns required for silencer modeling. The results obtained with the inclusion of sound absorbing materials, however, suggest that the parameters used to quantify their performance, may not be enough to obtain accurate results. By further developing the measurements of these material properties, and possibly including new properties, it is believed that there can be a better characterization of the material. Fortunately, there has been recent work in this area and papers by Peat and Rathi [12], Kirby and Cummings [13], Allard et al. [14], and Johnson et al. [15] discuss more complicated methods for obtaining and predicting the bulk properties and including them in the numerical model. It is the opinion of the author that this would be the final step in obtaining very accurate numerical representations for the silencers tested in this study.

7.2.5 Low Frequency Concerns

One final area for study is the examination of very low frequency noise control. It is often the case with large gas turbine installations, that there is a large amount of low frequency noise present. Typically, the higher frequency noise is not very difficult to attenuate, but the lower frequencies can be a large problem. At similar sound pressure levels, the lower frequency noise contains more energy than the high frequency noise. This coupled with the fact that low frequencies will be less impeded over large distances, means that controlling low frequency noise at the source is both difficult, and of great importance. Work in this area would include an in-depth look into the design of large-scale silencers with abundant amounts of sound absorbing material, as well as the inclusion of reactive type elements such as Helmholtz resonators and expansion chambers. Also, a further look into the bulk material properties and their inclusion in the numerical model at low frequencies is required as proposed by Kirby and Cummings [13]. In order to complete the work, a large-scale model would have to be constructed, with a large sound source to generate the high levels of low frequency noise required. The work already completed on broadband silencer modeling could be extended and concentrated on the low frequency range. One large advantage with dealing with low frequency noise, compared to higher frequencies, is that the FEM mesh does not need to be as finely discretized. If only the frequencies up to 200 Hz are required, for example, the element size would only need to be approximately 28cm, which is much larger than the 2cm size typically used for the models in this study. This means that much larger silencers could be modeled at faster rates than are currently done.

7.2.6 Optimization

One of the main advantages with the use of a numerical method, is the ability to incorporate an optimization scheme. With the many geometric and material variables which affect the performance of the silencing system, an optimization scheme which could sort through several design iterations would be advantageous. Several methods, such as using genetic algorithms, could be implemented, depending on the particular circumstances of the design, and which factors are able to be manipulated. With the use of an optimization scheme, the power and adaptability of the methods presented in the previous chapters could be harnessed and would prove much more beneficial.

7.3 Conclusions

With the basic work completed for numerical modeling of acoustical silencers, there still remains many steps which need to be completed to make the model more accurate. The first major step discussed was the numerical prediction of *IL*. This value is the most desirable by industry and designers. To achieve this, other considerations such as flow noise, break-out noise, a more in-depth look at sound absorbing materials, and low frequency noise control must be addressed. Finally, with all of the various parameters that can be manipulated, some sort of optimization scheme is desired to aid in the design stage and utilize the numerical methods to their full potential.

Appendix A: 2-D Acoustic FEM Derivation

The following details a derivation of a 2-dimensional finite element formulation. Note that the method presented is the Galerkin method and that there are other methods which will result in the same final formulation. Also note that the methods used can be applied to a 3-dimensional formulation as well. First, start with a forced 2-D pressure wave equation:

$$c^2 \frac{\partial^2 p}{\partial x^2} + c^2 \frac{\partial^2 p}{\partial y^2} - \frac{\partial^2 p}{\partial t^2} = F(t) \tag{40}$$

Now, using a Weighted Residual method (Galerkin), assume:

$$p = \{N\}^T \{p_e\} = R(x,y,t) \tag{41}$$

where:

$$\{N\} = \{N\}(x,y)$$

$$\{p_e\} = \{p(t)\}$$

The vector, $\{N\}$, is known as the mode shape vector for the element used. Note that the pressure vector has the subscript e. This is intended to show that this formulation is used for each element. The Galerkin equation in 2-D can be written as:

$$\int_A \{N\} R(x,y,t)\, dA = 0 \tag{42}$$

Now, plugging Eqs. (41) and (42) into (40) yields:

$$\int_A c^2 \{N\}\{N_{xx}\}^T \{p_e\} dA + \int_A c^2 \{N\}\{N_{yy}\}^T \{p_e\} dA - \int_A \{N\}\{N\}^T \{\ddot{p}_e\} dA = \int_l \{N\} F(t)\, dl \tag{43}$$

Where:

$$N_{xx} = \frac{\partial^2 N}{\partial x^2}, \quad N_{yy} = \frac{\partial^2 N}{\partial y^2}$$

Note that Eq. (43) has non-symmetric terms in the integrand. This can be dealt with by using integration by parts,

$$\int_A^B u\,dv = uv\Big|_A^B - \int_A^B v\,du \tag{44}$$

Using Eq. (44) in (43) results in:

$$\left[c^2\{N\}\{N_x\}^T\{p_e\}dA\right]_A - \int_A c^2\{N_x\}\{N_x\}^T\{p_e\}dA + \left[c^2\{N\}\{N_y\}^T\{p_e\}dA\right]_A - \int_A c^2\{N_y\}\{N_y\}^T\{p_e\}dA - \int_A \{N\}\{N\}^T\{\ddot{p}_e\}dA = \int_l \{N\}F(t)\,dl \tag{45}$$

Due to inter-element canceling and the application of boundary conditions, the first and third terms in Eq. (45) disappear. The resulting equation is:

$$\int_A c^2\{N_x\}\{N_x\}^T\{p_e\}dA + \int_A c^2\{N_y\}\{N_y\}^T\{p_e\}dA + \int_A \{N\}\{N\}^T\{\ddot{p}_e\}dA = -\int_l \{N\}F(t)\,dl \tag{46}$$

Now let the forcing function be a harmonic velocity:

$$F(t) = -j\omega\rho c^2\{v\}\cos(\omega t) \tag{47}$$

and assume:

$$\{p_e\} = \{p_e\}\cos(\omega t) \quad , \quad \{\ddot{p}_e\} = -\omega^2\{p_e\}\cos(\omega t) \tag{48}$$

(where ω is in rad/s) and substitute Eqs. (47) and (48) into (46):

$$c^2\left[\int_A \{N_x\}\{N_x\}^T dA + \int_A \{N_y\}\{N_y\}^T dA\right]\{p_e\} - \omega^2\int_A \{N\}\{N\}^T\{p_e\}dA = j\omega\rho c^2\int_l \{N\}\{v\}dl \tag{49}$$

Finally, with some manipulation, the more familiar form is derived as:

$$\left[[K_e] - k^2 [M_e]\right] \{p_e\} = \{F_e\} \tag{50}$$

Where:

$$[K] = \left[\int_A \{N_x\}\{N_x\}^T dA + \int_A \{N_y\}\{N_y\}^T dA \right], (unitless)$$

$$[M] = \int_A \{N\}\{N\}^T dA \ , \ (m^2)$$

$$\{F\} = j\omega\rho \int_l \{N\}\{v\} dl \ , \ (kg/m \cdot s^2)$$

$$k = \omega / c \ , \ (1/m)$$

$[K]$ is known as the stiffness matrix, and $[M]$ is known as the mass matrix, while $\{F\}$ is known as the forcing vector. Typically Eq. (50) is solved at several frequency values to obtain a frequency spectrum over the region of interest. In order to solve Eq. (50), the shape function, $\{N\}$, for the element must be known.

Appendix B: 2-D Acoustic Element Derivation

The following derivation is for a simple 4-node, linear, rectangular element. The principals presented can be used for many different shapes and configurations of element type. Also note that there are other techniques available for element derivations. This method was chosen since it is relatively simple and the steps can easily be followed.

Assume a 4-node, linear, rectangular element:

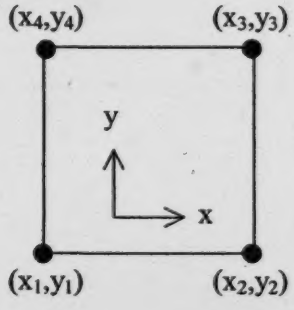

Acoustic Finite Element Illustration

For the case of an acoustic element, let there only be one degree of freedom per node, the pressure (p), which can be expressed as a function of the element dimensions:

$$p = a_1 + a_2 x + a_3 y + a_4 xy = \{g\}^T \{\alpha\} \tag{51}$$

Where:

$$\{g\} = \begin{Bmatrix} 1 \\ x \\ y \\ xy \end{Bmatrix} \quad , \quad \{\alpha\} = \begin{Bmatrix} a_1 \\ a_2 \\ a_3 \\ a_4 \end{Bmatrix}$$

At nodes 1 through 4, the pressure is expressed as:

$$
\begin{aligned}
p_1 &= a_1 + a_2 x_1 + a_3 y_1 + a_4 x_1 y_1 \\
p_2 &= a_1 + a_2 x_2 + a_3 y_2 + a_4 x_2 y_2 \\
p_3 &= a_1 + a_2 x_3 + a_3 y_3 + a_4 x_3 y_3 \\
p_4 &= a_1 + a_2 x_4 + a_3 y_4 + a_4 x_4 y_4
\end{aligned}
$$

Which can be written more conveniently as:

$$
\begin{Bmatrix} p_1 \\ p_2 \\ p_3 \\ p_4 \end{Bmatrix} = \underbrace{\begin{bmatrix} 1 & x_1 & y_1 & x_1 y_1 \\ 1 & x_2 & y_2 & x_2 y_2 \\ 1 & x_3 & y_3 & x_3 y_3 \\ 1 & x_4 & y_4 & x_4 y_4 \end{bmatrix}}_{[T]} \begin{Bmatrix} a_1 \\ a_2 \\ a_3 \\ a_4 \end{Bmatrix} \tag{52}
$$

Now the mode shape vector can be calculated by:

$$
\{N\}^T = \{g\}^T \left[T^{-1}\right] \tag{53}
$$

In order to calculate [K] and [M], the vector {N} must be computed for the element, given the x and y locations of the nodes, and then [K] and [M] can be computed over the area of the element. For a rectangular element, the limits of integration are simply the x and y dimensions of the element. A similar operation takes place for the forcing vector with the exception that the integration is a line integration between the nodes at which the velocity is applied. Once this has been done, [K] and [M] are assembled into global matrices encompassing all elements in the model. When this process is complete, Eq. (50) (without the subscript e's) can be solved for the entire model.

Appendix C: Global Stiffness Matrix Assembly Example

The following example illustrates how 3 elements may be linked together to form the global stiffness matrix. The numbers in brackets are the (x,y) coordinates, while the open numbers represent the node numbers. The italicized numbers represent the element numbers. Note that there are 3 elements, each with 4 nodes, but 4 of the nodes are interconnected, so the resulting global stiffness matrix will be of the size $[K]_{8x8}$.

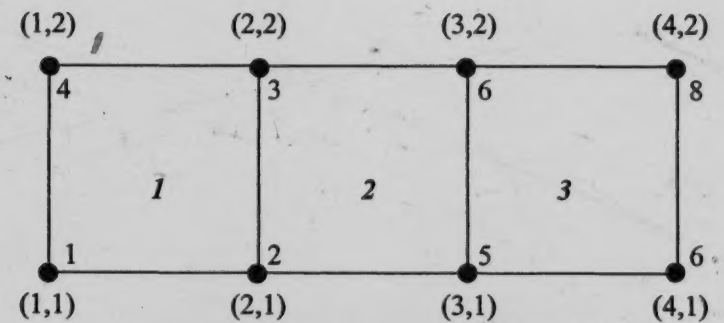

Global Element Assembly Illustration

For each of the elements, the $[T]$ matrices are expressed as:

$$[T_1]=\begin{bmatrix}1&1&1&1\\1&2&1&2\\1&2&2&4\\1&1&2&2\end{bmatrix}, \quad [T_2]=\begin{bmatrix}1&2&1&2\\1&3&1&3\\1&3&2&6\\1&2&2&4\end{bmatrix}, \quad [T_3]=\begin{bmatrix}1&3&1&3\\1&4&1&4\\1&4&2&8\\1&3&2&6\end{bmatrix}$$

Plugging the [T] values into Eq. (53) yields the mode shapes for each element as:

$$\{N_1\}=\begin{Bmatrix}4-2x-2y+xy\\-2+2x+y-xy\\1-x-y+xy\\-2+x+2y-xy\end{Bmatrix},\ \{N_2\}=\begin{Bmatrix}6-2x-3y+xy\\-4+2x+2y-xy\\2-x-2y+xy\\-3+x+3y-xy\end{Bmatrix},\ \{N_3\}=\begin{Bmatrix}8-2x-4y+xy\\-6+2x+3y-xy\\3-x-3y+xy\\-4+x+4y-xy\end{Bmatrix}$$

Now the [K] matrix from Eq. (50) can be computed for each element:

$$[K_1]=\begin{bmatrix}\frac{2}{3}&\frac{-1}{6}&\frac{-1}{3}&\frac{-1}{6}\\\frac{-1}{6}&\frac{2}{3}&\frac{-1}{6}&\frac{-1}{3}\\\frac{-1}{3}&\frac{-1}{6}&\frac{2}{3}&\frac{-1}{6}\\\frac{-1}{6}&\frac{-1}{3}&\frac{-1}{6}&\frac{2}{3}\end{bmatrix},\ [K_2]=\begin{bmatrix}\frac{8}{3}&\frac{-7}{6}&\frac{2}{3}&\frac{-13}{6}\\\frac{-7}{6}&\frac{2}{3}&\frac{-1}{6}&\frac{-2}{3}\\\frac{2}{3}&\frac{-1}{6}&\frac{2}{3}&\frac{-7}{6}\\\frac{-13}{6}&\frac{2}{3}&\frac{-7}{6}&\frac{8}{3}\end{bmatrix},\ [K_3]=\begin{bmatrix}\frac{20}{3}&\frac{-25}{6}&\frac{11}{3}&\frac{-37}{6}\\\frac{-25}{6}&\frac{8}{3}&\frac{-13}{6}&\frac{11}{3}\\\frac{11}{3}&\frac{-13}{6}&\frac{8}{3}&\frac{-25}{6}\\\frac{-37}{6}&\frac{11}{3}&\frac{-25}{6}&\frac{20}{3}\end{bmatrix}$$

Finally, the three elements can be assembled into the global stiffness matrix for the model:

$$[K_{global}]=\begin{bmatrix}2/3&-1/6&-1/3&-1/6&0&0&0&0\\-1/6&10/3&-8/3&-1/3&-7/6&2/3&0&0\\-1/3&-8/3&10/3&-1/6&2/3&-7/6&0&0\\-1/6&-1/3&-1/6&2/3&0&0&0&0\\0&-7/6&2/3&0&22/3&-19/3&-25/6&11/3\\0&2/3&-7/6&0&-19/3&22/3&11/3&-25/6\\0&0&0&0&-25/6&11/3&8/3&-13/6\\0&0&0&0&11/3&-25/6&-13/6&8/3\end{bmatrix}$$

The row and column numbers in the global matrix represent the node numbers in the entire (global) model. For example, at $[K_{global}]_{(1,1)}$ the value is 2/3 which is the same as $[K_1]_{(1,1)}$ since at node 1, the only element it is in contact with is element 1. At $[K_{global}]_{(2,2)}$ the node number is 2, which is in contact with elements 1 and 2. The

values of 2/3 (from element 1) and 8/3 (from element 2) are added together to get the 10/3 value. A similar process happens for the mass matrix, $[M]$, and the forcing function $\{F\}$. Note that the individual element stiffness matrices as well as the global stiffness matrix are symmetric. The global matrix may end up being tightly banded if care is taken when assigning node numbers. This is important when it comes time to solve the system for the pressure vector $\{p\}$ because faster solvers can be implemented.

Appendix D: Absorptive Material FEM Derivation

The following derivation outlines how the material properties can be included [5, 36], along with the assumptions involved. To begin with, make use of the continuity equation:

$$\Omega\left(\frac{\partial \delta}{\partial t}\right) - \rho_0 \, div(u) = 0 \tag{54}$$

where:

Ω = Porosity

δ = Density change when entering pores

ρ_0 = Density of fluid (kg/m^3)

$u(x,t)$ = Mean velocity of fluid particles (m/s)

The change in density can be related to the acoustic pressure by:

$$\delta = k_p \rho_0 P \tag{55}$$

where:

k_p = Effective Compressibility of the fluid in the pores = $1/(\rho_0 c^2)$ (ms^2/kg)

P = Acoustic pressure (Pa)

Combining Eqs. (54) and (55) yields:

$$k_p \Omega \frac{\partial P}{\partial t} = div(u) \tag{56}$$

For simple harmonic waves the following relation can be shown:

$$\frac{\partial P}{\partial t} = j\omega P \tag{57}$$

where:

ω = Angular frequency = $2\pi f$ (rad/s)

Combining Eqs. (56) and (57) yields:

$$\left(\frac{j\,\omega\,\Omega}{\rho_0\,c^2}\right)P = div(u) \tag{58}$$

Now, using the equation of motion:

$$\rho_a\left(\frac{\partial u}{\partial t}\right) + Ru - grad(P) = 0 \tag{59}$$

where:

ρ_a = Density of sound absorbing material (kg/m^3)

R = Flow resistivity of sound absorbing material

Again, for simple harmonic waves, the following can be shown:

$$\frac{\partial u}{\partial t} = u\,j\,\omega \tag{60}$$

Combining Eqs. (59) and (60) yields:

$$grad(P) = u(j\omega\rho_a + R) \tag{61}$$

Taking the divergence of Eq. (61) results in the following:

$$div\,grad(P) = div\left[\left(j\,\rho_a\,k_a\,c + R\right)u\right] \tag{62}$$

Finally, Eq. (58) can be combined with Eq. (62) to form:

$$div\, grad\,(P) = K_s k_a^2 P\, \Omega + \frac{j R k_a P \Omega}{\rho_0 c} \tag{63}$$

where:

K_s = Structural factor = ρ_a / ρ_0

Now make the following substitutions into Eq. (63):

$$Y_R = -k_a^2 K_s \Omega \quad , \quad Y_I = \frac{k_a R \Omega}{\rho_0 c} \quad , \quad P = (P_R + jP_I)e^{j\omega t}$$

where the sub I and sub R terms refer to incident and reflected waves respectfully. It can be shown that the following two equations result:

$$div\, grad\,(P_R) = Y_R P_R + Y_I P_I \tag{64a}$$

$$div\, grad\,(P_I) = Y_R P_I + Y_I P_R \tag{64b}$$

If it is assumed $\frac{\partial P}{\partial n} = 0$ at the boundary (normal gradient), then the following Functional can be formed:

$$F = \frac{1}{2} \int_v \left[\begin{array}{l} grad\,(P_R)\, grad\,(q_R) + grad\,(P_I)\, grad\,(q_I) + Y_R P_R q_R + \\ Y_I P_I q_R + Y_R P_I q_I + Y_I P_R q_I \end{array} \right] dv \tag{65}$$

where:

$q = (q_R + j q_I)e^{j\omega t}$ = adjoint acoustic pressure

Now let $\{P\}$ be the response vector of the real system and $\{q\}$ be the response vector of the adjoint system. The result is:

$$F = \frac{1}{2}\begin{bmatrix} \{P_R\}^T[K]\{q_R\} + \{P_I\}[K]\{q_I\} + Y_R\{P_R\}^T[M]\{q_R\} + Y_I\{P_I\}[M]\{q_R\} \\ + Y_R\{P_I\}^T[M]\{q_I\} + Y_I\{P_R\}[M]\{q_I\} \end{bmatrix} \tag{66}$$

where:

$[K]$ = The kinetic energy matrix (stiffness matrix)

$[M]$ = The strain energy matrix (mass matrix)

Now by setting $\{q_R\} = 0$ and F = 0, the following can be formed:

$$[K]\{P_R\} + Y_R[M]\{P_R\} + Y_I[M]\{P_I\} = 0 \tag{67a}$$

Similarly, by setting $\{q_I\} = 0$ and F = 0, the following can be formed:

$$[K]\{P_I\} + Y_R[M]\{P_I\} + Y_I[M]\{P_R\} = 0 \tag{67b}$$

In matrix form, and by substituting for Y_R and Y_I, the system of equations can be written as:

$$\begin{bmatrix} [K] - k_a^2 K_s \Omega[M] & \frac{k_a R \Omega}{\rho_0 c}[M] \\ \frac{k_a R \Omega}{\rho_0 c}[M] & [K] - k_a^2 K_s \Omega[M] \end{bmatrix} \begin{Bmatrix} \{P_R\} \\ \{P_I\} \end{Bmatrix} = \begin{Bmatrix} 0 \\ 0 \end{Bmatrix} \tag{68}$$

Making use of the first equation yields:

$$\left[[K]+\frac{jkR\Omega}{\rho c}[M]-k^2K_s\Omega[M]\right]\{p\}=\{0\} \tag{69}$$

where ρ_0 has been replaced by ρ, and k_a has been replaced by k and the subscript $_R$ has been removed from the pressure vector. The subscript m can be added to the stiffness and mass matrix terms, along with the pressure vector to denote that this formula is intended for the absorbing material. Finally, the forcing function can be added to the right hand side in place of the zero vector when the system is put into excitation. The resulting equation is the most familiar form as proposed by Craggs [6]:

$$\left[[K_m]+\frac{jkR\Omega}{\rho c}[M_m]-k^2K_s\Omega[M_m]\right]\{p_m\}=\{F_m\} \tag{70}$$

where:

$$[K_m]=\left[\int_A\{N_x\}\{N_x\}^T dA+\int_A\{N_y\}\{N_y\}^T dA\right],\ (unitless)$$

$$[M_m]=\int_A\{N\}\{N\}^T dA\ ,\ (m^2)$$

$$\{F_m\}=(j\omega\rho+R)\int_l\{N\}\{v\}dl\ ,\ (kg/m\cdot s^2)$$

$$k=\omega/c\ ,\ (1/m)$$

Note that in order to couple the absorptive elements (assemble into the same global matrix) with the fluid elements, Eq. (70) needs to be pre-multiplied by:

$$\frac{j\rho\omega}{(j\rho\omega + R)} \tag{71}$$

This will ensure that both the equality of nodal pressure **AND** surface velocity are satisfied [6].

At this point it is important to note all of the assumptions which were made for the previous derivation. The following is a list of the key assumptions made [36]:

- Pores of the material are interconnected in a random but isotropic way
- The solid, though porous, is perfectly rigid and incompressible
- At very high frequencies the compressibility of the fluid in the pores is adiabatic, and at low frequencies, it would be isothermal
- When fluid flows through a series of constrictions, its effective mass increases
- R is constant in all directions
- The adjoint system absorbs the energy dissipated by the real system governed by P and its inclusion ensures that total energy is conserved.
- $\frac{\partial P}{\partial n} = 0$ at the boundary. If this assumption is not made, then more surface integrals are required.
- When the air and absorptive material are coupled, it is assumed that there is a small volume of incompressible fluid at each node point, and that the dimensions of the volume are small compared with the wavelength. Therefore, the pressure in the air and material at the node are equal.

Appendix E: ANSYS Code for Mesh Generation

```
/title,Expansion Chamber Design 2D
!this is the code to generate the ANSYS drawing of the silencer model


! The following is ANSYS code for a simple 2 dimensional expansion chamber.
! This particular model incorporates different element types within the same
! geometry so that absorption can be assigned.  It also prompts the user for
! parameters so that the silencer can be customized.  Units in m


/PNUM,AREA,1
/prep7                  ! Enter the pre-processor
bopt,numb,off
et,1,plane82            !sets element #1 to type plane82
et,2,plane2             !sets element #2 to type plane2


*ask,slength,Enter the length of the silencer body (meters),3
*ask,sheight,Enter the height of the silencer body (meters),.6
*ask,size1,Enter the element size for silencer (default = 0.03m),.03
*ask,size2,Enter the element size for baffles (default = 0.03m),.03
*ask,blength,Enter the length of the baffles (meters),2.25
*ask,bheight,Enter the height of the baffles (meters),.1
*ask,nbaff,Enter the number of baffle rows (default = 1),2
*ask,Fname,Enter the name of the file you want to create(saves as a .cdb file),'test'


blocaty = (sheight-(nbaff*bheight))/(nbaff + 1)  !location of the bottom of each baffle
blocatx = (slength - blength)/2 !location of the start of the baffle

!make the main body
rectng,0,slength,(-sheight/2),(sheight/2)    !area 1

!create the baffles
count = 1
count2 = 0
*DO,i,1,nbaff,1                                  ! do i = 1, nbaff (in steps of one)
 sss = (-sheight/2)+(count*blocaty)+(count2*bheight)
 ssss = (-sheight/2)+(count*blocaty)+(count2*bheight)+(bheight)
 rectng,blocatx,(blocatx+blength),sss,ssss
 count = count+1
 count2 = count2+1
 *ENDDO

!subtract the baffles from the main body to get the main shape
asba,1,2
NUMCMP,AREA
count = nbaff
*DO,i,1,nbaff-1,1
 asba,(count),1
 NUMCMP,AREA
```

```
 count = count-1
 *ENDDO

!redraw the baffles
count = 1
count2 = 0
*DO,i,1,nbaff,1    ! do i = 1, nbaff (in steps of one)
 sss = (-sheight/2)+(count*blocaty)+(count2*bheight)
 ssss = (-sheight/2)+(count*blocaty)+(count2*bheight)+(bheight)
 rectng,blocatx,(blocatx+blength),sss,ssss
 count = count+1
 count2 = count2+1
 *ENDDO

!now we need to glue the areas together
*DO,i,1,nbaff,1
 aglue,1,2
 NUMCMP,AREA
 *ENDDO

!now we assign the element types and sizes to the areas
asel,s,area,,1   !selects area 1 for future work
aatt,,,1,      !assigns attribute of type=1 to area 1
aesize,1,size1          !sets element size for area 1
asel,u,area,,1   !unselects area 1

count = 2
*DO,i,1,nbaff,1
 asel,s,area,,count   !selects area 'count' for future work
 aatt,,,2,        !assigns attribute of type=2 to area 'count'
 aesize,count,size2   !sets the element size of 'size2' to area 'count'
 asel,u,area,,count       !unselects area 'count'
 count = count+1
 *ENDDO


!finally we can mesh the entire thing
asel,s,area,,1,(nbaff+1) !selects area's 1 through nbaff+1 for future work
amesh,all                  !meshes the entire silencer and baffles

cdwrite,all,Fname,cdb,

finish          ! Finish pre-processing
```

Appendix F: SYSNOISE Code for FEM Solution

```
close nosave return   {code for use with 3 point method}

Option  FEM Frequency Fluid Return
Import Mesh Format ansys File "filename".cdb Return
twodimensional return

{the following is a list of the variables for dimensions and boundary}
{conditions and material properties used in the code the values of these}
{variables need to be changed at this spot only and not at any other point.}

Environment
   section VARIABLES dummy = dummy
   section VARIABLES x1 = .22    {distance from inlet to point 1}
   section VARIABLES x2 = .24    {distance from inlet to point 2}
   section VARIABLES px1 = .22   {first measurement point location}
   section VARIABLES px2 = .24   {second measurement point location}
   section VARIABLES px3 = 2.76    {outlet measurement point location}
   section VARIABLES b1 = 0      {x location of inlet}
   section VARIABLES b2 = 3      {x location of outlet}
   section VARIABLES name = "name".tbl  {name of output table}
   section VARIABLES snd = 344.43  {speed of sound in m/s}
   section VARIABLES ro = 1.102  {density of the air}
   section VARIABLES imped = 379.56 {characteristic impedance}
   section VARIABLES c1 = .01824227 {Constant used in calculations}
   section VARIABLES ks = 1.3   {structural factor for the material}
   section VARIABLES res = 10614  {flow resistivity of the material}
   section VARIABLES por = .799 {porosity for the material}
   section VARIABLES lower = 10 {lower frequency range for calculation}
   section VARIABLES upper = 2840 {upper frequency range for calculation}
   return

Material Fluid
   Sound $snd  Rho $ro
   Elements all
   Return

Set 10 Name "source" faces x=$b1 Return
Boundary Velocity  Real 1 Imag 0
   faces Set 10
   Return

Set 20 Name  "termination" faces x=$b2 Return
boundary impedance real $imped imag 0
   faces set 20
   return

{select the element type to assign the absorptive properties to}
set 30 name "absorption" elements type tria6 return

{Sets the absorptive material properties to the absorptive element}
material absorbent
```

```
   name "light foam"
   sound $snd rho $ro structure-factor $ks porosity $por resistivity $res
   elements set 30
   return

point $px1 .3 0 return  {Picks points 1, 2, and 3 for the 3-point method}
point $px2 .3 0 return
point $px3 .3 0 return

Solve  Frequency $lower To $upper LogStep 1.04 Return

postprocess
  points all frequency $lower to $upper logstep 1.04
  near 2
  far 5
  quadrature 2 2 1
  save results step 1
  return

{calculation of TL using 3 point method}
combine
   read point 1 pressure return
   write function file $pnt1 return
   clear
   read point 2 pressure return
   write function file $pnt2 return
   clear
   read point 3 pressure return
   write function file $pnt3 return
   clear
   return

combine
   read point 1 pressure return
   amplitude
   frequency
   constant real $c1 imag 0
   multiply
   constant real $x1 imag 0
   multiply
   multiply
   read point 1 pressure return
   amplitude
   divide
   constant real 0 imag -1
   mulitply
   write table 50 return
   expon
   read point 1 pressure return
   multiply
   write table 10 return
   return

combine
   read point 2 pressure return
```

```
    amplitude
    frequency
    constant real $c1 imag 0
    multiply
    constant real $x2 imag 0
    multiply
    multiply
    read point 2 pressure return
    amplitude
    divide
    constant real 0 imag -1
    mulitply
    write table 60 return
    expon
    read point 2 pressure return
    multiply
    write table 20 return
    return

combine
    read table 50 return
    constant real 2 imag 0
    mulitply
    expon
    write table 30 return
    return

combine
    read table 60 return
    constant real 2 imag 0
    mulitply
    expon
    write table 40 return
    return

combine
    read table 10 return
    read table 20 return
    subtract
    read table 30 return
    read table 40 return
    subtract
    divide
    read point 3 pressure return
    divide
    amplitude
    log10
    constant real 20 imag 0
    multiply
    write table 2000 return
    write function file $name return
    return
```

References

[1] Bell L.H., 1994, *Industrial Noise Control*, Marcel Dekker, New York

[2] Gladwell, G.M.L., A finite element method for acoustics, *5^e Congres international D'Acoustique*, Liege, Belgium, Paper L33 (1965)

[3] Craggs, A., The use of simple three-dimensional acoustic finite elements for determining the natural modes and frequencies of complex shaped enclosures, J. Snd. Vib., 1972, 23(3); 331-339

[4] Munjal, M.L., 1987, *Acoustics of Ducts and Mufflers*, Wiley-Interscience, New York

[5] Craggs A. A finite element model for rigid porous absorbing materials. J. Sound Vib. 1978; 61(1), 101-111

[6] Craggs A. Coupling of finite element acoustic absorption models. J. Sound Vib. 1979; 66(4), 605-613

[7] Buma, Craggs, Faulkner. Data Report on the Measurement of Bulk Material Parameters of Acoustic-Absorptive Materials. University of Alberta, Mechanical Engineering Department. Sept 1988

[8] ASTM C522-87 (Reapproved 1997). Standard Test Method for Airflow Resistance of Acoustical Materials.

[9] Standard Test Method for Sound Absorption and Sound Absorption Coefficients By the Reverberation Room Method, ASTM C 423-99a

[10] Standard Test Method for Impedance and Absorption of Acoustical Materials Using a Tube, Two Microphones and a Digital Frequency Analysis System. ASTM E 1050-98.

[11] Attenborough K. Acoustical characteristics of porous materials. Physics Reports, 1982, 82(3), 179-227

[12] Peat K.S., Rathi K. L., A Finite Element Analysis of the convected acoustic wave motion in dissipative silencers, J. Sound Vib. 1995, 184(3); 529-545

[13] Kirby R., Cummings A. Prediction of the bulk acoustic properties of fibrous materials at low frequencies. Applied Acoustics, 1999, (56); 101-125

[14] Allard J-F., Herzog P., Lafarge D., Tamura M. Recent topics concerning the acoustics of fibrous and porous materials. Applied Acoustics. 1993, (39); 3-21

[15] Johnson D. L., Koplik J., Dashen R. Theory of dynamic permeability and tortuosity in fluid-saturated porous media. J. Fluid Mech. 1987, (176); 379-402

[16] Beranek L.L., Ver. I.L., 1992, *Noise and Vibration Control*, John Wiley & Sons, Inc.

[17] Seybert A.F., Ross D.F., Experimental determination of acoustic properties using a two-microphone random-excitation technique,, J. Acoust. Soc. Am., 1977; 61(5), 1362-1370

[18] Prasad, M.G. Acoustical modeling of automotive exhaust systems. P.HD. Thesis, Purdue University, 1980

[19] I.D.Idel'chik. Handbook of Hydraulic Resistance, Coefficients of Local Resistance and of Friction, translation from Russian by the Israel Program for Scientific Translations, Jerusalem 1966, U.S. Department of Commerce, Nat. Teck. Inf. Service AECTR-6630.

[20] Theodore J. Schultz, Ph.D. Acoustical Uses for Perforated Materials: Principles and Applications, 1986, Industrial Perforators Association Inc.

[21] Brandstatt P., Frommhold W., Program for the Computation of Absorptive Silencers in Straight Ducts. Applied Acoustics, 1994, (43); 19-38

[22] Standard test method for measuring insertion loss of pneumatic exhaust silencers. ASTM E 1265-90 (re-approved 1995)

[23] Measurement procedures for ducted silencers – Insertion loss, flow noise, and total pressure loss. ISO 7235:1991(E)

[24] Wu TW, Zhang P, Cheng CYR. Boundary element analysis of mufflers with an improved method for deriving the four-pole parameters. J. Sound Vib. 1998; 217(4), 767-779

[25] Seybert A.F., Cheng C.Y.R. Application of the boundary element method to acoustic cavity response and muffler analysis. J. Vib. Acoust. Stress and Reliab. 1987, (109); 15-21

[26] Reynolds D.D., 1981, *Engineering Principles of Acoustics*, Allyn and Bacon, Inc.Boston

[27] Cremers L., Fyfe K.R. On the use of variable order infinite acoustic wave envelope elements for acoustic radiation and scattering, J. Acoust. Soc. Am. 1995, 97(4); 2028-2040

[28] Manville Research and Development Center, PO Box 5108, Denver Colorado, USA. 80217-5108

[29] Chung J.Y., Blaser D.A. Transfer function method of measuring in-duct acoustic properties. J. Acoust. Soc. Am. 1980; 68(3), 907-921

[30] SYSNOISE Rev 5.4, LMS International, Interleuvenlann 68, 3001 Leuven, Belgium.

[31] ANSYS, Release 5.7.1, ANSYS Inc. Southpointe 275 Technology Drive Canonsburg, PA 15317

[32] MATLAB, Version 6.1.0.450 Release 12.1, The MathWorks, Inc. 3 Apple Hill Drive Natick, MA 01760-2098, UNITED STATES

[33] American National Standard Specification for Octave-Band and Fractional Octave Band Analog and Digital Filters. ANSI S1.11-1986

[34] Wu T.W, Wan G.C. Muffler performance studies using direct mixed-body boundary element method and a three-point method for evaluating transmission loss. J. Vib. And Acoust. 1996;118:479-484

[35] Istvan L. Ver. Prediction Scheme for the Self-Generated Noise of Silencers. Internoise 1972 Proceedings.

[36] Morse P.M., Ingard K.U., *Theoretical Acoustics*. McGraw-Hill Book Company, New York, 1968